To the Graduate Council:

I am submitting herewith a dissertation written by Jason Lasseter Pittman entitled "Studies of Electroosmotic Flow Dynamics During Electrophoretic Separations." I have examined the final electronic copy of this dissertation for form and content and recommend that it be accepted in partial fulfillment of the requirements for the degree of Doctor of Philosophy, with a major in Chemistry.

S. Douglass Gilman
Major Professor

We have read this dissertation
And recommend its acceptance:

James Q. Chambers

Robert N. Compton

David C. Joy

Acceptance for the Council:

Anne Mayhew
Vice Provost and Dean of
Graduate Studies

(Original signatures are on file with official student records.)

STUDIES OF ELECTROOSMOTIC FLOW DYNAMICS DURING ELECTROPHORETIC SEPARATIONS

A Dissertation
Presented for the
Doctor of Philosophy
Degree
The University of Tennessee, Knoxville

Jason Lasseter Pittman
May 2003

DEDICATION

I would like to dedicate this thesis to the memory of my grandparents that were not able to see me reach this important goal in my life.

Mrs. Floy Lasseter Pittman

Mr. Edward Mollison, Jr.

Mrs. Lorraine Clay

Major Sherman Clay

ACKNOWLEDGMENTS

First, I would like to thank Jasna for being a source of strength for me over the last five and a half years. Thank you for being such an important part of my life and becoming my wife. I truly believe that without Jasna's support and encouragement, the task of finishing graduate school and this thesis would have been much harder.

I would also like to thank my family for their support. Dad and Becky for their belief in me as well as their support for my desire to pursue my education to the extent that I have. I promise that I am really not a professional student. My mother and Terry for believing in me. Pop for believing in and supporting my desire for an education.

I would like to thank many people at the University of Tennessee Department of Chemistry for their help and support over the last five years. Doug for his patience with me and for teaching me to be stubborn when I needed to be. Everyone in the Gilman Group (Angela, Yohannes, Amber, Courtney, Christi, Colin and Jessica) who have made graduate school more enjoyable. Steve (a.k.a. Stevil), Anton, Eloise and Herman for giving up their summers and their spare time to work with me. Kim Schrum for all of her help on my first series of papers as well as for helping me with my research proposal. Dr. Steve for reviewing parts of this thesis and for his support when I was doubting whether or not I could finish and Deb for her help in reviewing portions of this thesis. Bill for taking the time to talk to me about computers when I really didn't have anything important to talk about. Marilyn and Rachelle for always being so kind. Tim for his help with technical drawing and many machine shop projects. Eddie for helping me out so many times when I needed to borrow tools or ask how to get something done.

I especially want to thank my Knoxville family at the Knoxville Volunteer Emergency Rescue Squad. Tony, Linny, Beeler and Weaver have been more than just friends over the last four years. I would trust each of them with my life and thank them for their friendship. Corky, Neil and Thomas for their friendship as well. There are many others at the "Squad" that have played an important part in my life here in Knoxville.

ABSTRACT

Instrumentation and techniques for monitoring electroosmotic flow (EOF) during capillary electrophoretic (CE) separations in both fused-silica capillaries and glass microfluidic devices are presented. These techniques were applied under conventional and sample stacking separation conditions. The instrumentation developed for monitoring EOF was also used to develop optically gated vacancy separations in microfluidic devices.

A recently developed technique for monitoring EOF in capillary electrophoresis by periodic photobleaching of a neutral fluorophore added to the running buffer was further characterized and optimized and then applied to monitoring EOF during a typical capillary electrophoresis separation. The concentration of neutral fluorophore (rhodamine B) added to the running buffer for monitoring EOF was decreased by one order of magnitude to 40 nM. The rate at which EOF can be measured was increased from 0.2 to 1.0 Hz by decreasing the distance between the bleaching beam and the laser-induced fluorescence detector from 6.13 mm to 0.635 mm. The precision of the measured EOF ranged from 0.2 to 1.8%. Under typical experimental conditions, the dynamic range for flow measurements was 0.066 to 0.73 cm/s. Experimental factors affecting precision, signal-to-noise (S/N) ratio and dynamic range for EOF monitoring were studied. This technique was applied to measure EOF during a separation of phenolic acids with analyte detection by UV/VIS absorbance. The EOF monitoring method was shown not to interfere with UV/VIS absorbance detection of analytes.

EOF was monitored in glass microfluidic devices at rates up to 2 Hz with a precision of 0.2 – 1.0% using the periodic photobleaching method. This EOF monitoring method was used to examine the performance of the current monitoring technique for measuring an average electroosmotic flow in a microfluidic device with a cross-T design. Flow measurements made with the current monitoring method gave a precision of 0.4 – 2.2%, but the periodic photobleaching method showed that the current monitoring technique caused changes in EOF as high as 41% during a single experiment. The periodic photobleaching method for EOF monitoring was also used to study EOF in channels on opposite sides of a cross-channel intersection. The opposite channels were shown to exhibit substantially different EOF dynamics during a current monitoring experiment as well as different steady state EOF rates during normal operating conditions.

Electroosmotic flow dynamics during a field-amplified sample stacking experiment have been studied experimentally using the periodic photobleaching of a dilute, neutral fluorophore added to the separation buffer. Changes in electroosmotic flow during a separation of arsenic compounds with field-amplified sample stacking have been monitored at a rate of 1 Hz. The effects of hydrodynamically injecting different sample plug lengths of analyte dissolved in 0.125 mM (120, 240, and 600 s) and 41.7 μM (27, 45, and 74 s) phosphate buffer with a separation buffer concentration of 12.5 mM

phosphate buffer were examined. The observed effects of increasing the sample plug length on electroosmotic flow and electrophoretic current agreed qualitatively with predictions by theoretical models presented in the literature. Electroosmotic flow changes greater than 100% (1.6 – 3.3 mm/s) have been observed. Broadening of the flow monitoring peaks has been used to examine laminar flow due to the discontinuous buffer systems used for sample stacking.

Using the instrumentation and methods developed for monitoring EOF, electrophoretic vacancy separations with optically gated injections were developed as an alternative method of performing separations in microfluidic devices. Vacancy electrophoretic separations of FITC-labeled amino acids were performed over a separation distance of 0.9 cm at a field strength of 353 V/cm, with an injection every 8.0 s. For a series of 10 vacancy electrophoretic separations with 100-ms (177 pL) optically gated injections, the RSD for retention times was 0.17% and the RSD for peak height was 1.6%. The performance of optically gated vacancy electrophoresis was quantitatively compared to the performance of standard optically gated electrophoresis for the same separation using the same microfluidic device and identical experimental conditions. For these separations, the overall performance of the two optically gated injection methods was similar. The resolution obtained with the electrophoretic vacancy separations was slightly lower (6-14%) than with the standard electrophoretic separations due to the larger injection volume for optically gated vacancy injection, using the same injection time.

TABLE OF CONTENTS

Chapter *Page*

I. INTRODUCTION....1

Electroosmotic Flow....3
Fundamentals of Electroosmotic Flow....3
The Importance of Electroosmotic Flow....7
The Impact of Electroosmotic Flow on Separations....7
Methods of Measuring Electroosmotic Flow....9
Methods Which Measure Average EOF....9
Neutral Marker Method....9
Current Monitoring Methods....10
Weighing of Effluent....11
Methods Which Monitor EOF....12
Weighing of Effluent....12
Single-point Fluorescence Methods....12
Heat Index Flow Monitoring....13
Periodic Photobleaching of a Neutral Fluorophore....14
EOF Imaging Methods....14
Laser Induced Fluorescence (LIF) Detection....15
Analyte Injection by Optical Gating....15
Goals of This Research....16

II. ON-LINE MONITORING OF ELECTROOSMOTIC FLOW FOR CAPILLARY ELECTROPHORETIC SEPARATIONS....17

Abstract....17
Introduction....17
Experimental....19
Chemicals....19
EOF Monitoring Instrument....19
Capillary Electrophoresis....21
Instrument Control and Data Acquisition....21
Fluorescence and Absorbance Spectra....21
Limit of Detection (LOD) Determination....21
Bleaching Pulse Power and Duration Studies....22
Characterization of the Photobleached Region as a Function of Flow Rate and Bleaching Pulse Duration....22
Rhodamine B Neutrality Study....23
Phenolic Acid Separation....23
Results and Discussion....23
Fluorophore Concentration....24

Distance Between F1 and F2 24
Rhodamine B Photobleaching....24
Effect of Bleaching Duration of Photobleached Zone Width....28
EOF Measurement Precision 32
Application of EOF Monitoring to a Separation with Absorbance Detection....35
Acknowledgments....37

III. EXPERIMENTAL STUDIES OF ELECTROOSMOTIC FLOW DYNAMICS IN MICROFABRICATED DEVICES DURING CURRENT MONITORING EXPERIMENTS....38

Abstract....38
Introduction....38
Experimental....39
Chemicals....39
Microfabricated Devices....40
Flow Monitoring Instrument....40
Flow Rate Measurments 42
EOF Simulation 44
EOF Monitoring and Current Monitoring Experiments 44
Instrument Control, Data Acquisition and Data Analysis 44
Safety Precautions....45
Results and Discussion 45
EOF vs. Applied Potential 45
Attempts to Monitor EOF in PDMS/Glass Devices 47
EOF Measurement Using the Current Monitoring Method....47
Conclusions....59
Acknowledgments....59

IV. EXPERIMENTAL STUDIES OF ELECTROOSMOTIC FLOW DYNAMICS DURING SAMPLE STACKING FOR CAPILLARY ELECTROPHORESIS....60

Abstract....60
Introduction....60
Experimental....62
Chemicals....62
EOF Monitoring....62
Capillary Electrophoresis....64
Coumarin 334 Neutrality Studies....64
Coumarin 334 Detection Limit Studies 64
Sample Stacking Studies....65
Instrument Control, Data Acquisition and Data Analysis 66
Results and Discussion 66

Coumarin 334....66
Electroosmotic Flow Dynamics During Sample Stacking....66
FASS Induced Pressure Gradients....71
Impact of Shorter, More Dilute Sample Plug Injections....74
Conclusions....76
Acknowledgments....76

V. OPTICALLY GATED VACANCY ELECTROPHORESIS IN MICROFLUIDIC DEVICES....77

Abstract....77
Introduction....77
Experimental....79
Chemicals....79
Microfluidic Chip....79
Optical Gating and LIF Instrument....80
Derivatization of Amino Acids with FITC....82
Optically Gated Injections and Electrophoretic Separations....82
Instrument Control, Data Acquisition and Analysis....82
Results and Discussion....83
Optically Gated *Vacancy* Electrophoresis....83
Optically Gated *Vacancy* Electrophoresis Versus Standard Optically Gated Electrophoresis....86
Conclusions....92
Acknowledgments....93

VI. CONCLUSIONS....94

LIST OF REFERENCES....96

APPENDIX....107

Data Acquisition and Analysis Programs....108
Refractive Index Flow Monitoring....116

VITA....131

LIST OF FIGURES

Figure *Page*

1-1. The individual factors contributing to the separation and elution order of analytes in a capillary electrophoretic separation. 2

1-2. The design of microfluidic devices can be as simple as (A) using two intersecting channels to create sample and separation channels or as complex as (B) where the intersection of multiple channels is used to perform a serial dilution of a sample 4

1-3. Illustration of the (A) formation of the electric double layer along the wall of a fused-silica capillary or microfluidic channel and the (B) plug-like flow profile characteristic of electroosmotic flow 5

2-1. Schematic of the (A) EOF monitoring instrument and (B) an enlarged view of the capillary indicating the position of the bleaching beam (F1) relative to the detection beam (F2) on the capillary 20

2-2. Percent rhodamine B photobleached as detected at F2 vs. bleaching power at F1 25

2-3. Percent rhodamine B photobleached as detected at F2 vs. bleaching pulse duration (F1) for bleaching pulses delivered to 40 nM rhodamine B in 50 mM borate buffer (pH = 9.0) 27

2-4. Electropherograms showing a bleaching pulse (positive peak) and the resulting decrease in fluorescence intensity (negative peak)....30

2-5 Examples of photobleaching sequences with a positive peak overlapping with the photobleached zone....31

2-6. S/N vs. flow rate for the detection of photobleached zones with a 75-ms bleaching pulse....34

2-7. Separation of phenolic acids with simultaneous EOF monitoring....36

3-1 Diagram of the EOF monitoring and LIF detection instrument for microfabricated devices 41

3-2 EOF measurements made in the microfluidic device at applied fields of (A) 353 V/cm (EOF = 0.253 ± 0.001 cm/s) and (B) 118 V/cm (EOF = 0.0856 ± 0.0002 cm/s) 43

3-3 EOF (cm/s) versus applied field (V/cm) as measured by periodic photobleaching of a neutral fluorophore in a microfluidic device....46

3-4 EOF (cm/s, top points) and current (μA, bottom curves) measurements versus time as 20 mM borate buffer (pH = 9.0) is replaced by (A) 19 mM, (B) 10 mM, and (C) 40 mM borate buffer (pH = 9.0) 50

3-5 Simple schematic of the microfluidic device 53

3-6 The (A) EOF (cm/s) and (B) photobleached zone width (fwhm) upstream from the cross-channel intersection (•) and downstream from the cross-channel intersection (o) versus time as 20 mM borate buffer (pH = 9.0) is replaced by 10 mM borate buffer (pH = 9.0) 54

3-7 The (A) EOF (cm/s) and (B) photobleached zone width (fwhm) upstream from the cross-channel intersection (•) and downstream from the cross-channel intersection (o) versus time as 20 mM borate buffer (pH = 9.0) is replaced by 40 mM borate buffer (pH = 9.0) 55

4-1 Schematic and data illustrating the EOF monitoring technique 63

4-2 Structures of (A) coumarin 334 and (B) the zwitterionic form of rhodamine B 67

4-3 Electropherogram of a separation of arsenic compounds dissolved in (A) 12.5 mM phosphate buffer and (B) 0.125 mM phosphate buffer 69

4-4 An (A) electropherogram with (B) EOF (•) and current (solid line) for a separation of three arsenic containing compounds after a 4.0-min hydrodynamic injection of sample dissolved in 0.125 mM phosphate buffer 70

4-5 An (A) electropherogram with (B) EOF (•) and current (solid line) for a separation of three arsenic containing compounds after a 10.0-min hydrodynamic injection of sample dissolved in 0.125 mM phosphate buffer 72

4-6 Peak widths of the photobleached zones (fwhm) during FASS experiments 73

4-7 An (A) Electropherogram with (B) EOF (•) and current (solid line) for a separation of three arsenic containing compounds after a 74-s hydrodynamic injection of sample dissolved in 41.7 μM phosphate buffer 75

5-1 Diagram of the microfluidic device 81

5-2 Series of 3 vacancy electrophoretic separations 84

5-3 Peak height for Arg versus optically gated vacancy injection time 85

5-4 Resolution of Arg/Phe peaks as a function of injection time for optically gated vacancy (•) and standard optically gated (o) separations 88

5-5 Schematic of the injection process for optically gated vacancy electrophoresis (A, C, E) and standard optically gated electrophoresis (B, D, F) 89

5-6 Electrophoretic separations following a 50-ms (A) optically gated vacancy and (B) standard optically gated injection of 3 FITC-labeled amino acids. Electrophoretic separations after a 500-ms (C) optically gated vacancy and (D) standard optically gated injection 91

A1-1 Relationship between TTL output by LabVIEW data acquisition and instrument control and shutter function 109

A2-1 Refractive index flow monitoring instrument 119

A2-2 Illustration of the interference pattern as observed at the PMT (A) before heating and (B) after heating the solution filling the fused-silica capillary 120

A2-3 Primary (3.8 s) and secondary (5.7 s) peaks observed during a flow monitoring experiment using a RI detector and laser heating of the running buffer (10 mM borate buffer; pH = 9.0) containing 0.5 mM phenol red 122

A2-4 Flow rates measured using the secondary peak observed with 0.5 mM phenol red in 10 mM borate buffer (pH = 9.0) 124

A2-5 Flow rates measured using the secondary peak observed with 0.5 mM rhodamine B in 10 mM borate buffer (pH = 9.0) 125

A2-6 Flow rates measured using the secondary peak observed with 0.5 mM fluorescein in 10 mM borate buffer (pH = 9.0) 126

A2-7 The (A) distance vs. calibrated flow rate measured from the center of the thermal peak 128

LIST OF TABLES

Table		*Page*
2-1	Photobleached zone width at fwhm for different values of EOF and bleaching pulse durations	29
3-1	EOF values for 20 mM borate buffer in the separation channel being replaced with each buffer listed	48
5-1	Theoretical plates for Arg with optically gated vacancy and standard optically gated electrophoretic separations	87

CHAPTER I

Introduction

Capillary electrophoretic (CE) separations were first demonstrated in their modern form by Jorgenson and Lukacs in 1981.[1] This work was the culmination of previous independent work by other researchers dating back to 1967.[2,3] CE separations are based on two processes that occur when an electrical potential is applied across a fused-silica capillary filled with a buffering solution. The first of these two processes is electrophoresis, or the separation of charged species in an applied electric field.[4-6] When a mixture of charged molecules is injected into a capillary and an electric field is applied, cationic species migrate towards the cathode, anionic species migrate towards the anode and neutral species remain stationary (Figure 1-1). The magnitude and direction of the electrophoretic velocity ($v_{\text{electrophoresis}}$) is dependent on the charge and size of the analyte molecule and the magnitude of the applied potential field:

$$v_{electrophoresis} = \mu \frac{V}{L} \tag{1-1}$$

where μ is the electrophoretic mobility of an analyte, V is the total voltage applied across the capillary and L is the length of the capillary.[1] Differences in size and charge of the analytes result in the separation of cationic and anionic species:

$$\mu = \frac{q}{6\pi\eta r} \tag{1-2}$$

where q is the charge of the analyte molecule, η is the viscosity of the buffer and r is the radius of the analyte molecule.[6,7] If electrophoresis is the only force acting on the analytes, and a positive potential is applied across the capillary, only cationic analytes migrate past the detector at the cathodic end of the capillary and are detected. Anionic species migrate away from the detector towards the anode and neutrals remain at the point of injection, and neither is detected. Under typical CE operating conditions, electrophoresis is not the only process acting on the injected analyte molecules.

In a fused-silica capillary, when a positive electrical potential is applied across the capillary, electroosmotic flow (EOF) of the buffer solution filling the capillary is generated and typically flows from anode to cathode. The total velocity (v_{total}) of an analyte traveling through a capillary is the sum of $v_{\text{electrophoresis}}$ and v_{EOF} (Figure 1-1):

$$v_{total} = (\mu + \mu_{EOF})\frac{V}{L} \tag{1-3}$$

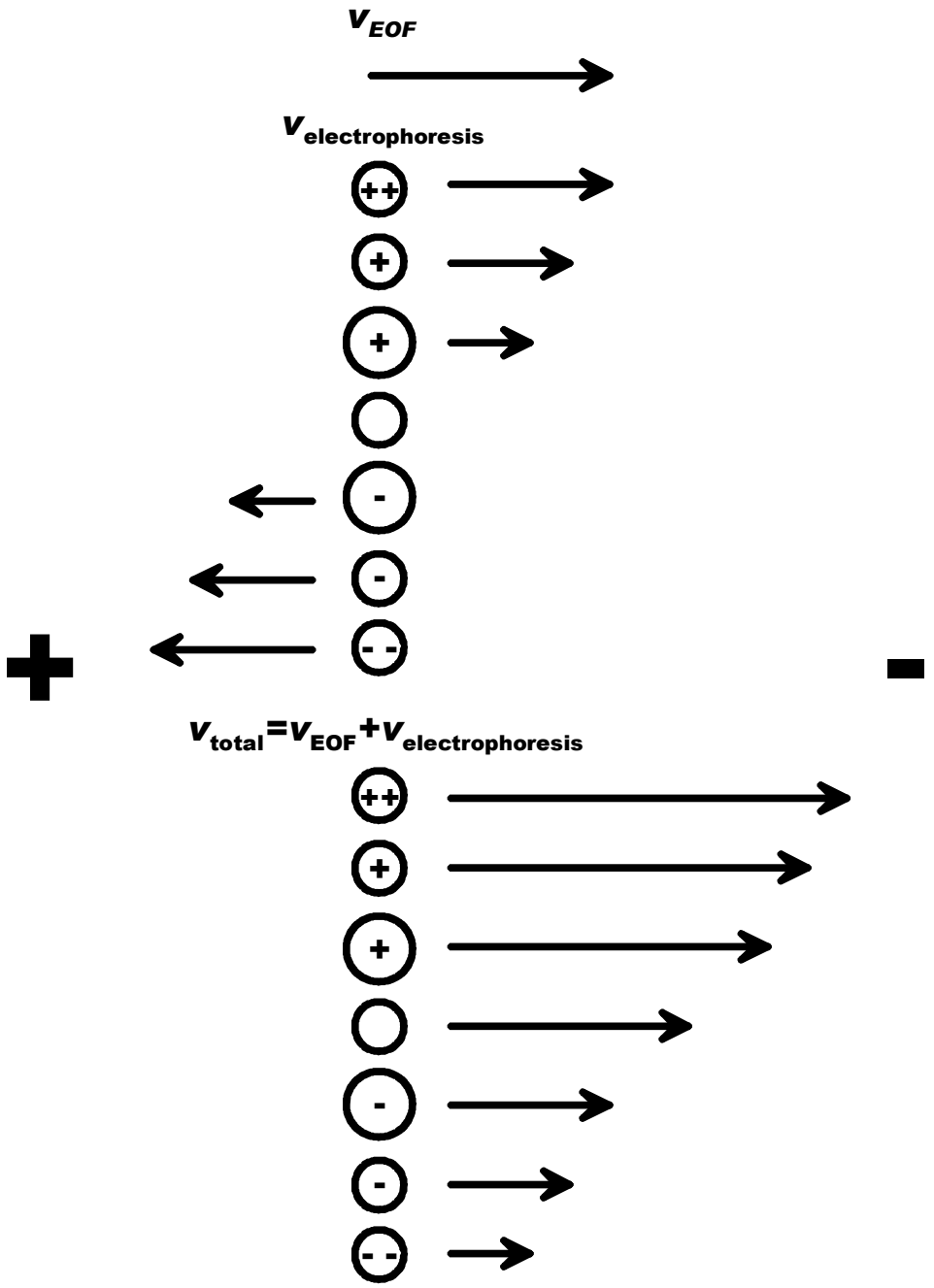

Figure 1-1. The individual factors contributing to the separation and elution order of analytes in a capillary electrophoretic separation. (Adapted from Skoog, D. A.; West, D. M.; Holler, F. J.; Crouch, S. R. *Analytical Chemistry: An Introduction*, 7th ed.; Saunders College Publishing: Fort Worth, 1999).

where μ_{EOF} is the electrophoretic mobility due to electroosmotic flow. In order for all anionic species to be detected, v_{EOF} must be larger than $v_{electrophoresis}$ for these anionic species. Typically, cationic and most anionic species can be detected in a single experiment.

Capillary electrophoretic separations are not limited to being performed only in fused-silica capillaries. In 1992, Harrison *et al.* introduced glass microfluidic chips for the performance of capillary electrophoretic separations.[8] Since that time, a large body of work has been performed demonstrating the use of electroosmotic flow for the movement and control of solutions in both simple and complex microfluidic devices (Figure 1-2) as well as describing the rapid separation of mixtures in microfluidic devices using electrophoresis.[9-20]

Electroosmotic Flow

Fundamentals of Electroosmotic Flow

The theory of electroosmotic flow in a glass capillary was first described in 1967 by Rice and Whitehead.[21] The inner surfaces of fused-silica capillaries and glass microfluidic channels contain weakly acidic silanol (SiOH) groups ($pK_a \approx 5.3 - 6.3$),[22,23] some percentage of which become negatively charged when the capillary or channel is filled with a solution of pH 3.0 or greater.[7] Due to the presence of the negatively charged SiO^- groups, a layer of positively charged, hydrated ions forms at the interface of the solution and the inner wall of the capillary or channel to form what is called the electric double layer (EDL) (Figure 1-3A).[24-28] The portion of the EDL closest to the wall of the capillary or microfluidic channel is composed primarily of hydrated ionic species which are assumed to be adsorbed to the surface of the capillary or channel wall and to be immobile.[27] This layer of adsorbed species is called the Stern layer.[24,28] Beyond the Stern layer, hydrated ions are attracted to the wall of the capillary or microfluidic device by weak, electrostatic forces and form the diffuse layer which extends from the Stern layer into the bulk solution filling the capillary or microfluidic channel.[24,27]

When an electric field is applied across the length of the capillary or microfluidic channel, the hydrated ions present in the diffuse region of the EDL experience an electrophoretic force causing them to migrate along the wall of the capillary or channel.[25,26,28] As the positively charged ions migrate along the capillary wall, the solvating molecules surrounding the ions present in the EDL are also pulled through the capillary. The movement of the hydrated ions of the EDL induces a viscous flow of the bulk solution through the capillary or channel, the electroosmotic flow (EOF), with a velocity (v_{EOF}) which has a value of zero at the wall.[21,25-27,29] Since EOF is generated at the walls of the capillary or channel, it is characterized by a plug-like flow (Figure 1-3B) compared to the laminar flow profile observed with hydrodynamic flow.[21,29-34] This plug-like flow results in the minimal dispersion of analyte bands during a separation and contributes to the high resolution of capillary electrophoretic separations.[1,29]

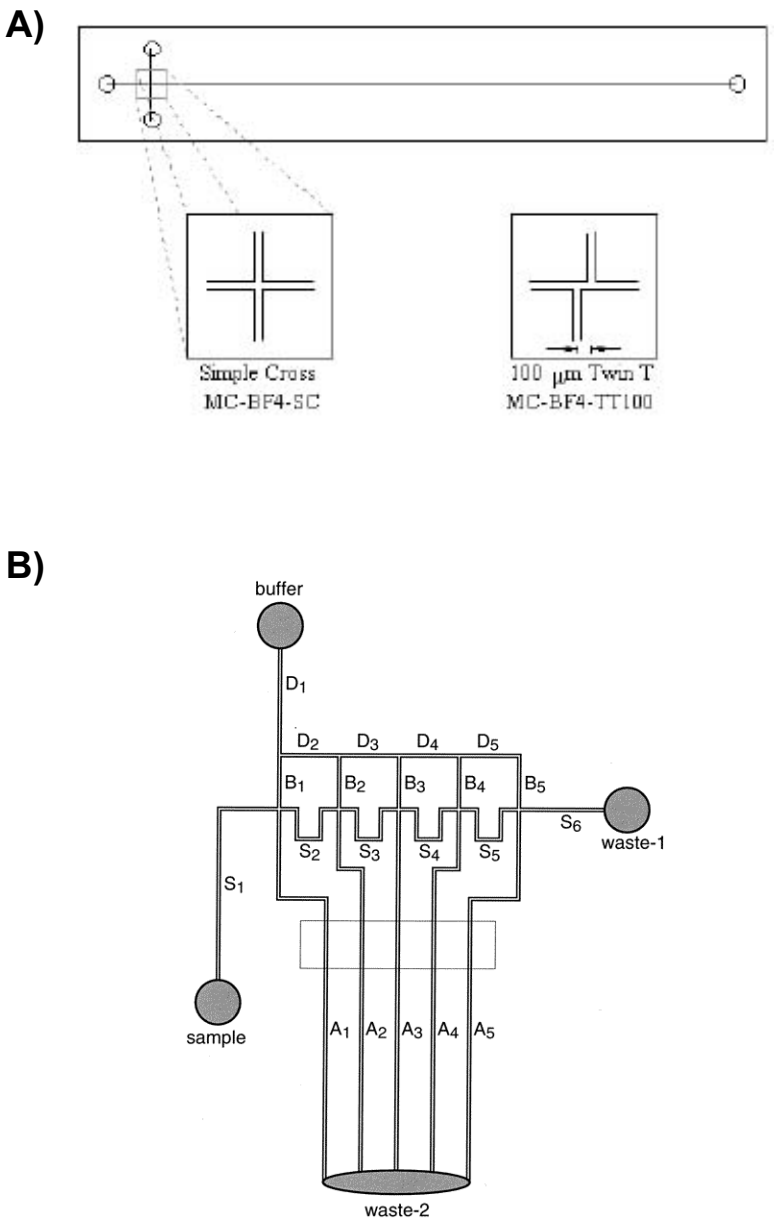

Figure 1-2. The design of microfluidic devices can be as simple as (A) using two intersecting channels to create sample and separation channels or as complex as (B) where the intersection of multiple channels is used to perform a serial dilution of a sample. (Source for Figure 1-2A was http://www.micralyne.com/technology42b.html; Figure 1-2B was Jacobson, S. C.; McKnight, T. E.; Ramsey, J. M. *Anal. Chem.* **1999**, *71*, 4455-4459).

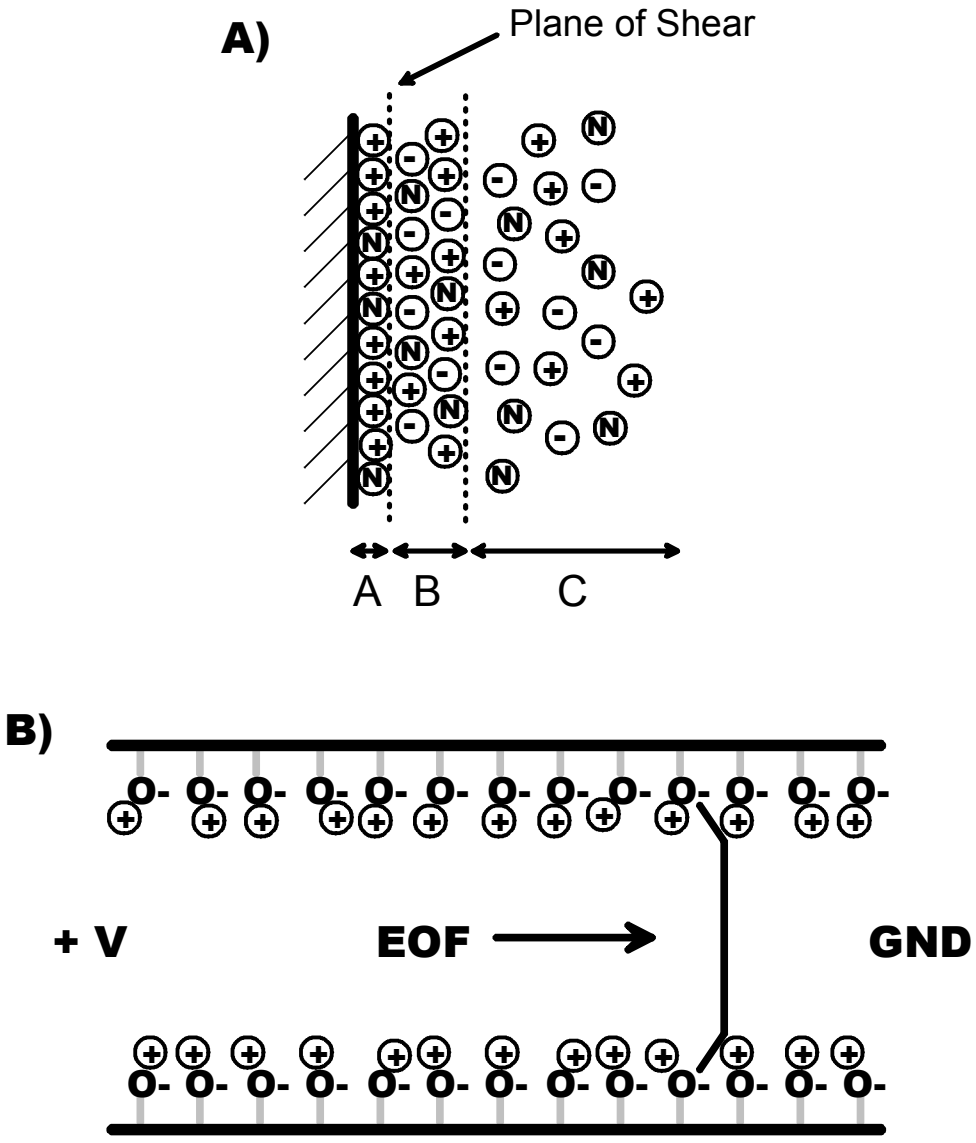

Figure 1-3. Illustration of the (A) formation of the electric double layer along the wall of a fused-silica capillary or microfluidic channel and the (B) plug-like flow profile characteristic of electroosmotic flow. The parts of the electric double layer are the A) Stern layer, B) Compact layer and C) Diffuse layer.

The rate at which the bulk solution flows through the capillary or channel due to EOF is described by:

$$v_{EOF} = \mu_{EOF} E \tag{1-4}$$

where μ_{EOF} is the electrophoretic mobility due to EOF and E is the applied electric field (V/cm).[1] The Smoluchowski equation further describes μ_{EOF}:

$$\mu_{EOF} = \frac{\varepsilon \zeta E}{\eta} \tag{1-5}$$

where ε is the dielectric constant of the buffer, E is the applied field strength and η is the viscosity of the buffer solution.[35,36] The ζ-potential is the electrical potential at the plane of shear occurring at the interface of the immobile Stern layer and the diffuse layer of the buffer solution filling the capillary or channel.[26,27]

The electrophoretic mobility due to EOF (μ_{EOF}) is directly proportional to the ζ-potential. The ζ-potential is dependent on the charge of the capillary wall and is therefore upon the pH and ionic strength of the buffer solution filling the capillary or microfluidic channel.[6] The ζ-potential is described by the following equation:

$$\begin{aligned} \zeta &= GV\delta - \frac{\sigma_w \delta}{\varepsilon \varepsilon_0}, \\ G &= \frac{\varepsilon_1}{\varepsilon r_w}\left(\ln\frac{r_0}{r_2} + \frac{\varepsilon_1}{\varepsilon_2}\ln\frac{r_c}{r_0} \right)^{-1} \end{aligned} \tag{1-6}$$

where G is a geometrical factor, V is the applied electrical potential, δ is the Debye-Hückel radius, σ_w is the surface density of the immobilized electric charge, ε is the dielectric constant of the buffer solution and ε_0 is the dielectric permittivity of a vacuum, r_w is the inner capillary radius, r_0 is the capillary outer radius, r_c is the radius of an imaginary grounded outer cylinder, r_2 is the radius of the space between the capillary wall and the grounded parts of the CE instrument, ε_1 and ε_2 are the dielectric constants of the capillary wall and the substance filling the space between the capillary and the grounded parts of the CE apparatus.[37] The Debye-Hückel radius is defined as:

$$\delta = \frac{1}{F}\sqrt{\frac{\varepsilon_0 \varepsilon RT}{\sum_i C_{i0} z_i^2}} \tag{1-7}$$

where F is Faraday's constant, R is the gas constant, T is the absolute temperature, z_i is the charge of the buffer ion *i* and C_{i0} is the bulk concentration of the buffer ion *i*. This relation details the dependence of the ζ-potential on the ionic strength and composition of the buffer as well as the temperature of the separation environment.[37]

The Importance of Electroosmotic Flow

In capillary electrophoresis, the presence of electroosmotic flow allows the simultaneous analysis of both anions and cations and often results in a decrease of the total amount of time required for a given analysis.[1] However, under normal operating conditions for a negatively charged analyte to be detected in the presence of electroosmotic flow its electrophoretic mobility must be less than the electroosmotic flow (Equation 1-1).[1,29] If an analyte has an electrophoretic mobility greater than that of the electroosmotic flow and in a direction opposite the direction of flow, the analyte will elute out the injection end of the capillary and never be detected at the opposite end of the capillary. In addition to allowing the simultaneous analysis of cationic and anionic species, EOF has additional utility beyond its application to electrophoretic separations.

Pressure based flow, capillary flow and EOF have all been used in microfluidic devices to control the flow of solutions through complex fluid channels. While hydrodynamic flow is well understood and characterized, the laminar flow profile leads to the dispersion of sample zones as they are manipulated in the microfluidic device, while the plug-like flow profile of EOF allows sample plugs to be manipulated with minimal dispersion.[10-12,16-18,38] As the dimensions of microfluidic channels continue to decrease, the scalability of hydrodynamic flow becomes a limiting factor where EOF is easily applied in channels < 10 μm without the use of external pumps or the limitations of designing a system to be used under high applied pressures. EOF, however, can be difficult to control in a reproducible manner due to its dependence on the composition of the solutions being moved through the device as well as the surface chemistry of the device.[18]

The Impact of Electroosmotic Flow on Separations

One reason for the great success of high-performance liquid chromatography (HPLC) is the ability to precisely control the flow rate through the separation column, resulting in separations with a precision and run-to-run reproducibility approximately one order of magnitude better than those obtained with CE.[39] EOF is a surface sensitive phenomenon and can be affected by adsorption of sample components,[40] local changes in temperature, changes in buffer pH, ionic strength or composition, or inhomogeneities in the composition of the capillary or channel wall.[25,26,41] Electrophoretic separations performed in capillaries and microfluidic devices typically have a quantitative precision of 1-10% RSD.[42-44] The relatively poor precision in capillary and chip-based electrophoretic separations is primarily due to the difficulty in maintaining a constant rate of EOF.[41,45]

This lack of reproducibility in retention times of analytes greatly affects the quantitation of analytes following a separation.[43,46] Electrophoretic separations typically have run-to-run reproducibility of 1-5%.[41,43-45] As an analyte travels past a detector, the width of the analyte peak is due to both the physical width of the analyte zone in the channel or capillary and the rate at which it travels past the detector.[43] For instance, an analyte band moving with the EOF will appear to be narrower than an analyte band of the

same physical length moving against the EOF. The variable migration rates of each analyte can be accounted for by calibrating the detector response for each analyte. However, if the EOF changes between the calibration and the analytical separation, the quantitative results obtained are not reliable. Irreproducible EOF further affects the ability to reliably identify analyte peaks in repetitive separations. Jumppanen and Riekkola used multiple marker compounds of known electrophoretic mobility to correct values for the run-to-run v_{EOF} and to achieve a RSD of 0.01-0.03% for the calculated mobility for analyte peaks in a separation.[47]

In microfluidic devices, inconsistent EOF results in irreproducible injection and separation conditions.[48] Many microfluidic devices use electrical potentials applied to multiple channels of the device to control the flow of solution into adjoining channels during separations or to manipulate solutions from multiple sample wells on the device. These "pull-back" potentials are often determined for an individual device prior to the beginning of an experiment. Over time, as v_{EOF} changes, the potentials required to control solutions within a given channel will change as well. Crabtree *et al.* have directly observed an increase in the flow of solution with time from a side channel into the separation channel of a simple microfluidic device.[48] This indicates that unless an understanding and better control of EOF is achieved, the ability to perform reproducible and reliable analyses using microfluidic devices will be hindered.

While lack of reproducible EOF is known to contribute to a decrease in the precision of the quantitative results obtained using CE, some separation methods induce dynamic changes in the bulk flow of solution through a capillary. In sample stacking, a sample dissolved in a dilute buffer is introduced into a capillary filled by a higher concentration buffer.[49] The analyte molecules are concentrated at the interface between the dilute and concentrated buffer zones and are then separated prior to being detected. The introduction of a buffer of differing concentration or conductivity results in a change in the local ζ-potential and impacts the bulk EOF through the capillary.[50,51] As the dilute sample plug migrates through the capillary, hydrodynamic and diffusional processes cause the sample plug to change in size and concentration. As the size and concentration of the dilute sample plug change with time, dynamic changes in the bulk EOF are observed. The bulk EOF continually changes throughout the separation until the dilute sample plug elutes from the end of the capillary. If the size of the dilute sample plug introduced during the injection step of a separation changes from experiment to experiment, the effects of the dilute sample plug on EOF will change.

In other sample stacking experiments, an organic solvent is used to modify the conductivity of the sample solution, resulting in a change of the EOF through the capillary.[52] The effects of organic solvents on EOF and the ζ-potential have been described by Schwer and Kenndler.[22] The increasing concentration of an organic solvent in the running buffer filling a capillary results in a decrease in EOF and also results in a shift of the observed pKa of the surface silanol groups to a higher value.[22] The resulting local changes in ζ-potential and their dynamic effects on the bulk EOF will decrease the precision and accuracy of analytical separations performed under sample stacking conditions both with and without the addition of an organic solvent in the sample plug.

In order for CE techniques such as sample stacking to be applied in a reproducible and quantitative manner, the dynamic changes in EOF induced by the introduction of a discontinuous buffer system into a capillary or microfluidic channel must be fully understood.

Methods of Measuring Electroosmotic Flow

Methods Which Measure Average EOF

Neutral Marker Method

The most common method of measuring an average EOF rate during CE separations is measuring the elution time of a neutral compound.[42,53,54] The ideal neutral marker is any compound which has no electrophoretic mobility under the conditions of the experiment being performed, is easily detected using the method of analyte detection, and does not interact with the wall of the separation capillary.[55] Some common neutral markers are dimethyl sulfoxide, mesityl oxide, methanol, phenol and benzyl alcohol.[42,53,55-57]

The neutral marker is typically injected with the sample plug at the beginning of the experiment, prior to the application of the separation potential. Once the separation potential is applied, the amount of time required for the neutral marker to elute past the detector is used to calculate EOF by $EOF = t_0/L$, where t_0 is the elution time of the neutral marker and L is the length of capillary to the detector. Sandoval and Chen reported a RSD for the neutral marker method of 0.9% (N = 15).[55]

A modified version of the neutral marker method has been demonstrated for measuring reduced EOF in capillaries where the inner surface has been chemically modified.[55-57] In some chemically modified capillaries, the magnitude of the EOF is decreased and results in long migration times. Under conditions of slow or diminished EOF, the traditional neutral marker method becomes impractical. Ermakov *et al.* developed a method in which a plug of neutral marker is electrophoretically injected onto the capillary and then pressure-based flow is used to "rinse" the neutral marker past the detector. The peak area of the electrophoretically injected neutral marker is compared to the peak area of a reference injection of neutral marker injected separately by pressure based injection. Since the amount of neutral marker injected electrophoretically is proportional to the EOF rate, the ratio of the two peak areas can be used to calculate a value for EOF. This modified neutral marker method deviated from the standard method by up to 15%.[56]

Sandoval and Chen developed a similar method in which a neutral marker plug is hydrodynamically injected into the capillary followed by the application of an electrophoretic potential for a short period of time. A second plug of neutral marker is then hydrodynamically injected behind the first, separated by a short plug of running buffer. The two plugs of neutral marker are then hydrodynamically pushed through the capillary and past the detector. The time separation between the two neutral marker

peaks is used to calculate a value for EOF. A RSD of 0.8% was reported for this method (N = 15) with a 0.9% deviation from the standard neutral marker method.[55]

Williams and Vigh have also reported a modified neutral marker method where three discrete injections of a neutral marker were used to measure an average EOF.[57] A band of neutral marker is first hydrodynamically injected into the capillary followed by a region of running buffer. A second band of neutral marker is then hydrodynamically injected into the capillary followed by another region of running buffer. The electrophoretic potential is then applied across the capillary and the two bands of neutral marker migrate with the EOF. The applied potential is removed after a predetermined amount of time and prior to the elution of the bands of neutral marker past the detector. A third band of neutral marker is then hydrodynamically injected into the capillary followed by the hydrodynamic elution of all three neutral marker bands from the capillary. The EOF rate is then determined through a series of calculations which relate the multiple injection times, the applied potential time and the elution times of all three neutral marker bands. This method exhibited a RSD of 6% and deviated from the standard neutral marker method by 4%.[57]

The neutral marker method is an easily implemented technique for measuring an average EOF rate during a separation. The EOF rate measured using the neutral marker method, however, is an average of the EOF during the time that the neutral marker is migrating through the capillary to the detector. Depending on the separation conditions and the sample mixture, it is possible that either cationic or anionic species may not have eluted past the detector at the time of the neutral marker's detection. Any changes in EOF that occur after the elution of the neutral marker past the detector will not be accounted for in the average EOF value measured.

Current Monitoring Method

The current monitoring method provides an alternative to the neutral marker method for measuring an average EOF rate through a capillary or microfluidic device.[27,58-72] Developed by Huang *et al.* the current monitoring method makes an average EOF measurement by determining the amount of time required for a replacement buffer of different concentration to migrate through a capillary, displacing the buffer which originally filled the capillary.[58] As the replacement buffer migrates through the capillary, the capillary is filled with a buffer of different ionic strength and therefore a different resistivity. As the capillary fills with this new buffer, a change in the electrophoretic current through the capillary is observed. The change in current is most easily explained by imagining the buffer filling the capillary as a resistor. When the capillary is filled by a homogeneous solution, the current (I) through the capillary is defined by Ohm's law as $I= V/R$ where V is the applied voltage and R is the resistance of the buffer solution. When the replacement buffer is introduced into the capillary, a circuit with two resistors in series is created and the simple description becomes $I = V/(R_1+R_2)$. The resistance of the concentrated and replacement buffer zones (R_1 and R_2) is dependent on the length of capillary filled by each buffer as well as the conductivities of each buffer. As the replacement buffer continues to fill the capillary, the values of R_1

and R_2 continually change until the capillary is completely filled by the replacement buffer.

Once the replacement buffer has completely filled the capillary, the current through the capillary reaches equilibrium at a new value characteristic of the replacement buffer. The time that is required for the capillary to be filled by the replacement buffer is determined by measuring the time where the current first reaches its new equilibrium value on a plot of current versus time. The average EOF rate is determined by the total length of the capillary divided by the migration time of the replacement buffer. The EOF measurements made by Huang, Gordon and Zare had an accuracy of 0.3 – 0.5% versus a neutral marker measurement and a precision of 1.7 – 1.8%.[58] This method, however, suffers from the same limitations that were previously described for the neutral marker method.

The simplicity of the current monitoring method allows it to be easily applied to measuring EOF rates in microfluidic devices.[61-67,69-72] Initially, Huang, Gordon and Zare used a replacement buffer which was a 5% dilution of the stock buffer (i.e. 19 mM replacement buffer made from 20 mM stock buffer).[58] Since the size of the microfluidic channels is after smaller, the magnitude of the current through a channel is typically smaller than that through a capillary. In order to compensate for the smaller change in current observed in microfluidic channels, many researchers have increased the dilution factor of the replacement buffer relative to the stock buffer in order to exaggerate the change in current as the replacement buffer fills the microfluidic device.[61,62,64-67,69-72] The precision of EOF measurements made using the current monitoring method in microfluidic devices has ranged from 2.5 – 13%.[61-64,69,70]

An alternative to the current monitoring method using conductivity detection to measure the change in buffer concentrations has also been used in both capillaries and microfluidic devices.[58,69,73,74] In this adaptation of the current monitoring method, changes in conductivity at the detection end of the capillary or at the waste end of the microfluidic channel are monitored rather than changes in current through the capillary or microfluidic device. Liu *et al.* reported a RSD for the conductivity monitoring method of 1.9% versus the 5.9% measured for the current monitoring method, indicating that the conductivity monitoring method is an improvement over the standard current monitoring method.[69] However, the conductivity monitoring method is more difficult to implement than the current monitoring method due to the requirement that the conductivity detector be placed near the end of the capillary or integrated into a microfluidic device.

Weighing of Effluent

The weighing of capillary effluent has also been used to determine average EOF values both on- and off-line.[35,75,76] Measuring the change in mass of the reservoir at the detection end of the capillary, Altria and Simpson were able to measure average EOF rates with a precision of 1.3%.[76] Due to the small volumes being collected by this method, it is necessary to take precautions to prevent the evaporation of buffer from the detection end reservoir during the experiment. Just as the neutral marker and the current monitoring methods mentioned previously, this method provides a single, time-averaged

value for EOF. The greatest advantage of this method is that no modification of the running buffer and no introduction of sample is necessary. It is also possible to measure the average EOF over the course of an entire separation unlike the neutral marker and current monitoring methods.

Methods Which Monitor EOF

Weighing of Effluent

Van de Goor *et al.* further adapted the method of Altria and Simpson into an on-line method for measuring EOF.[35] Placing the detection end reservoir on an analytical balance during the electrophoretic experiment, van de Goor *et al.* were able to measure changes in the mass of the effluent with a time resolution of 5 min, however, no other figures of merit were reported for this EOF monitoring method.

Single-point Fluorescence Methods

Changes in the flow rate of a solution through a capillary have also been measured by detecting changes in the fluorescence intensity of a fluorophore traveling past a single-point fluorescence detector.[77] The effects of photobleaching on the fluorescence intensity of single-point laser-induced fluorescence (LIF) detectors has been examined in order to optimize conditions for detection of derivatized or natively fluorescent compounds in CE.[77-79] It has been shown that the intensity of the fluorescence detected from a constant concentration of fluorophore is dependent on the flow rate of fluorophore past a LIF detector.[77,78,80,81] As the flow rate past the detector increases, the amount of time a given fluorophore is exposed to the LIF detection beam is decreased, resulting in a decrease in the amount of photobleaching that occurs. This increases the amount of fluorescence observed at the single-point detector. The opposite is true for a decrease in the flow rate past the detector. As the flow rate decreases, the residence time for a single fluorophore in the LIF detection beam is increased and the likelihood of photobleaching occurring increases as well. This results in a decrease in the amount of fluorescence observed at the detector.

The approximate flow rates studied by Sugarman and Prud'homme using their technique were 0.13-2 nL/s (0.26-2.5 cm/s).[77] These flow rates are up to one order of magnitude greater than the flow rates typically encountered in capillary or microfluidic electrophoretic separations. This observation raises a question of whether or not this technique will be able to detect changes in flow rate on a scale smaller than that demonstrated here. In addition to this concern, this technique is limited by the stability of the intensity of the light source used to excite fluorescence. The calibration curve used for determining the flow rates measured using this technique must be determined for each test buffer due to the influence of solvent properties on fluorescein and photobleaching. Sugarman and Prud'homme reported no figures of merit for this technique.[77]

A second method for measuring EOF using a single point fluorescence detector has been reported by Lee *et al.*[82] A fluorescent dye is added to the running buffer at a constant rate, at the far end of the separation capillary and fluorescence is then detected

by LIF. The intensity of the detected fluorescence is dependent on the rate of the EOF leaving the separation capillary. As the flow rate in the separation column increases, the amount by which the added fluorophore is diluted by the running buffer increases, resulting in a decrease in the fluorescence signal. As the flow rate decreases, fluorescence intensity increases as expected. Lee *et al.* reported a response time of ~1 s and an ability to detect changes in EOF as small as 1%.[82] While this technique has high precision and good time resolution, due to the need to create a junction between two capillary halves and introduce the fluorescent marker at the junction, it is technically difficult to implement. No further reports or applications of this technique have appeared in the literature.

Heat Index Flow Monitoring

Two different approaches to monitoring hydrodynamic flow in capillaries and microfluidic devices using changes in refractive index following heating of the solution flowing through the capillary have been demonstrated.[83-85] Weimer and Dovichi used two intersecting laser beams, one pump and one probe beam, to measure the deflection of the probe beam by the change in the optical properties of the solution flowing through a square capillary by creating a thermal lens in the center of the capillary.[83] The energy from the pump beam was absorbed by a chromophore introduced into the solution filling the capillary, resulting in a localized change in refractive index. This change in refractive index caused the probe beam to deviate from the center of the probe axis and resulted in a change in the intensity of the probe beam at the detector. This deflection was proportional to the local temperature of the solution and the return of the probe beam to the center of the probe axis was dependent on the rate of solution flow through the capillary. This method sampled the flow at a rate of 25 Hz with a dynamic range of 0.2 to 30 mm/s and a precision of 1.9% in a capillary of approximately 1 mm i.d. Typically, flow rates of up to ~0.4 cm/s are observed in CE separations in capillaries of up to 100 μm i.d.

In a second method using a change in refractive index of a solution filling a capillary, StClaire and Hayes used a heating coil wrapped around a fused silica capillary to heat a small region of solution flowing through a 184 μm i.d. capillary.[84] Using a refractive index (RI) detector, a shift in the RI downstream from the heating coil was detected as the region of heated solution flowed through the detector window. By monitoring the amount of time it took for the shift in RI to occur relative to the beginning of the heating event, a flow rate was measured. Hydrodynamic flow rates of 2-25 cm/s were monitored with an accuracy of 1%.[84] No precision was reported for this technique. In a similar approach, Markov and Bornhop used an IR laser to induce a thermal gradient in the solution flowing through a 250 μm capillary and then detected the heated solution with a RI detector downstream from the IR laser.[85] In this version of RI flow monitoring, a change in the phase of the Fourier transforms of the computer signal which triggers the heating beam and the RI signal was used to measure flow rate. Flow rates of 1 to 10 μl/min (0.034 to 0.34 cm/s) were quantified.[85]

Periodic Photobleaching of a Neutral Fluorophore

Schrum *et al.* have reported monitoring of EOF by the periodic photobleaching of a dilute, neutral fluorophore added to the running buffer.[86] Using this method, EOF was monitored at a rate of 0.2 Hz in a 50 μm i.d. capillary with a precision of 0.7% or better using rhodamine B as a neutral, zwitterionic additive in the running buffer. The estimated dynamic range of this EOF monitoring method was 0.10 to 2.4 cm/s. It was further demonstrated that this EOF monitoring method could be used to measure EOF during a CE separation of fluorescent analytes.[86]

EOF Imaging Methods

Various imaging methods have been used to examine the flow in capillaries and microfluidic devices.[19,20,30-34,65,87-101] The electrophoretic flow of a fluorophore across a capillary gap junction was first reported by Kuhr *et al.*[87] Fluorescence imaging has also been used to examine the profile of a solution front as it flowed through a capillary by either hydrodynamic and electroosmotic flows.[30-32] Preisler and Yeung continuously monitored the electroosmotic flow down the length of a coated capillary by following a fluorescent, neutral marker using whole-column imaging with a time resolution of 1-5 min.[94] The effects of nonuniform ζ-potentials in a capillary on the electroosmotic flow profile has been examined using a caged dye technique with fluorescence imaging.[99] In order to observe the development of the EOF profile, the capillary is filled with a solution containing a caged dye. This caged dye in the capillary is exposed to a well-defined and focused laser beam, which breaks the bond between the fluorophore and the caging moiety making the dye fluorescent. The initial plug-like profile can then be examined using fluorescence imaging, allowing changes in the profile of the sample zone as it travels down the capillary to be observed.[99] Nuclear magnetic resonance imaging has also been used to examine the development of the EOF as a function of time.[91,92]

J. Michael Ramsey's group at Oak Ridge National Laboratory has used imaging of microfluidic devices to examine the flow dynamics of sample injection techniques[88,95,100] as well as the flow dynamics of electroosmotically induced hydraulic pumping.[97] Fluorescence imaging of microfluidic devices was used by Lichtenberg *et al.* to observe the flow of sample solutions in a microfluidic device designed for sample preconcentration using sample stacking.[101] Using fluorescein dye and fluorescence imaging Seiler *et al.* observed electroosmotic pumping and the flow of solutions through a valveless manifold in a microfluidic device.[89] Each of these studies used simple fluorescence imaging to qualitatively observe the flow of solutions through various microfluidic devices. The information gained from such studies is important to understanding the behavior of solutions in complex microfluidic geometries, however, no quantitative information is obtained regarding the magnitude of electroosmotic flow and whether or not it is reproducible.

Laser-Induced Fluorescence (LIF) Detection

LIF is a sensitive method of analyte detection for electrophoretic separations performed in capillaries and microfluidic devices, with detection limits as low as 10^{-15} M.[78] When using LIF as a detection method, it is desirable to optimize the detection conditions so that the maximum the number of photons are obtained from a single fluorophore before photodecomposition occurs. The optimization of conditions for LIF detection includes consideration of both laser power and flow rate of the fluorophore across the detection axis.[78,79] In LIF detection, the intensity of the laser beam at the point of detection is high enough that the excited state of the fluorophore becomes the most populated state. Once the excited state has become populated, any increase in laser power will result in a decreased signal-to-noise ratio, due to an increase in the amount of light scattered from the capillary and no increase in fluorescence intensity.[78] As the amount of time that the fluorophore is illuminated increases, the fluorescence intensity decreases due to photodestruction of the fluorophore molecule.[78]

A large volume of work has been reported developing LIF detection for capillary electrophoretic and microfluidic separations.[102-105] The greatest challenge to performing LIF, is the small number of analytes that are natively fluorescent. Often, pre- or post-column derivatization is utilized to attach a fluorophore to non-fluorescent analytes.[103-105] An approach which negates the need for derivatization of the analytes is indirect fluorescence detection. In indirect fluorescence detection, a fluorophore is added to the running buffer and fills the entire capillary. A zone of analyte moving through the capillary displaces the fluorophore and is detected as a decrease in the background fluorescence intensity.[104] As diode-based lasers become more readily available, LIF detection becomes more affordable.[104]

Analyte Injection by Optical Gating

Optical gating has been demonstrated as a rapid, reproducible method of injecting fluorescently derivatized analytes into the separation length of a capillary or microfluidic device.[106-113] Optically gated injection in capillaries was first demonstrated by Monnig and Jorgenson in 1991.[106] Monnig performed a separation of FITC-labeled amino acids in as short as 1.5 s over a distance of 1.2 cm. In order to perform the optically gated electrophoretic separation, the capillary was filled with the analyte solution and the separation potential applied. A high power laser beam, the gating beam, was directed onto the capillary at a point upstream from the LIF detector. The gating beam irradiated the sample flowing through the capillary, photobleaching the fluorophore labels attached to the analyte molecules, resulting in a baseline signal with little fluorescence at the LIF detector. When the gating beam was blocked, an injection of analyte was performed. The analyte molecules migrated normally from the point of injection to the LIF detector, where the analytes were detected as positive, fluorescent peaks.[106]

The photodestruction of a fluorophore is believed to occur by the interaction of an excited state with another reactant present in the system[77] or the molecule can relax from

an excited state into a reactive state and photodecompose.[78,79,114-116] The ability to photobleach or photodestroy a given fluorophore is dependent upon its photostability. For instance, sodium-fluorescein, an easily photobleached fluorophore, has a bleaching efficiency of 7.4 x 10^{12} molecules/W·s·cm^3 which is 15 times higher than the bleaching efficiency of rhodamine B (0.5 x 10^{12} molecules/W·s·cm^3).[117] These values indicate that a higher total laser power will be required to bleach the same number of rhodamine B molecules as fluorescein molecules in a given period of time.

Goals of This Research

The importance of separation techniques for the analysis of complex samples is well established. Capillary electrophoretic separations in both fused-silica capillaries and microfabricated devices have allowed increasingly small sample volumes to be separated and analyzed. The lack of reproducibility in capillary electrophoretic separations, however has greatly hindered the use of techniques for quantitative analysis. The quantitative measurement of electroosmotic flow and flow dynamics in capillaries and microfabricated devices will have a direct impact on performing reproducible and quantitative separations.

The primary goal of the research presented here is to study the flow dynamics of electroosmotic flow in capillary and microfluidic devices during electrophoretic separations. The technique developed to monitor EOF was applied to measuring EOF during a typical CE separation using UV/Vis absorbance detection of analytes as well as during a separation where the preconcentration of analytes by sample stacking was applied. The instrumentation developed for measuring EOF was also used to perform reproducible, serial, vacancy injections of fluorescently labeled analytes for separations in microfluidic devices. Optically gated vacancy injections were directly compared to standard optically gated injections. The optically gated vacancy injections were also used to directly compare separation efficiencies of microfluidic devices fabricated from glass and PDMS.

CHAPTER II

On-Line Monitoring of Electroosmotic Flow For Capillary Electrophoretic Separations

This chapter is a slightly revised version of a paper by the same title published in the journal *The Analyst* in 2001 by Jason L. Pittman, Kimberley F. Schrum and S. Douglass Gilman:

Pittman, J. L.; Schrum, K. F.; Gilman, S. D. *Analyst* **2001**, *126*, 1240-1247.

Abstract

A recently developed technique for monitoring electroosmotic flow (EOF) in capillary electrophoresis by periodic photobleaching of a neutral fluorophore added to the running buffer has been further characterized and optimized and then applied to monitoring EOF during a typical capillary electrophoresis separation. The concentration of neutral fluorophore (rhodamine B) added to the running buffer for monitoring EOF has been decreased by one order of magnitude. The rate at which EOF can be measured has been increased from 0.2 to 1.0 Hz by decreasing the distance between the bleaching beam and the laser-induced fluorescence detector from 6.13 mm to 0.635 mm. The precision of the measured EOF ranges from 0.2 to 1.8%. Under typical experimental conditions, the dynamic range for flow measurements is 0.066 to 0.73 cm/s. Experimental factors affecting precision, signal-to-noise (S/N) ratio and dynamic range for EOF monitoring have been examined. This technique has been applied to measure EOF during a separation of phenolic acids with analyte detection by UV/VIS absorbance. The EOF monitoring method has been shown not to interfere with UV/VIS absorbance detection of analytes.

Introduction

Precision limits the wide acceptance of capillary electrophoresis (CE) in laboratories required to submit results to regulatory agencies.[39,43,118] The precision of retention times, peak areas and peak heights obtained with CE are typically an order of magnitude poorer than that obtained with HPLC.[39] Fluctuations in electroosmotic flow (EOF) often result in variations of retention times of 3-5%, hindering the ability to identify and quantify analytes.[39,43,118] Therefore, it is important to measure and understand EOF for CE separations.

Typically, EOF is measured by injecting a neutral marker with the sample.[42,53] The migration time of the neutral marker provides a single, average value of EOF. However, this method has two significant shortcomings. Fluctuations of EOF that take

place on a time scale faster than the neutral marker's elution time cannot be resolved. Also, the average EOF value does not include changes that occur after detection of the neutral marker although charged analytes may be detected after this time. Therefore, it is desirable to monitor EOF over an entire separation with time resolution faster than the total separation time. This will enable measurement and study of EOF fluctuations and correction of CE data for variations in EOF.

A variety of approaches have been used to continuously monitor or image EOF in capillaries.[30-32,35,82,86,94,99,119,120] Most imaging studies have focused on observing flow profiles of electrokinetic and pressure-driven flow in capillaries, but these techniques have not been used for continuous monitoring of EOF.[30-32,99,119,120] Only two reported techniques for continuous EOF monitoring provide time resolution of less than 10 s and measurement precision of better than 1%.[82,86] Zare and coworkers monitored EOF by measuring the dilution of a fluorophore stream mixed with the effluent from the separation capillary.[82] The concentration of the fluorophore downstream from the post-column mixing device was inversely proportional to the rate of EOF in the separation capillary. These measurements were made with a time resolution of ~1 s and a precision of better than 1%.[82] Schrum et al. reported a method for EOF monitoring based on periodic photobleaching and laser-induced fluorescence (LIF) detection of a neutral fluorophore added to the running buffer at nanomolar concentrations.[86] Electroosmotic flow was measured by determining the time for a photobleached zone generated on-column to migrate ~6 mm to a downstream LIF detector. This measurement was repeated for EOF monitoring, providing a time resolution of 5.0 s and a precision of 0.7% or better.

Two related approaches for measuring flow in capillaries have been demonstrated.[77,84] Sugarman and Prud'homme measured flow by monitoring the change of fluorescence signal for a single-point LIF detector at high laser power.[77] They showed that fluorescein fluorescence under these conditions was dependent on the rate of Poiseuille flow in a 25-μm i.d. capillary for flow rates on the order of 100 nL/min. StClaire and Hayes used a heating coil to periodically raise the temperature of a solution zone in a capillary.[84] This heated zone was detected 9 mm downstream based on the resulting change in refractive index. The migration time of the heated zone was used to determine the rate of Poiseuille flow in a 184-μm i.d. capillary.[84] The time resolution and precision obtained were not reported for either of these methods.

The goals of the research presented in this paper are to improve the performance of the EOF monitoring technique reported by Schrum et al.[86] and to demonstrate the application of this technique to a typical CE separation with UV/VIS absorbance detection. The instrument has been modified to improve the time resolution of EOF monitoring. This is important for studying rapid fluctuations in EOF and for applying the technique to fast CE separations.[106,109,121] The concentration of the neutral fluorescent dye added to the running buffer for EOF monitoring has been reduced, which will decrease the potential for interference of the dye with analyte detection. We demonstrate that this method for EOF monitoring can be used with a CE separation and does not

interfere with simultaneous detection of analytes using a separate UV/VIS absorbance detector.

Experimental

Chemicals

Laser grade rhodamine B, syringic acid, 4-hydroxy-3-methoxybenzoic acid, p-hydroxycinnamic acid, 3,4-dihydroxybenzoic acid, 3,4-dihydroxycinnamic acid, and gallic acid were obtained from Acros (Pittsburgh, PA). Mesityl oxide was purchased from Aldrich (Milwaukee, WI). Dimethyl sulfoxide (DMSO) was obtained from Mallinckrodt (Phillipsburg, NJ). Boric acid, sodium bicarbonate and HPLC grade methanol were purchased from Fisher Scientific (Pittsburgh, PA). All solutions were prepared in doubly distilled water.

EOF Monitoring Instrument

The previously reported instrument for EOF monitoring was modified to simplify monitoring of the opening of the computer-controlled shutter.[86] A single fiber optic (147.0 μm core; 164.0 μm cladding; Polymicro Technologies; Phoenix, AZ) was used to direct a portion of the bleaching beam to the PMT so that a small positive signal indicating the opening of the computer-controlled shutter was detected. Dichroic mirrors and cut-on filters were changed as needed for LIF detection with excitation at either 457.9 nm or 514.5 nm.

The remainder of the instrument was described in detail previously.[86] The modified instrument is illustrated in Figure 2-1. Briefly, the 457.9 nm or 514.5 nm line from an Argon-ion (Ar^+) laser (Coherent Innova 90C-5; Santa Clara, CA) was split with a broadband cubic beamsplitter. The bleaching portion of the beam was directed through a computer-controlled shutter (Uniblitz 310 B; Vincent Associates; Rochester, NY), and focused through a fused-silica plano convex lens (f = 38 mm) onto the bore of the capillary at position F1. The detection portion of the beam was attenuated with neutral density filters (not shown). The detection beam was directed by a dichroic mirror (475DRLP for 457.9 nm or 540DRLP for 514.5 nm; Omega Optical; Brattleboro, VT) to a 20X microscope objective (0.4 NA) and focused on to the capillary bore at position F2. Fluorescence was collected at 180° and passed through two glass cut-on filters (LP-560-1.00 and CG-OG-550-1.00-2 for excitation at 514.5 nm or LP-475-1.00 and FCG-465-1.00 for excitation at 457.9 nm; CVI Laser Corporation; Albuquerque, NM) and spatially filtered (1.5 mm pinhole) prior to being detected with a PMT (Hamamatsu HC120; Bridgewater, NJ). The distance, d, between F1 and F2 (Figure 2-1B) was determined daily using the method described previously.[86] The value of $d_{F1\text{-}F2}$ is:

$$d_{F1-F2} = mean\ photobleached\ zone\ migration\ time \times \frac{injection\ end\ to\ F2\ distance}{neutral\ marker\ migration\ time} \quad (2\text{-}1)$$

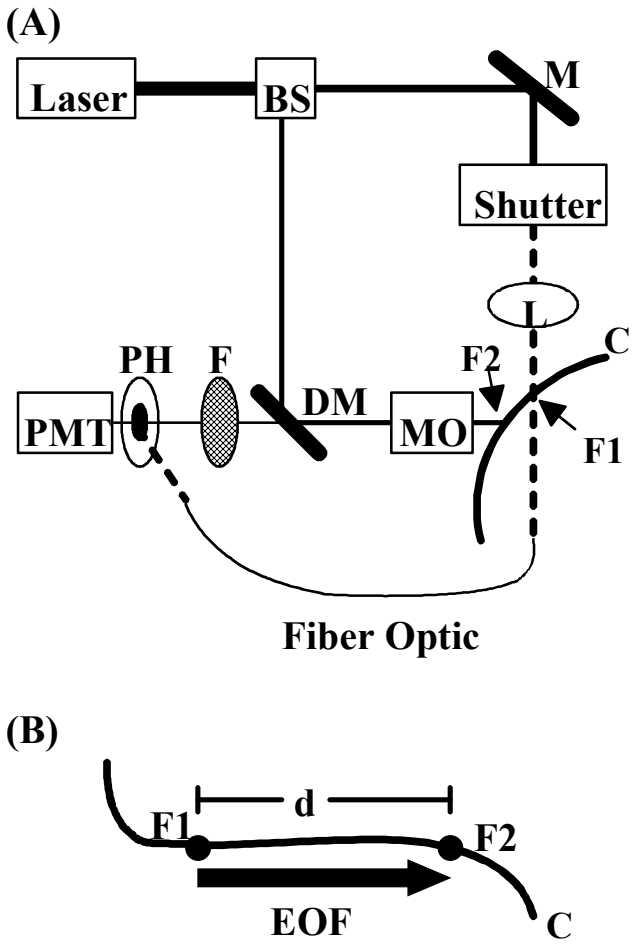

Figure 2-1. Schematic of the (A) EOF monitoring instrument and (B) an enlarged view of the capillary indicating the position of the bleaching beam (F1) relative to the detection beam (F2) on the capillary. BS, beamsplitter; M, mirror; L, plano-convex lens; C, capillary; F1, bleaching point on the capillary; F2, detection point on the capillary; MO, microscope objective; DM, dichroic mirror; F, long-pass filters; PH, pinhole; PMT, photomultiplier tube. The distance between F1 and F2 is *d*.

Capillary Electrophoresis

Fused silica capillary (50 μm i.d./220 μm o.d.) was obtained from SGE (Austin, TX) and used for all experiments. A Spellman CZE1000R high voltage power supply was used to apply the electrophoretic potential (Hauppauge, NY). The home-built CE instrument was described previously.[86] A Linear UVIS 204 detector (Linear Instruments; Reno, NV) with an on-column capillary cell was used for absorbance detection. The detection wavelength was 210 nm. The rise time for the absorbance detector was 1.0 s.

Instrument Control and Data Acquisition

A program written in LabVIEW (National Instruments; Austin, TX) was used for data acquisition and instrument control. All data were acquired with a National Instruments PCI-6024E data acquisition board. All signals were filtered with a low-pass RC filter prior to acquisition. All data were analyzed with either Peak Fit 4.0 (SPSS Science; Chicago, IL) or Microsoft Excel (Microsoft Corp.; Redmond, WA).

Fluorescence and Absorbance Spectra

Fluorescence excitation and emission spectra were obtained for 2.5 μM rhodamine B in 50 mM borate buffer (pH = 9.0) with a Model SQ-340 Aminco/Bowman Series 2 Luminescence Spectrometer (SLM Aminco; Urbana, IL). For the acquisition of the emission and excitation spectra, the excitation and emission monochromators were set at 552 and 577 nm, respectively. Absorbance spectra of the same solution of rhodamine B were obtained with a Model 8452A Diode Array Spectrophotometer (Hewlett Packard; Boise, ID).

Limit of Detection (LOD) Determination

The capillary was filled with 50 mM, pH 9.0 borate buffer solution containing rhodamine B at concentrations from 10 μM to 7.0 nM. At each rhodamine B concentration, a series of bleaching pulses were delivered to the running buffer at F1 as it flowed through the capillary. Signal was determined by measuring the difference between the fluorescence signal at each rhodamine B concentration with the shutter closed and the minimum value of the photobleached zone (negative peak) detected at F2. The LOD was defined as the concentration at which the signal was 3 times greater than the rms fluctuation of the fluorescence signal from unbleached rhodamine B. Conditions for the LOD study at 457.9 nm were based on the experimental conditions previously published.[86] The conditions for excitation at 457.9 nm were: bleaching power = 56 mW; detection power = 23 mW; bleaching pulse duration = 250 ms; applied potential = 188 V/cm; data acquisition and filtering rates = 100 Hz/50 Hz, respectively; capillary length = 80 cm; length to detector = 70 cm. For excitation at 514.5 nm conditions were: bleaching power = 230 mW; detection power = 13 mW; bleaching pulse duration = 75 ms; applied potential = 138 V/cm; data acquisition and filtering rates = 150 Hz/50 Hz, respectively; capillary length = 80 cm; length to detector = 70 cm.

Bleaching Pulse Power and Duration Studies

The percentage of rhodamine B photobleached as a function of laser power was studied by exposing the fluorophore in the running buffer to 75-ms bleaching pulses. Experimental conditions were as follows: applied potential = 250 V/cm; running buffer = 50 mM borate buffer (pH = 9.0) containing 40 nM rhodamine B; flow rate = 0.200 cm/s; bleaching power = 29 - 232 mW; detection power = 14 mW; $d_{F1-F2} = 1.32 \pm 0.01$ mm; capillary length = 80 cm; length to detector = 70 cm; data acquisition and filtering rates = 150 Hz/50 Hz, respectively. The capillary was filled with blank borate buffer prior to each run and the fluorescence background in the absence of rhodamine B was measured. The baseline fluorescence signal was then determined by measuring the fluorescence due to the rhodamine B present in the running buffer with no photobleaching taking place (shutter closed). Then the computer-controlled shutter was allowed to open, exposing the rhodamine B in the running buffer to the bleaching beam. After the photobleaching event occurred at F1, the photobleached zone was detected as a negative peak at F2. The decrease in fluorescence due to photobleaching was measured at the minimum of the photobleached zone. The blank signal was subtracted from both the baseline fluorescence signal and the minimum value for the photobleached zone. The percentage of rhodamine B photobleached was determined by dividing the minimum value of the photobleached zone by the baseline fluorescence signal. Measurements were made for a series of 10 consecutive bleaching pulses (n = 10).

The effect of the bleaching pulse duration at F1 on the percent photobleaching observed at F2 was studied by varying the length of the bleaching pulse from 10 to 300 ms. Experimental conditions were as follows: bleaching power = 230 mW; detection power = 20 mW; running buffer = 50 mM borate buffer (pH = 9.0) containing 40 nM rhodamine B; applied potential = 188 V/cm; flow rate = 0.119 cm/s; $d_{F1-F2} = 0.709 \pm 0.001$ mm. The data were filtered at a rate 3 times $(\text{pulse width})^{-1}$ and acquired at 10 times $(\text{pulse width})^{-1}$ (e.g. 10 Hz filtering and 33 Hz acquisition for a 300 ms pulse).

Characterization of The Photobleached Region as a Function of Flow Rate and Bleaching Pulse Duration

The capillary was filled with 50 mM borate buffer (pH = 9.0) containing 40 nM rhodamine B. The effect of flow rate on the photobleached region was examined using 75-ms bleaching pulses. The laser power was adjusted so that the bleaching power at F1 was 250 mW and the detection power at F2 was 12 mW. Data were filtered at 50 Hz and acquired at 150 Hz. The applied potential field was varied between 62.5 and 250 V/cm. The effect of bleaching pulse duration was examined by varying the duration of the bleaching pulses delivered at position F1 from 10 to 500 ms at each applied potential. Delay times between bleaching pulses were selected so that the negative peak observed at position F2 did not overlap with the start of the next bleaching pulse. The separation between F1 and F2 was $d_{F1-F2} = 0.635$ mm.

Rhodamine B Neutrality Study

In order to confirm the neutrality of rhodamine B, samples of rhodamine B were coinjected electrokinetically with either mesityl oxide or DMSO (neutral markers) for 3 s at a potential of 235 V/cm and detected by absorbance. Replicate injections were conducted in both 50 mM borate buffer (pH = 9.0) and 50 mM bicarbonate buffer (pH = 8.35). The detection wavelength was 220 nm. The capillary used for these experiments was 85.0 cm long and 40.0 cm to the detector. All separations were carried out at 235 V/cm.

Phenolic Acid Separation

The UV/VIS absorbance detector was placed 40.0 cm from the injection end of the 85.0-cm capillary. The EOF monitoring instrument was located 75.0 cm from the injection end, after the absorbance detector. A solution containing syringic acid, 4-hydroxy-3-methoxybenzoic acid, p-hydroxycinnamic acid, 3,4-dihydroxybenzoic acid, 3,4-dihydroxycinnamic acid, and gallic acid was prepared in 1 + 1 (v + v) methanol/water. The capillary was first flushed with a 2.0 min electrokinetic injection (290 V/cm) of 0.1 M NaOH. The capillary was next flushed electrophoretically with 50 mM sodium bicarbonate buffer (pH = 8.35) for 1 hr.[122] The buffer was then replaced with 50 mM sodium bicarbonate buffer (pH = 8.35) containing 400 nM rhodamine B and was allowed to flush electrophoretically for 30 min prior to any sample injections. A single 3.0-s electrokinetic injection of the phenolic acid mixture was then made at an applied potential of 290 V/cm. The separation potential was 290 V/cm. EOF data were filtered at 300 Hz and acquired at 900 Hz.

Results and Discussion

Our initial report of the photobleaching method for EOF monitoring demonstrated EOF measurement every 5.00 s throughout the course of a CE separation with a precision of 0.7% or better.[86] A neutral fluorophore is added to the running buffer at nanomolar concentrations. A computer-controlled shutter is opened briefly (10-500 ms in the work presented here), and a focused laser beam passes through the shutter, irradiating the dye-filled capillary at position F1 as indicated in Figure 2-1. This creates a photobleached zone at F1, which flows to position F2 where it is detected by LIF as a negative peak. The measured flow rate is:

$$flow\ rate = \frac{d_{F1-F2}}{\Delta t_{F1-F2}} \tag{2-2}$$

where d_{F1-F2} is the distance between positions F1 and F2 on the capillary and Δt_{F1-F2} is the time required for the photobleached zone to migrate from F1 to F2. When the shutter is opened, a positive peak is observed at the LIF detector (F2) due to light from the bleaching beam at F1 that is delivered to the PMT by an optical fiber (Figure 2-1A). This

positive peak serves as a time stamp, indicating the time at which the shutter was opened and the photobleached zone was created at F1.[86]

Fluorophore Concentration

The effect of the wavelength of light used for photobleaching and LIF detection was examined in order to decrease the concentration of neutral fluorophore required in the running buffer for EOF monitoring. Rhodamine B has been used as a neutral fluorophore here and in our previous work.[86] The excitation maximum for rhodamine B in 50 mM borate buffer at pH 9.0 is 552 nm. In our previous work, an irradiation wavelength of 457.9 nm was used.[86] The excitation spectrum of rhodamine B in borate buffer suggests that lower dye concentrations could be used with excitation by the 488.0 or 514.5-nm line from the Ar^+ laser used in this work. The absorbance of rhodamine B is 4 times greater at 488.0 nm and 10 times greater at 514.5 nm relative to 457.9 nm.

We compared the minimum rhodamine B concentrations required to monitor EOF using irradiation at 457.9 nm and 514.5 nm based on a S/N of 3. The minimum concentration for irradiation at 457.9 nm was 60 nM, and the minimum concentration at 514.5 nm was 7 nM. This improvement is expected based on the fluorescence excitation spectrum for rhodamine B. Differences in the bleaching power, pulse width and EOF rates between the experiments at 457.9 nm and 514.5 nm will also impact the detection limits obtained as discussed in the following sections. It is important to use low concentrations of neutral fluorescent buffer additive to minimize interference by the EOF monitoring method with a concurrent method of analyte detection such as UV/VIS absorbance. In our previous work, the concentration of rhodamine B was typically 400 nM.[86] Irradiation at 514.5 nm was used for all other experiments presented here.

Distance Between F1 and F2

As $d_{F1\text{-}F2}$ is decreased, the frequency at which the flow rate can be measured is increased. We have reduced $d_{F1\text{-}F2}$ to 0.635 mm, about an order of magnitude lower than in our previous work.[86] By decreasing $d_{F1\text{-}F2}$, the amount of time necessary for the photobleached zone created at F1 to reach the LIF detector at position F2 is reduced for a given flow rate. Previously, EOF was measured at a rate of 0.20 Hz ($d_{F1\text{-}F2}$ = 6.13 mm).[86] In the work presented here, we have measured EOF at frequencies of 0.7-1.0 Hz ($d_{F1\text{-}F2}$ = 0.635-1.33 mm). As examined in this paper, when $d_{F1\text{-}F2}$ is decreased, it becomes necessary to use shorter bleaching pulses and faster data acquisition in order to maintain the dynamic range and precision of EOF measurements obtained at greater values of $d_{F1\text{-}F2}$.

Rhodamine B Photobleaching

Figure 2-2 shows a plot of the percentage of rhodamine B photobleaching observed at F2 as the power of the bleaching pulses delivered at F1 is increased. The percentage of rhodamine B photobleached was determined by measuring the minimum

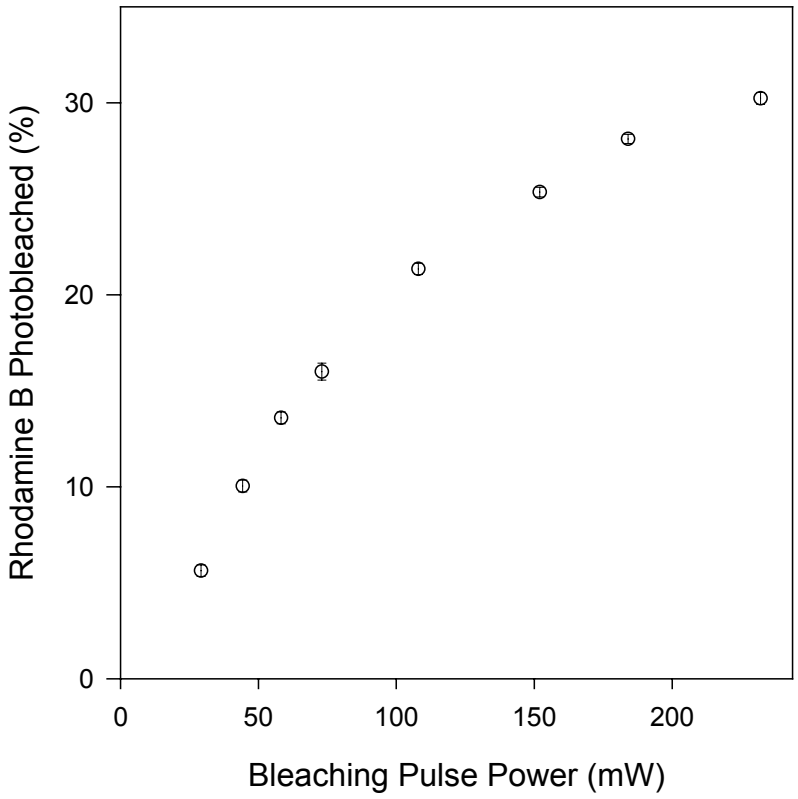

Figure 2-2. Percent rhodamine B photobleached as detected at F2 vs. bleaching power at F1. Bleaching pulses (75 ms) were delivered to 40 nM rhodamine B in 50 mM borate buffer (pH = 9.0). (Flow rate = 0.200 cm/s; $d_{F1\text{-}F2}$ = 1.32 mm). Error bars are ± 1 SD.

fluorescence for the negative photobleached peak observed at F2 and dividing this value by the total fluorescence observed in the absence of bleaching (shutter closed). As expected, the percentage of rhodamine B photobleached increases with increasing laser power at F1.[78,79,106,109] As the power of the bleaching pulses increases, the percentage of rhodamine B photobleached begins to reach a plateau. The primary pathway for the photodegredation of rhodamine dyes is believed to take place from the excited triplet state.[79,114,123-125] The low quantum yield for formation of the excited triplet state of rhodamine B reduces the likelihood of complete photobleaching during a 75-ms exposure.[79,116,123]

Maximum photostability from a fluorophore is desired for sensitive LIF detection.[78,79] However, for flow monitoring based on photobleaching of a fluorophore[77,86] or optically gated injection of samples for CE,[106,109] it is desirable to use a fluorophore that is easily photobleached. Rhodamine B is photostable relative to many fluorescent dyes. For example, rhodamine B has a bleaching quantum efficiency of 0.5 x 10^{12} molecules photobleached W^{-1} s^{-1} cm^{-3}, which is 15 times smaller than that for fluorescein (7.4 x 10^{12} molecules photobleached W^{-1} s^{-1} cm^{-3}).[117] Fluorescein was not used in this work because it is a charged species at the pH's used in these experiments. Due to the photostability of rhodamine B, high laser powers were used in this work in order to achieve adequate photobleaching of rhodamine B.

Figure 2-3 shows a plot of the percentage of rhodamine B photobleached as a function of the bleaching pulse duration. As expected, the percentage of rhodamine B photobleached increases as the duration of the bleaching pulse is increased.[77-79,109] When short bleaching pulses are applied, the percentage of rhodamine B photobleached (observed at F2) is determined by the total duration of exposure to the bleaching beam as well as diffusional broadening of the photobleached zone as it travels from position F1 to F2. As the bleaching pulse duration is increased, the amount of time that the fluorophore is exposed to the bleaching beam is lengthened, increasing the percentage of rhodamine B photobleached. Also, as the width of the bleached zone increases, the effect of diffusional broadening on the depth of the negative peak observed at F2 is reduced.

The plateau observed in the photobleaching efficiency of rhodamine B as a function of bleaching pulse duration occurs when two criteria are met: 1) the volume of flow during the time that the shutter is open exceeds the volume irradiated by the bleaching beam, and 2) the attenuation of the photobleached peak minimum due to diffusional broadening is negligible. Both of these criteria are flow rate dependent. As the flow rate increases, the volume flowing past F1 during a given period of time that the shutter is open will increase. This will decrease the bleaching pulse duration at which the percent photobleaching reaches a plateau. The effect of diffusional broadening will be reduced at higher flow rates, again reducing the bleaching pulse width at which a plateau is reached. The flow rate was 0.119 ± 0.001 cm/s (Δt_{F1-F2} = 0.595 ± 0.002 s) for the data in Figure 2-3, and the percent rhodamine B photobleached reaches 90% of it's maximum value at ~100 ms. As the flow rate decreases (at constant bleaching power and pulse duration), the percentage of rhodamine B photobleached will increase due to an increase in the amount of time that the fluorophore is exposed to the bleaching beam.[77-79,109]

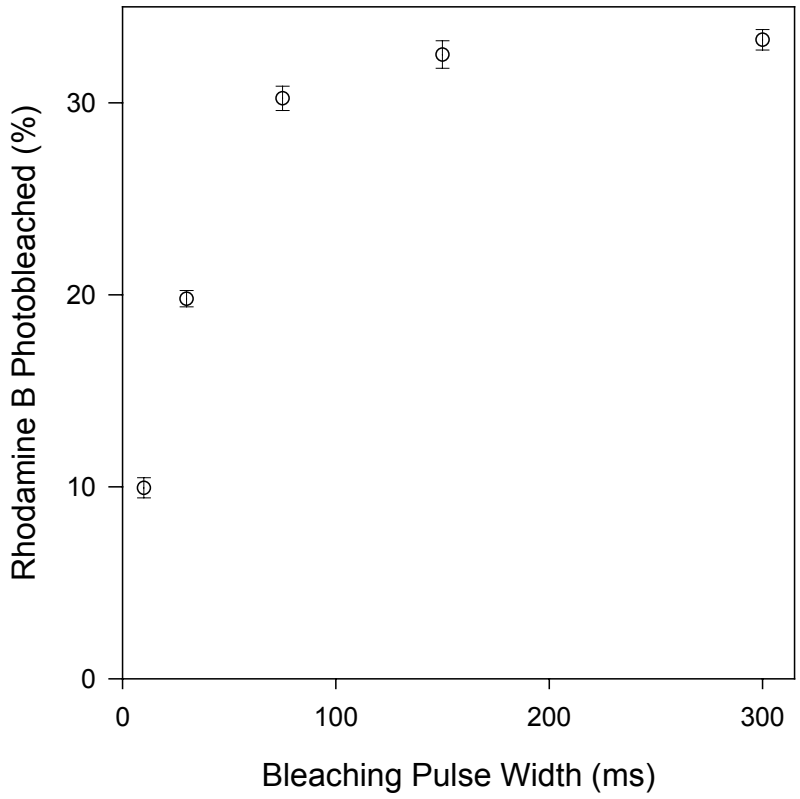

Figure 2-3. Percent rhodamine B photobleached as detected at F2 vs. bleaching pulse duration (F1) for bleaching pulses delivered to 40 nM rhodamine B in 50 mM borate buffer (pH = 9.0). (Bleaching power = 230 mW; flow rate = 0.119 cm/s; $d_{F1\text{-}F2}$ = 0.709 mm). Error bars are ± 1 SD.

Effect of Bleaching Pulse Duration on Photobleached Zone Width

A series of 10 to 500-ms bleaching pulses were delivered to a dye-filled capillary (40 nM rhodamine B) at flow rates ranging from 0.0317 to 0.160 cm/s. These experiments were performed in order to observe the effects of flow rate and bleaching pulse duration on the photobleached zone as observed at F2. Data from this study are presented in Table 2-1 and Figure 2-4. As expected, the width of the photobleached zone increases as the duration of the bleaching pulse is increased.

Figure 2-4 illustrates what is observed at the extremes of bleaching pulse duration and flow rate used in this study. At a flow rate of 0.158 cm/s and $d_{F1\text{-}F2}$ of 0.635 mm, $\Delta t_{F1\text{-}F2}$ is 402 ± 4 ms, and the application of a 500-ms bleaching pulse is not completed before the leading edge of the photobleached zone reaches the LIF detector at F2 (Figure 2-4a). Under identical conditions, a 10-ms bleaching pulse is well resolved from the photobleached zone (Figure 2-4b). Figure 2-4c shows the results for a 500-ms bleaching pulse at a flow rate of 0.0327 cm/s. Since $\Delta t_{F1\text{-}F2}$ is 1.94 ± 0.01 s, the photobleached zone is well resolved from the bleaching pulse. However, the photobleached zone for a 10-ms bleaching pulse (Figure 2-4d) is barely perceptible due to diffusional broadening over 1.94 s. Table 2-1 includes an estimated dynamic range for flow measurements calculated for different bleaching pulse durations, a pulse repetition rate of 1 Hz and $d_{F1\text{-}F2}$ of 0.635 mm. In our previous work, a 250-ms pulse length was used with $d_{F1\text{-}F2}$ of 6.13 mm, resulting in a dynamic range for flow measurements of 0.10 to 2.4 cm/s.[86] Ideally, the distance between F1 and F2 would be as short as possible and the duration of the bleaching pulse would be infinitely short, thus allowing the rate at which EOF is monitored to be increased beyond 1 Hz with unlimited dynamic range.

Extremely narrow pulses provide the best dynamic range; however, the data in Figures 2-3 and 2-4 illustrate that narrower bleaching pulses also result in decreased S/N for detection of the photobleached zone at F2 due to decreased bleaching and increased effects of diffusional broadening on the photobleached zone. Selection of a bleaching pulse width for an experiment is necessarily a compromise between pulse width and the minimum dye concentration required for adequate S/N. This compromise should include consideration of the desired measurement frequency and the range of flow rates expected for the experiment.

Inspection of the electropherograms from these experiments reveals an unexpected but reproducible feature that was unnoticed in earlier work.[86] This feature can be seen in Figure 2-4 and is shown more clearly in Figure 2-5. In Figure 2-5a, a positive peak precedes and overlaps with the negative peak created by a 200-ms bleaching pulse (50 mM borate buffer; pH = 9.0 with 40 nM rhodamine B). The same phenomenon is shown in Figure 2-5b for a 75-ms bleaching pulse (50 mM sodium bicarbonate buffer; pH = 8.35 with 400 nM rhodamine B), but diffusional broadening has obscured the stepped structure that is apparent in Figure 2-5a. As discussed below the cause of this positive peak is not understood, but it is reproducible, and it is observed in nearly every experiment.

Table 2-1. Photobleached zone width at fwhm for different values of EOF and bleaching pulse durations.[a]

Bleaching Pulse Duration (ms)	Photobleached Zone Width (ms) as a Function of EOF			Estimated Dynamic Range (1 Hz)[b]
	0.160 cm/s	0.113 cm/s	0.0317 cm/s	
10	34.9 ± 2.5	59.8 ± 4.5	---[c]	0.066 – 2.8 cm/s
30	47.5 ± 1.3	58.2 ± 2.1	276 ± 15	0.067 – 1.6 cm/s
100	96.0 ± 2.0	97.7 ± 2.3	291 ± 8	0.070 – 0.65 cm/s
200	204 ± 2	200 ± 3	353 ± 12	0.080 – 0.31 cm/s
500	---[d]	517 ± 3	518 ± 12	---[d]

[a] Bleaching pulse duration at F1 and photobleached zone width (fwhm) at F2 were determined for a $d_{F1\text{-}F2}$ of 0.635 mm with 40 nM rhodamine B in 50 mM borate buffer (pH = 9.0) with bleaching pulse and detection laser powers of 250 and 12 mW, respectively. Applied potentials were 250 V/cm, 187.5 V/cm, and 62.5 V/cm with average EOF rates of 0.160 cm/s, 0.113 cm/s and 0.0317 cm/s, respectively. (n = 10 consecutive bleaching pulses)

[b] Values for the estimated dynamic range were calculated for an EOF sampling rate of 1 Hz.

[c] A photobleached zone width could not be calculated due to poor S/N.

[d] A photobleached zone width could not be calculated due to overlap of the bleaching pulse and the photobleached zone.

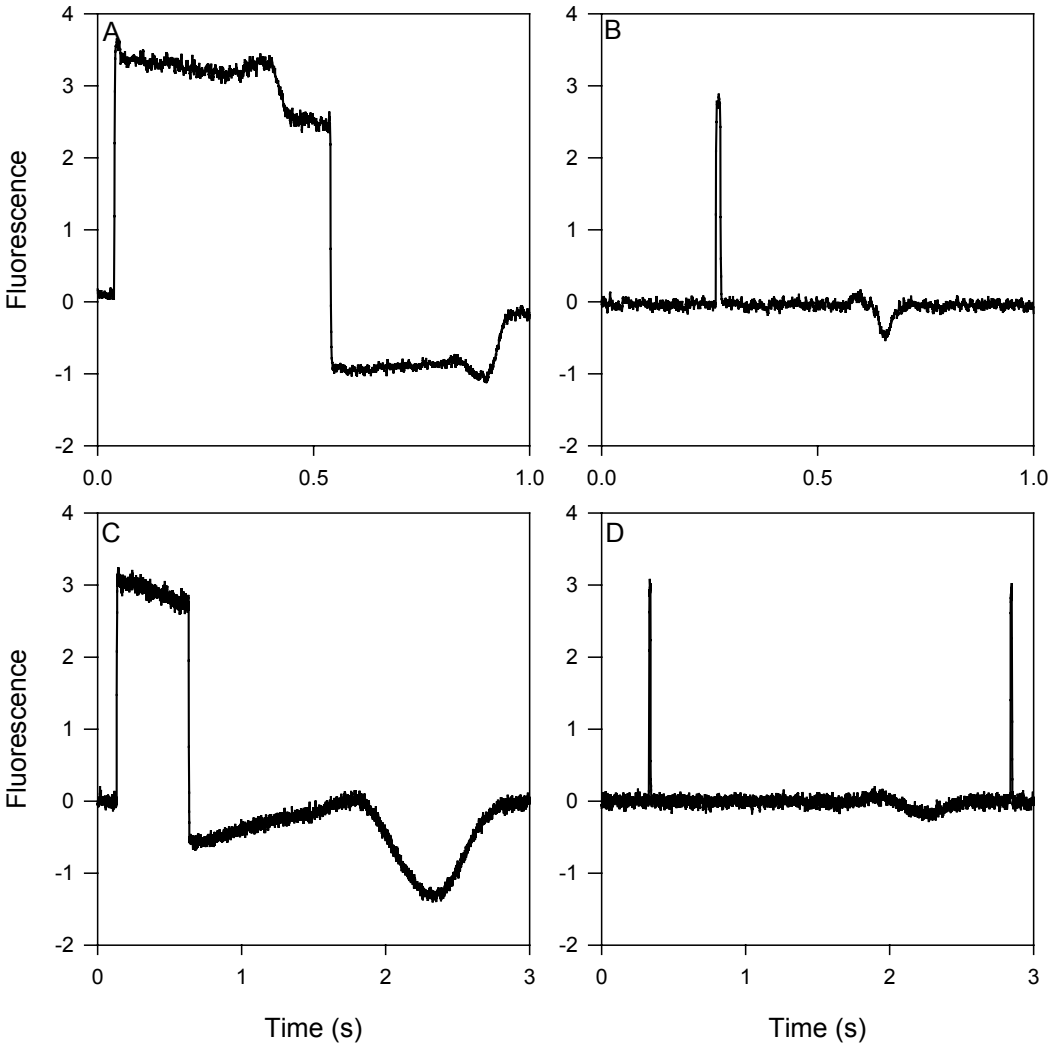

Figure 2-4. Electropherograms showing a bleaching pulse (positive peak) and the resulting decrease in fluorescence intensity (negative peak). (A) 500-ms bleaching pulse at a flow rate of 0.158 cm/s. (B) 10-ms bleaching pulse at a flow rate of 0.158 cm/s. (C) 500-ms bleaching pulse at a flow rate of 0.0327 cm/s. (D) 10-ms bleaching pulse at a flow rate of 0.0327 cm/s. The second positive peak observed (D) is the beginning of the next EOF measurement. Experimental conditions are as listed in Table 2-1.

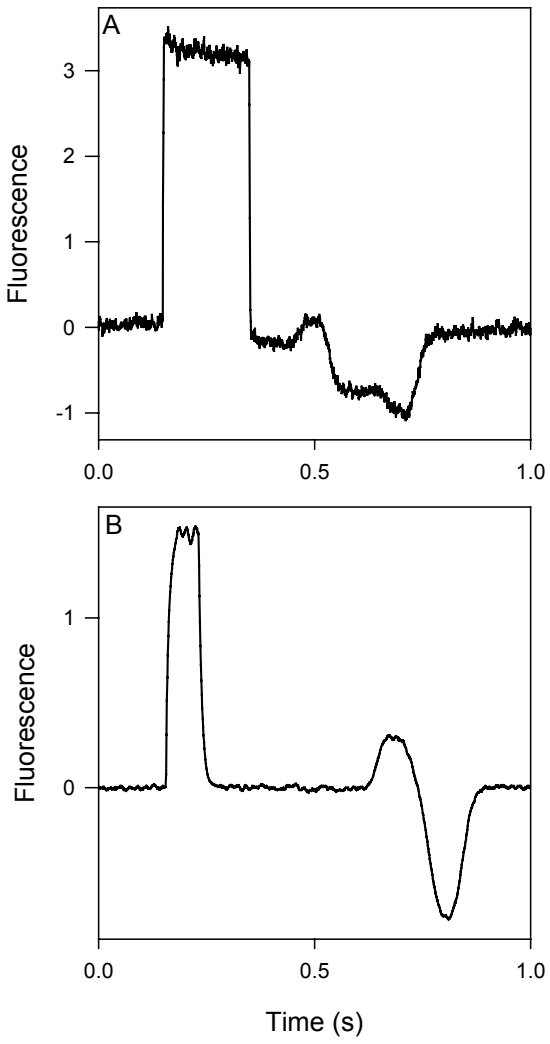

Figure 2-5. Examples of photobleaching sequences with a positive peak overlapping with the photobleached zone. (A) Conditions are the same as those for Table 2-1. (Bleaching pulse duration = 200 ms; flow rate = 0.160 cm/s). (B) Capillary filled with 400 nM rhodamine B in 50 mM sodium bicarbonate buffer (pH = 8.35). (Bleaching power = 245 mW; detection power = 13 mW; flow rate = 0.211 cm/s, $d_{F1\text{-}F2}$ = 1.29 mm, Bleaching pulse duration = 75 ms).

One hypothesis to explain these observations is that the positive peak is caused by changes in the refractive index of the solution due to heating during application of the photobleaching pulse.[84] This hypothesis requires rhodamine B to have a partial negative charge so that the photobleached zone separates from the heated solution zone as it travels from F1 to F2. We carefully reexamined the neutrality of rhodamine B to test this hypothesis, but these experiments give no indication that rhodamine B is negatively charged.

Other hypotheses have been considered but not tested experimentally. Rhodamine B fluorescence has been shown to decrease with increasing temperature in water, but this would lead to an effect opposite to our observations.[126] Several forms of rhodamine B are known to exist in aqueous solution, (neutral zwitterions, neutral lactones, cations and dimers), and the zwitterion is the expected form for the conditions used in this work.[126-131] A highly fluorescent cationic species would be consistent with our observations, but the cationic form of rhodamine B is present only at acidic pH's (pKa = 3.1), and should be less fluorescent than the zwitterion with irradiation at 514 nm.[128,130,131]

The presence of this positive peak does not preclude making flow measurements using our method, but it must be considered when analyzing the data generated by this technique. In previous work, $\Delta t_{F1\text{-}F2}$ was measured from the half-maximum of the leading edge of the positive peak to the half-maximum of the leading edge of the negative peaks due to the photobleached zone.[86] The positive peak, overlapping with the photobleached zone will shift the apparent half-maximum of the leading edge of the negative peak and could shift the trailing edge of the negative peak depending on the extent of overlap. The calibration method used for our EOF measurements (EOF Monitoring Instrument in the Experimental section and in our previous publication)[86] will yield the same EOF rate regardless of whether the measurement is based on the leading or trailing edge of the peak. The only difference will be the calculated value for $d_{F1\text{-}F2}$. However, the precision of EOF measurement may differ depending on whether the leading or trailing edge is used for measurement. All data reported in this paper use the trailing edge for EOF measurement.

EOF Measurement Precision

In our previous work, the precision of our EOF measurements ranged from 0.2% to 0.7%.[86] For the data presented in this paper, the measured EOF precision ranges from 0.2% to 1.8%. The lower values for EOF measurement precision indicate that precision has not been sacrificed substantially by decreasing $d_{F1\text{-}F2}$, decreasing $\Delta t_{F1\text{-}F2}$ and increasing the measurement frequency. It is useful to consider the factors that affect EOF measurement precision using our method.

The first limitation to EOF measurement precision that must be considered is real fluctuations in EOF that occur on the time scale of our measurements. What this technique does is to repeatedly measure the EOF rate averaged over $\Delta t_{F1\text{-}F2}$ as the photobleached zone travels from F1 to F2. Values for $\Delta t_{F1\text{-}F2}$ in this work range from

0.393 to 1.94 s. For a value of Δt_{F1-F2} of 393 ms, measured with a precision of 0.5%, the standard deviation of Δt_{F1-F2} will be only 2.0 ms. It is not easy to determine whether the measurement precision is limited by the technique or if it is limited by real fluctuations of EOF on the time scale of the measurement.

One factor that could lead to fluctuations in flow is variability in the voltage output from the electrophoresis power supply. The specifications for the power supply used in this work indicate an output noise of 0.1% peak-to-peak. This value is small relative to the observed precision of measured EOF. Current measurements during our experiments also indicate an RC time constant for the electrophoretic circuit on the order of 2 s.[132] Data presented later in this manuscript indicate that in some cases real fluctuations in EOF are determining the apparent measurement precision; however, it is unlikely that these are the result of fluctuations of the applied potential.

The time required for the shutter to close will impact the measurement precision. We measured the closing time of the shutter by directly observing the light from the bleaching beam detected at the PMT as indicated in Figure 2-1. The shutter required 4 ± 1 ms to close (n = 14). The contribution of a 1-ms variation in the shutter opening to Δt_{F1-F2} measurement error is less than 0.3% for Δt_{F1-F2} = 0.393 s and 0.05% for Δt_{F1-F2} = 1.94 s.

Precision of EOF rate measurement is also affected by the rate at which the data are filtered and acquired. The data presented in Table 2-1 were filtered at 500 Hz and acquired at 1500 Hz. The contribution of the data filtering and acquisition rates is similar in magnitude to that of the shutter transfer time. As the data acquisition rate is increased, the possible precision of EOF measurements increases. Ideally, data would be acquired from all data channels at the maximum rate possible. However, the amount of data generated by acquiring multiple data channels at a high acquisition rate can be prohibitive. For example, a text file containing data acquired from 3 channels at 1500 Hz for 10 min is 17 MB in size. A compromise must be made between data acquisition rate and total acquisition time due to practical limitations of current computer resources.

The S/N for the photobleached zones detected will also impact the EOF measurement precision. If the S/N is too low, imprecise measured flow values will result. If S/N limits EOF measurement precision, this can be addressed by increasing the neutral dye concentration, increasing the bleaching power, or increasing fluorescence detection sensitivity.

The S/N for the photobleached zones is also affected by the EOF rate. As shown in Figure 2-6, for a bleaching pulse of 75-ms, the S/N increases with increasing flow rate until a peak S/N value is reached near 0.1 cm/s. The S/N then decreases as the flow rate rises above 0.1 cm/s. As the flow rate drops below 0.1 cm/s, diffusion of the photobleached zone begins to decrease the S/N due to broadening of the photobleached zone prior to its detection at F2. As the flow rate increases above 0.1 cm/s, the percentage of rhodamine B photobleached decreases, and the S/N decreases accordingly. The decrease in S/N is due to a decrease in the effective exposure time of the rhodamine

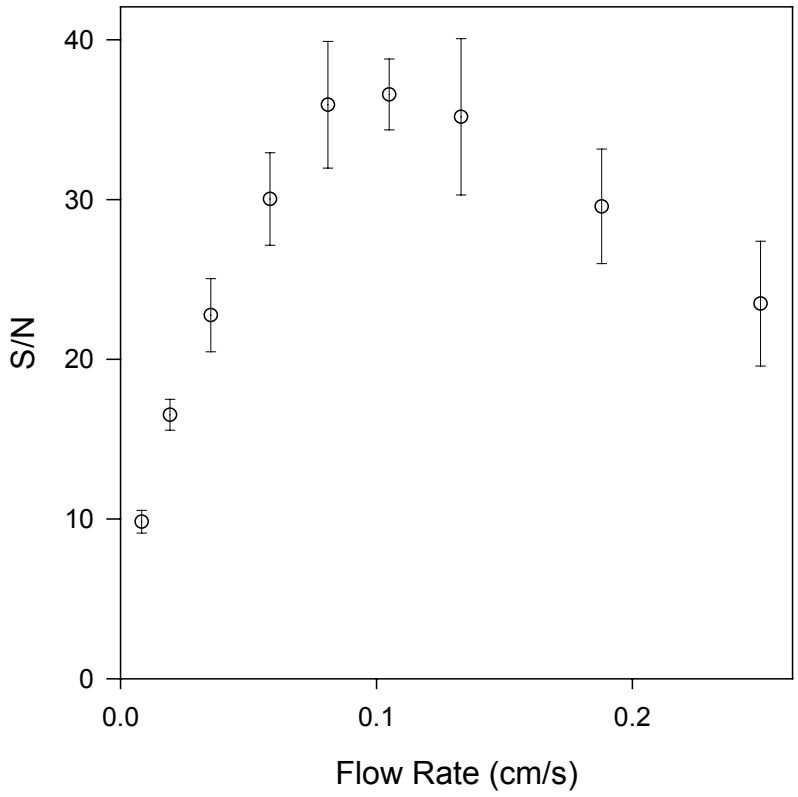

Figure 2-6. S/N vs. flow rate for the detection of photobleached zones with a 75-ms bleaching pulse. All experiments were conducted with 40 nM rhodamine B in 50 mM borate buffer (pH = 9.0). (Bleaching power = 250 mW; detection power = 12 mW; d_{F1-F2} = 0.747 mm; data acquisition and filtering frequencies = 150 Hz/40 Hz, respectively). Error bars are ± 1 SD.

B to the bleaching beam at F1 as the flow rate increases.[77,78,109] This is further supported by the data in Figure 2-3.

The frequency at which the data is filtered and acquired will also affect the S/N. S/N can be improved by decreasing the frequency at which the input signal is filtered and acquired. However, as mentioned earlier in this section, the precision of the EOF measurement will be sacrificed.

Application of EOF Monitoring to a Separation with Absorbance Detection

One of the most common methods of detection used for CE is UV/VIS absorbance.[133] In order to demonstrate that our method of monitoring EOF does not interfere with concurrent methods of detection, a UV/VIS absorbance detector was used for analyte detection with EOF monitoring for a separation of six phenolic acids.[122] The UV/VIS absorbance detector was placed before the EOF detector (closer to the injection end) on the capillary. Bleaching pulses of 75-ms were used to measure EOF every 1.08 s. Data were filtered at 300 Hz and acquired at 900 Hz. In order to ensure a high S/N for flow measurements, the concentration of rhodamine B added to the CE running buffer was 400 nM. The separation and detection conditions (detection wavelength = 210 nm) were based on a published separation of phenolic acids by Cartoni and coworkers.[122]

Figure 2-7a shows the elution of the phenolic acids as well as a peak from the methanol/water mixture as detected at the UV/VIS detector 40.0 cm from the injection end of the capillary. Figure 2-7b shows a plot of EOF rate values as measured 80.0 cm from the injection end of the capillary. The separation was also carried out on the same instrument using only UV/VIS detection without Rhodamine B added to the running buffer (data not shown). The separation and baseline obtained with the rhodamine B present in the running buffer is indistinguishable from the control experiment without rhodamine B, and our results are almost identical to the published separation.[122] Clearly, monitoring EOF using our method is not influencing the separation and analyte detection by UV/VIS absorbance.

The average EOF rate over the entire experiment was determined to be 0.211 cm/s as measured with the methanol/water neutral peak at 202 s. When the flow rates measured by our EOF monitoring technique over the course of the separation are plotted (Figure 2-7b), it can be seen that the flow actually fluctuates between 0.200 to 0.222 cm/s with an average flow rate of 0.211 ± 0.003 cm/s (RSD = 1.6%; n = 482) measured over 545 s. The overall average flow rate measured by our technique until the neutral marker elutes past the UV/Vis absorbance detector at 202 s is 0.211 ± 0.002 cm/s. From 203 s to 556 s, our technique measures a flow rate of 0.211 ± 0.003 cm/s. In this case, the overall flow rate is indistinguishable before and after the neutral marker elutes past the UV/Vis absorbance detector. However, in cases where the EOF is less stable over long periods of time, only our method is capable of observing a difference.

In order to determine whether fluctuations in EOF were due to instabilities in the EOF from interactions between the sample and the capillary, EOF was monitored for approximately 20 s when no sample had been injected into the capillary. A precision of

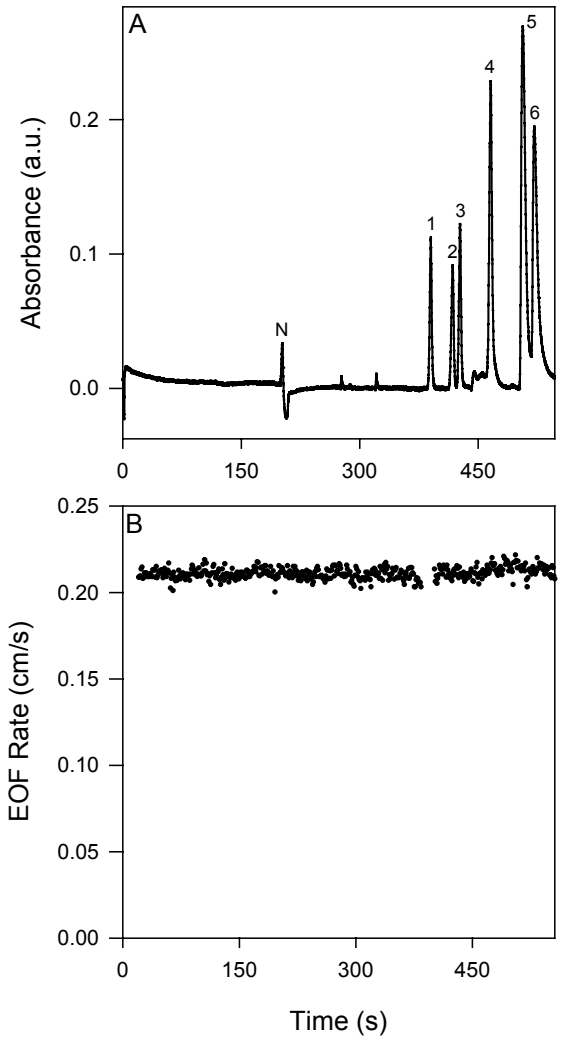

Figure 2-7. Separation of phenolic acids with simultaneous EOF monitoring. (A) Electropherogram of a separation of 6 phenolic acids (detection λ = 210 nm). Peaks are identified as (N) methanol/water, (1) syringic acid (380 μM), (2) p-hydroxycinnamic acid (490 μM), (3) 4-hydroxy-3-methoxybenzoic acid (410 μM), (4) 3,4-dihydroxycinnamic acid (1.5 mM), (5) 3,4-dihydroxybenzoic acid (1.4 mM) and (6) gallic acid (3.0 mM). (B) EOF rate vs. time for EOF monitoring performed during the phenolic acid separation. The capillary was filled with 400 nM rhodamine B in 50 mM sodium bicarbonate buffer (pH = 8.35). The sample was electrokinetically injected for 3.0 s at an applied potential of 290 V/cm. (Bleaching power = 245 mW; detection power = 13 mW; bleaching pulse duration = 75 ms; average flow rate = 0.211 cm/s; $d_{F1\text{-}F2}$ = 1.29 mm).

1.0% (n = 19 consecutive bleaching pulses) was observed for the EOF without sample injection. This precision measured in the absence of sample indicates that the 1.6% precision in EOF observed during the separation of the phenolic acids is affected by the presence of the sample. The nature of these fluctuations due to sample injection is not yet understood and is under investigation.

Acknowledgments

The authors would like to thank Joseph Batts for his contributions to this work. This research was supported by startup funds from the University of Tennessee. K. F. S. was supported by the National Science Foundation RSEC Program at UT (9974734).

CHAPTER III

Experimental Studies of Electroosmotic Flow Dynamics in Microfabricated Devices During Current Monitoring Experiments

This chapter is a slightly revised version of a paper by the same title accepted for publication in the journal *Analytical Chemistry* in 2003 by Jason L. Pittman, Charles S. Henry and S. Douglass Gilman:

Pittman, J. L.; Henry, C. S.; Gilman, S. D. *Anal. Chem.* **2003,** *Accepted for Publication.*

Abstract

Electroosmotic flow was monitored in glass microfluidic devices at rates up to 2 Hz with a precision of 0.2 – 1.0% using a technique based on the periodic photobleaching of a dilute, neutral fluorophore added to the running buffer. This EOF monitoring method was used to examine the performance of the current monitoring technique for measuring an average electroosmotic flow in a microfluidic device with a cross-T design. Flow measurements made with the current monitoring method gave a precision of 0.4 – 2.2%, but the periodic photobleaching method shows that the current monitoring technique causes changes in EOF as high as 41% during a single experiment. The periodic photobleaching method for EOF monitoring was also used to study EOF in channels on opposite sides of a cross-channel intersection. The opposite channels were shown to exhibit substantially different EOF dynamics during a current monitoring experiment as well as different steady state EOF rates during normal operating conditions.

Introduction

The manipulation of fluids in microfabricated channels by applied potential fields has been an active area of investigation since the introduction of microfabricated devices for electrokinetic analysis in the early 1990's.[13,14,18,61-64,66,67,69-71,88,89,95-97,101,134-144] Electroosmotic flow (EOF) provides an easily scalable method for manipulating small quantities of fluids in microfabricated devices in a controlled manner with a well defined flow profile. The adsorption of analyte molecules onto the surface of the microfluidic channel or a change in the composition, pH, ionic strength or temperature of the solutions filling the channels will alter EOF during an experiment. Changes in EOF that occur during an experiment in a capillary or in a microfluidic channel decrease the reproducibility of peak retention times and the precision of analyte quantitation. In complex microfluidic systems where there are multiple channels that intersect and multiple solutions filling these channels, unexpected or uncontrolled changes in EOF can result in the failure of the analytical method. It is important to measure and understand

flow dynamics in microfluidic devices so that the full potential of these devices may be realized.[13,14,18,63,88,89,96,97,101,134,136,140,142]

Fluorescence imaging techniques have been used to examine flow dynamics in microfluidic devices.[88,89,95-97,101,134] These fluorescence imaging methods have been used to visualize the effects of injection schemes, channel coatings, microfabrication methods, and materials on the electrokinetic transport of fluids through microfluidic channels. The shape of electroosmotic and hydrodynamic flow profiles have been described by fluorescence imaging using caged fluorescent dyes in microfluidic channels.[96] Fluorescence imaging has also been used to observe the path of fluorescent solutions through microfabricated devices.[88,89,95,97,101,134] In most cases, fluorescence imaging has been used to acquire qualitative data about flow in microfluidic devices.

The most common method used for quantitative studies of EOF in microfabricated devices has been the current monitoring method.[61-64,66,67,70,71,96,139] Originally developed for use in capillaries,[58] the experimental simplicity of the current monitoring method allows it to be easily adapted to measure average EOF in glass or polymer microfluidic devices. In this method, the buffer filling the microfluidic device is electrophoretically replaced by a buffer of different concentration. As the channel is filled with the different concentration buffer, the current through the microfabricated device changes until a new, constant current is reached. The time required for the changing current to stabilize at the new current is used to calculate the average EOF in the channel using $EOF = L/t$, where L is the total length of the microfabricated channel and t is the time required for the current to reach the new value. A modified version of the current monitoring method used a microfabricated conductivity detector to detect the change in conductivity as one buffer was replaced by a more dilute buffer.[69] The neutral marker method has also been used in microfabrciated devices.[97,145] Current monitoring and the neutral marker method are limited to providing a single, average EOF value on the time scale of the flow through the length of a microfluidic channel.

In this paper, we demonstrate monitoring of EOF in microfluidic devices using periodic photobleaching of a dilute, neutral fluorophore added to the running buffer filling the microfluidic channel.[86,146] Flow monitoring has also been used to determine if the current monitoring method causes significant changes in EOF in a microfabricated channel. EOF dynamics have been studied in channels on opposing sides of a cross-channel intersection during current monitoring experiments.

Experimental Section

Chemicals

Laser grade coumarin 334 and rhodamine B were obtained from Acrōs Organics (Pittsburgh, PA). Sulfuric acid, sodium hydroxide, hydrogen peroxide and 2-propanol were purchased from Fisher Scientific (Fair Lawn, NJ). Boric acid was obtained from

Mallinckrodt (Phillipsburg, NJ), and methanol was purchased from Aldrich (Milwaukee, WI). All solutions were prepared in doubly distilled water.

Microfabricated Devices

A cross-T microfluidic chip made from low fluorescence Borofloat glass was purchased from Micralyne (MC-BF4-SC, Edmonton, Alberta, Canada). The separation channel was 50 μm wide x 20 μm deep x 85.0 mm long with an 8.0 mm long cross-channel intersecting the separation channel 5.0 mm from the sample reservoir. Buffer reservoirs were fashioned on the glass chip by attaching pieces of plastic micropipette tips (1000 μl Fisher*brand* Redi-Tip, Fisher Scientific, Pittsburgh, PA) with 5 Minute Epoxy (Devcon, Danvers, MA).

Poly(dimethylsiloxane) (PDMS) devices were fabricated as described previously.[69] The separation channel was 83 μm wide x 17 μm deep x 45.0 mm long with a 20.0 mm long cross-channel intersecting the separation channel 8.0 mm from the sample reservoir. The PDMS chip was reversibly sealed to a glass plate daily, prior to experiments. The glass plate was cleaned by immersion in piranha solution (2:1 H_2SO_4:30% H_2O_2) for 10 min. The glass plate was then rinsed with doubly distilled water for 2 min followed by immersion in a 2-propanol bath for 2 min. After being removed from the 2-propanol bath, the plate was again rinsed with doubly distilled water followed by a methanol rinse. The PDMS chip was rinsed with methanol and placed on to the glass plate. The PDMS/glass assembly was placed in an oven at 70 °C for 10 min. After removal from the oven, any air bubbles between the glass plate and PDMS were removed, and the assembly allowed to cool to room temperature while covered.

The channels in both devices were filled with running buffer by filling the sample reservoir and two cross-channel reservoirs with buffer and then applying a mild vacuum to the waste reservoir until no air bubbles were observed in any of the channels. Electrical connections were made to the microfluidic devices with platinum electrodes placed into the sample and waste reservoirs at the ends of the separation channel. A positive potential was applied to the sample reservoir with a Bertan Associates Model 215 3000 V power supply (Hicksville, NY) while the waste reservoir was connected to ground. The reservoirs at each end of the cross-channel were allowed to float electrically. The cross-channel was not directly used for any of the experiments presented here.

Flow Monitoring Instrument

The EOF monitoring instrument used in this work (Figure 3-1) is a modified version of an instrument described previously.[86,146] The capillary in the previous system has been replaced by a microfabricated device mounted horizontally on an XY-translation stage (TSX-10; Newport, Irvine, CA), and the photobleaching and detection optics were modified accordingly. Briefly, a laser beam from an Argon-ion (Ar^+) laser (457.9-nm laser line; Coherent Innova 90C-5; Santa Clara, CA) was split with a cubic beam splitter (Figure 3-1). One split beam was used for laser-induced fluorescence (LIF)

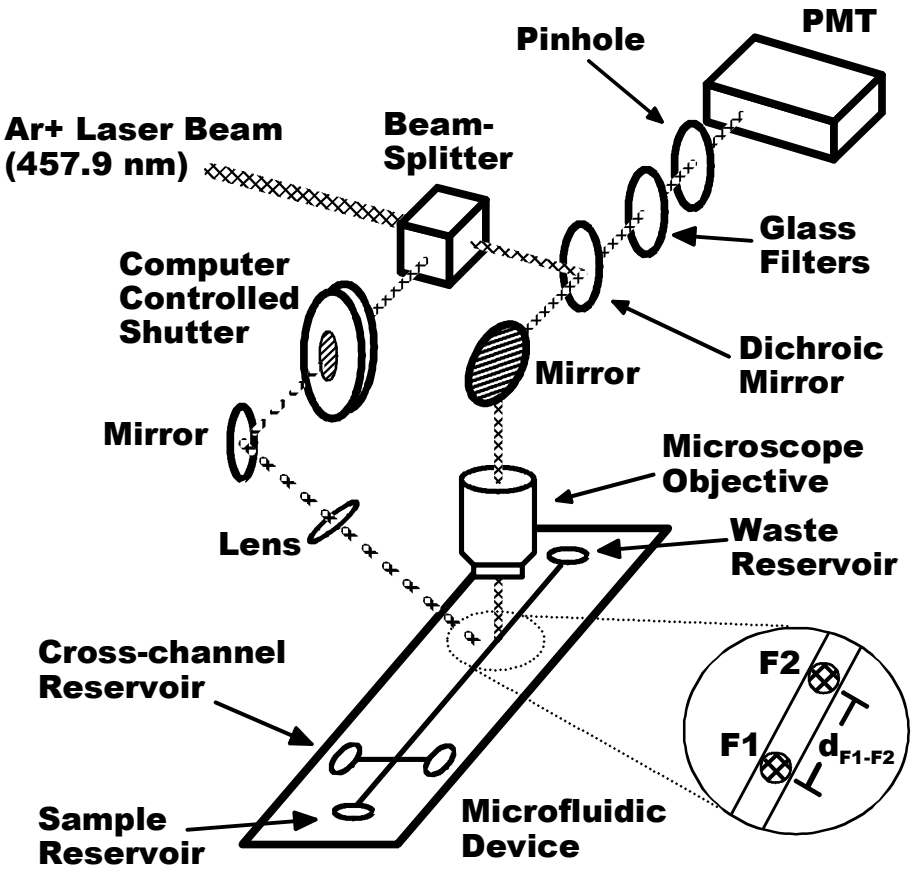

Figure 3-1. Diagram of the EOF monitoring and LIF detection instrument for microfabricated devices. The inset shows a magnified view of the position of the photobleaching beam (F1) and the LIF detection beam (F2) on the separation channel of the microfluidic device. The distance between the two beams is d_{F1-F2}.

detection, and the other split beam was used for photobleaching of the dilute fluorophore in the microfluidic channel. The LIF detection beam was attenuated to 12.1 mW with neutral density filters (not shown) prior to being turned 90° with a dichroic mirror (475DRLP; Omega Optical; Brattleboro, VT). The detection beam was then turned downward by a mirror and directed through a 5× (N.A. = 0.12) microscope objective. The microscope objective was mounted vertically on a XYZ-mount (LP-1-XYZ; Newport, Irvine, CA) over the separation channel in the microfluidic device (Position F2, Figure 3-1). The fluorescence was collected by the microscope objective at 180° and directed through the dichroic mirror. The fluorescence was then spectrally filtered with two glass cut-on filters (LP-475-1.00 and FCG-465-1.00; CVI Laser Corporation; Albuquerque, NM) and spatially filtered (1.4-mm diameter pinhole) prior to being detected by a PMT (Hamamatsu HC120; Bridgewater, NJ). The bleaching beam (40.0 mW) was directed through a computer-controlled shutter (Uniblitz LS6Z2; Vincent Associates; Rochester, NY) and then focused onto the separation channel (Position F1, Figure 3-1) by a fused-silica plano-convex lens (f = 100 mm). The focusing lens for the bleaching beam was mounted on an XYZ-translation stage for positioning and focusing of the bleaching beam along the separation channel. A single fiber optic (not shown) (147.0 μm core; 164.0 μm cladding; Polymicro Technologies; Phoenix, AZ) was used to direct a small portion of the bleaching beam to the PMT to generate the positive peaks seen in the electropherogram in Figure 3-2.

Flow Rate Measurements

EOF rates were measured as described previously for capillaries.[86,146] Calibration of $d_{F1\text{-}F2}$ was carried out by first filling all the channels with 200 nM coumarin 334 dissolved in 20 mM borate buffer (pH = 9.0). The buffer in the sample reservoir (Figure 3-1) was then replaced with 400 nM coumarin 334 dissolved in the same buffer. Using an applied potential of 1500 V (176 V/cm), the separation channel was filled with 400 nM coumarin 334. The time required for the 400 nM coumarin 334 front to travel from the sample reservoir to the LIF detector at position F2 (d = 4.7 cm) was used to determine an average EOF rate. As the separation channel was filled with 400 nM coumarin, EOF was monitored at a rate of 1 Hz. The shutter blocking the bleaching beam was opened for 50 ms for all experiments. The distance between the two laser spots ($d_{F1\text{-}F2}$) was determined using the following equation:

$$d_{F1-F2} = flow\ rate \bullet \Delta t_{F1-F2} \tag{3-1}$$

where $\Delta t_{F1\text{-}F2}$ is the time required for the photobleached zone to migrate from the bleaching beam (F1) to the LIF beam (F2, Figure 3-1). The average of $\Delta t_{F1\text{-}F2}$ for all 36 flow measurements made as the fluorescent front migrated to the LIF detector and the average flow rate were used to calculate a value for $d_{F1\text{-}F2}$.

Following calibration to determine $d_{F1\text{-}F2}$, Equation 3-1 was used to calculate an EOF value (using $\Delta t_{F1\text{-}F2}$ measured) for each time the shutter was opened to produce a photobleached zone. The positive peaks shown in Figure 3-2 were generated when the

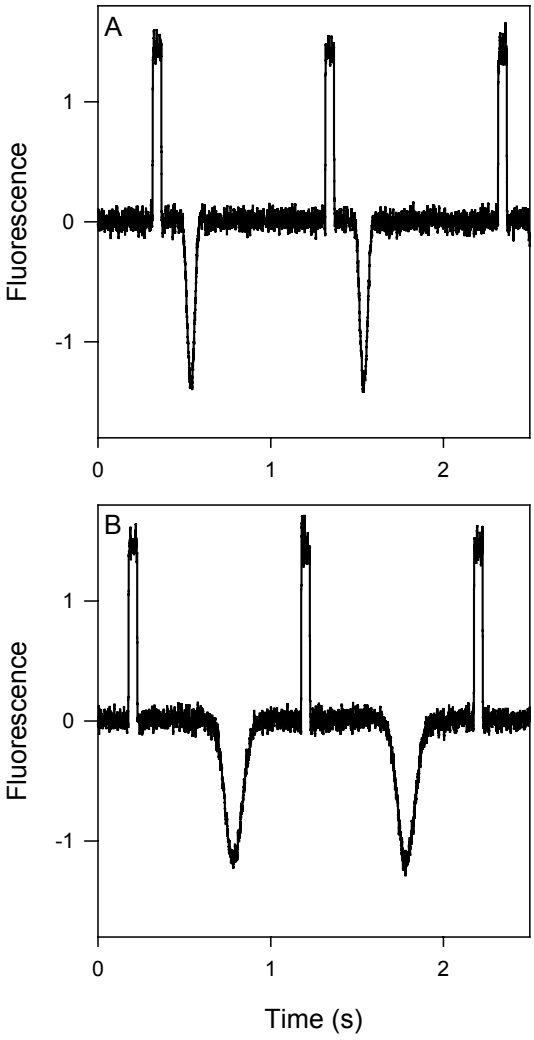

Figure 3-2. EOF measurements made in the microfluidic device at applied fields of (A) 353 V/cm (EOF = 0.253 ± 0.001 cm/s) and (B) 118 V/cm (EOF = 0.0856 ± 0.0002 cm/s). The separation channel was filled with 200 nM coumarin 334 dissolved in 20 mM borate buffer (pH = 9.0). The shutter was opened for 50 ms every 1.00 s to measure EOF (d_{F1-F2} = 497 ± 2 μm).

shutter blocking the bleaching beam was opened to create the photobleached zone at F1, and a portion of this bleaching beam was redirected to the PMT through a fiber-optic. This positive signal provides a time stamp, indicating the start of a flow measurement (t_{F1}). The negative peak (t_{F2}) is the zone of photobleached fluorophore as it is detected at the LIF detector at F2, downstream from the photobleaching beam. Values for $\Delta t_{F1\text{-}F2}$ were measured at the maximum and minimum of each positive and negative peak, respectively.

EOF Simulation

EOF was calculated as a function of time using a MatLAB program based on a model for EOF in a channel containing two solutions at different concentrations (Equation 3-2).[49,50] The calculated bulk flow rate v_b was used to determine the fraction of the capillary filled by the replacement buffer after 0.1 s. A new value of v_b was calculated and used to determine x after the next 0.1 s interval. This process was repeated at 0.1 s intervals for values of x from 0 to 1.

EOF Monitoring and Current Monitoring Experiments

The potential applied across the separation channel was changed in increments of 250 V from 500 to 3000 V (59-353 V/cm) to evaluate EOF in the glass microfluidic device versus applied potential. All device channels were filled with 200 nM coumarin 334 dissolved in 20 mM borate buffer (pH = 9.0). EOF was monitored at a rate of 0.6 – 1.0 Hz.

For current monitoring studies, the primary running buffer was 20 mM borate buffer (pH = 9.0) containing 200 nM coumarin 334. Four test buffers were made at concentrations of 5, 10, 19 and 40 mM borate, all containing 200 nM coumarin 334. All channels were first filled with the 20 mM borate buffer. The 20 mM borate buffer in the sample reservoir was then replaced with the 5, 10, 19 or 40 mM borate buffer, and a potential of 3000 V (353 V/cm) was applied across the separation channel. The current through the separation channel was recorded by measuring the potential across a 100-kΩ resistor. The time required for the replacement buffer to fill the separation channel was measured by determining the intersection of the line tangent to the changing current and the line tangent to the new equilibrium current. While average EOF measurements were made by current monitoring, EOF was also monitored at a rate of 2 Hz using the periodic photobleaching method.

Instrument Control, Data Acquisition and Data Analysis

The instrument was controlled using a program written with LabVIEW (National Instruments; Austin, TX). All data were acquired at 1000 Hz with a PCI-6024E data acquisition board (National Instruments; Austin, TX). All data were filtered using a 500 Hz low-pass RC filter prior to acquisition. A program written in MatLAB (The MathWorks, Natick, MA) was used for baseline subtraction and measurement of time values of the peak maxima and minima of each EOF measurement. The method of

Cardot *et al.* was used to identify peaks.[147] This program also identifies the peak full-width at half-maximum time values used for evaluation of zone broadening. The output from the MatLAB program was imported into Peak Fit 4.0 (SPSS Science, Chicago, IL) or Microsoft Excel (Microsoft Corp., Redmond, WA) for further analysis. All reported precision values are ± 1 SD.

Safety Precautions

Piranha solution is a powerful oxidizer and reacts violently with organic materials or solvents and should be handled with extreme care. Caution should be exercised to avoid contact with the exposed high-voltage contacts in this system.

Results and Discussion

EOF vs. Applied Potential

We have monitored EOF at rates up to 2.0 Hz in glass microfabricated devices by periodically photobleaching a dilute, neutral fluorophore added to the running buffer. Figures 3-2A and B show several individual flow measurements made at applied potentials of 353 and 118 V/cm with corresponding EOF rates of 0.253 ± 0.001 and 0.0856 ± 0.0002 cm/s (n = 60 consecutive flow measurements), respectively. The amount of time required for the photobleached zone to migrate from the bleaching beam (position F1, Figure 3-1) to the LIF detection beam (position F2, Figure 3-1) increases as the applied potential is decreased. The average $\Delta t_{F1\text{-}F2}$ values for the series of EOF monitoring measurements from which Figures 3-2A and B are excerpted are 196 ± 1 ms and 580 ± 1 ms, respectively. Due to diffusional broadening of the photobleached zone, the width of the negative peak increases as the flow rate decreases and the migration time from F1 to F2 increases.[107,146] The appearance of the data obtained in the microfluidic device with the neutral fluorophore additive coumarin 334 is similar to that obtained for experiments conducted in fused-silica capillaries with rhodamine B.[86,146]

The EOF measured in the glass microfabricated device ranged from 0.0436 ± 0.0002 cm/s to 0.253 ± 0.001 cm/s at applied fields from 59 to 353 V/cm (Figure 3-3). The EOF measurements made in the glass device exhibited a precision of 0.2 to 0.6%, which is comparable to the 0.2 - 1.8% precision observed in fused silica capillaries.[86,146] The EOF increases linearly with increasing potential field in contrast with previously published data for fused-silica capillaries at similar field strengths.[86,148,149] More efficient heat dissipation by the glass microfabricated devices decreases the effects of Joule heating on EOF and allows higher potential fields to be applied relative to fused-silica capillaries.[95,150,151]

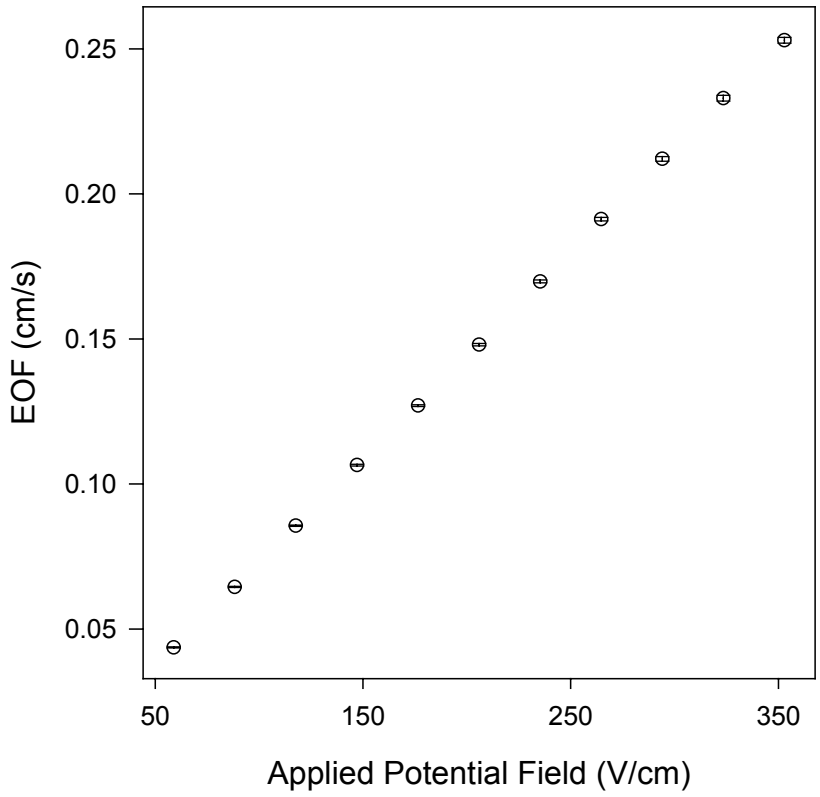

Figure 3-3. EOF (cm/s) versus applied field (V/cm) as measured by periodic photobleaching of a neutral fluorophore in a microfluidic device. Error bars are ± 1 SD.

Attempts to Monitor EOF in PDMS/Glass Devices

Monitoring of EOF in microfluidic devices fabricated from PDMS on glass was attempted without success using both rhodamine B and coumarin 334 as neutral fluorescent buffer additives. Fluorescence was observed in the channel with both fluorophores; however, flow monitoring peaks could not be detected, even at long shutter opening times. We suspect that the neutral coumarin 334 and zwitterionic rhodamine B both absorb irreversibly into the hydrophobic walls of the PDMS microfluidic device,[62,63] and the photobleached zones did not migrate from the bleaching beam (F1) to the LIF detector (F2). The negative photobleached zones were observed when a solution of fluorescein was used to fill the channel; however, because it has a negative charge, fluorescein moves slower than the electroosmotic flow and cannot be used to make direct, quantitative measurements of EOF. Previously, both rhodamine B and coumarin 334 have been successfully used in fused-silica capillaries, and coumarin 334 has been used in the work presented here.[86,94,146] Previous and current work with rhodamine B and coumarin 334 suggest that they do not interact with a quartz capillary as indicated by co-elution with other neutral markers and symmetrical peak shapes.[146] Methanol or 2-propanol were added to the running buffer at concentrations of 5 - 10% (% vol.) in an unsuccessful attempt to limit absorption of the fluorophore into the PDMS. In order for this method of monitoring EOF to be applied to microfluidic devices fabricated from polymers, a neutral dye that does not absorb into the channel walls must be used. The interaction of the hydrophobic, fluorescent buffer additives with the walls of the polymer chips illustrates a limitation of this EOF monitoring technique.

EOF Measurement Using the Current Monitoring Method

We measured average EOF by the current monitoring technique and simultaneously monitored EOF at 2 Hz using the periodic photobleaching method. Current monitoring measurements were made by replacing the 20 mM borate buffer filling the separation channel with either a 5 mM, 10 mM, 19 mM or 40 mM borate buffer. The flow rates measured using both techniques are presented in Table 3-1. Flow rates with the separation channel filled with only one buffer concentration (i.e. 100% 5 mM, 10 mM, 19 mM, 20 mM, or 40 mM borate) were also measured using the periodic photobleaching method and are presented in Table 3-1. For the original report of the current monitoring method in capillaries, a 5% difference in buffer concentrations (19 replacing 20 mM) was used.[58] In order to facilitate end-point detection in microfabricated devices, many researchers have increased the difference in buffer concentration from 5% to as much as 10x so that the differences in current are exaggerated.[61,62,64,66,67,70,71,96] The use of a dilute buffer to replace a more concentrated buffer, creates a discontinuous buffer system in the separation channel and could cause significant changes in EOF to occur during the current monitoring experiment.[49-51,58,152]

The effect of discontinuous buffer systems on EOF in capillaries has been discussed in the literature with regards to sample stacking and other on-column

Table 3-1. EOF values for 20 mM borate buffer in the separation channel being replaced with each buffer listed.[a]

Replacement Buffer Concentration (mM)	EOF in Channel with 100% Replacement Buffer (cm/s)[b]	Current Monitoring	EOF Monitoring[d]		
		Average EOF (cm/s)[c]	*Min. EOF (cm/s)*	*Max EOF (cm/s)*	*Average EOF (cm/s)*
5	0.314 ± 0.003	0.273 ± 0.006	0.239	0.338	0.302 ± 0.040
10	0.290 ± 0.002	0.252 ± 0.003	0.245	0.299	0.278 ± 0.021
19	0.268 ± 0.002	0.249 ± 0.001	0.259	0.269	0.264 ± 0.003
20	0.254 ± 0.002	-[e]	0.250	0.258	0.254 ± 0.002
40	0.224 ± 0.001	0.231 ± 0.005	0.233	0.275	0.254 ± 0.018

[a] All errors in table are ± 1 SD.

[b] n = 60 consecutive EOF monitoring measurements

[c] n = 3 current monitoring measurements

[d] Max. EOF and Min. EOF values are single values taken from three current monitoring experiments. For Average EOF, n = the number of EOF measurements from t=0 to the current monitoring measurement endpoint and is averaged from three current monitoring experiments.

[e] No current change.

preconcentration techniques that make use of capillaries filled with buffers of different concentrations.[49-51,152] It is well known that EOF is dependent upon the ionic strength of the running buffer, with higher ionic strength solutions resulting in reduced EOF rates.[49-51] Also, solution zones in a channel with different ionic strengths will experience different potential fields. A simple model to describe the bulk flow (ν_b) in a microfluidic channel containing two buffers of different concentrations was developed by Chien and Burgi.[49,50]

$$\nu_b = \frac{\left[\gamma x \nu_{eo1} + (1-x)\nu_{eo2}\right]}{\left[\gamma x + (1-x)\right]} \tag{3-2}$$

where γ is the ratio of buffer resistivities ($\gamma = \rho_1/\rho_2$), x is the fraction of the total channel length filled by buffer 1 and ν_{eo1} and ν_{eo2} are the EOF rates in a channel filled with only buffer 1 or buffer 2, respectively. As buffer 1 replaces buffer 2 in the channel, the relative contribution of buffer 1 to ν_b increases, resulting in a change of ν_b from the initial flow conditions in the channel. Equation 3-2 indicates that during the time required for the concentrated buffer in the channel to be replaced by a more dilute buffer, the bulk flow will increase until the channel is completely filled with the new buffer.[49] Thormann and coworkers have published a more detailed computer model to predict changes in EOF due to the presence of a discontinuous buffer system during sample stacking.[51] In the original description of the current monitoring technique, a 19 mM buffer replaced a 20 mM buffer, and this discontinuous buffer system was observed to have no significant impact on EOF when compared to the EOF rate measured with a neutral marker.[58]

The average EOF from triplicate measurements using the current monitoring method for a channel filled with 20 mM borate buffer and replaced with 19 mM borate buffer is 0.249 ± 0.001 cm/s (RSD = 0.4%) (Table 3-1). Under similar conditions, Huang and Zare measured EOF in capillaries with a RSD of 1.7 – 1.8%.[58] It can also be seen in Figure 3-4A that the electrophoretic current changes only 0.2 μA (9%) during the experiment described above while the EOF remains nearly constant. The average, maximum and minimum EOF values measured with the periodic photobleaching method during the current monitoring measurements are shown in Table 3-1. The average value for the EOF data shown in Figure 3-4A was 0.262 ± 0.002 cm/s in the first 8.0 s as the 19 mM buffer replaced the 20 mM buffer and 0.265 ± 0.002 cm/s in the last 8.0 s (26.1 – 34.1 s) of the current monitoring experiment. This result is consistent with Huang and Zare's observation that the current monitoring method does not lead to large flow changes if buffers with small conductivity differences (5.0%) are used.[58] The average EOF value (0.249 ± 0.001 cm/s) obtained with the current monitoring method where 20 mM buffer is replaced by 19 mM buffer is 2.0% less than the EOF rate for a channel filled with only 20 mM borate buffer as measured using the periodic photobleaching method. While the current monitoring method provided an accurate (2.0%) value for EOF if the separation channel were filled only with 20 mM buffer, this value is 5.7% lower than the actual average EOF (0.264 ± 0.003 cm/s) measured by the periodic photobleaching technique during the current monitoring experiment.

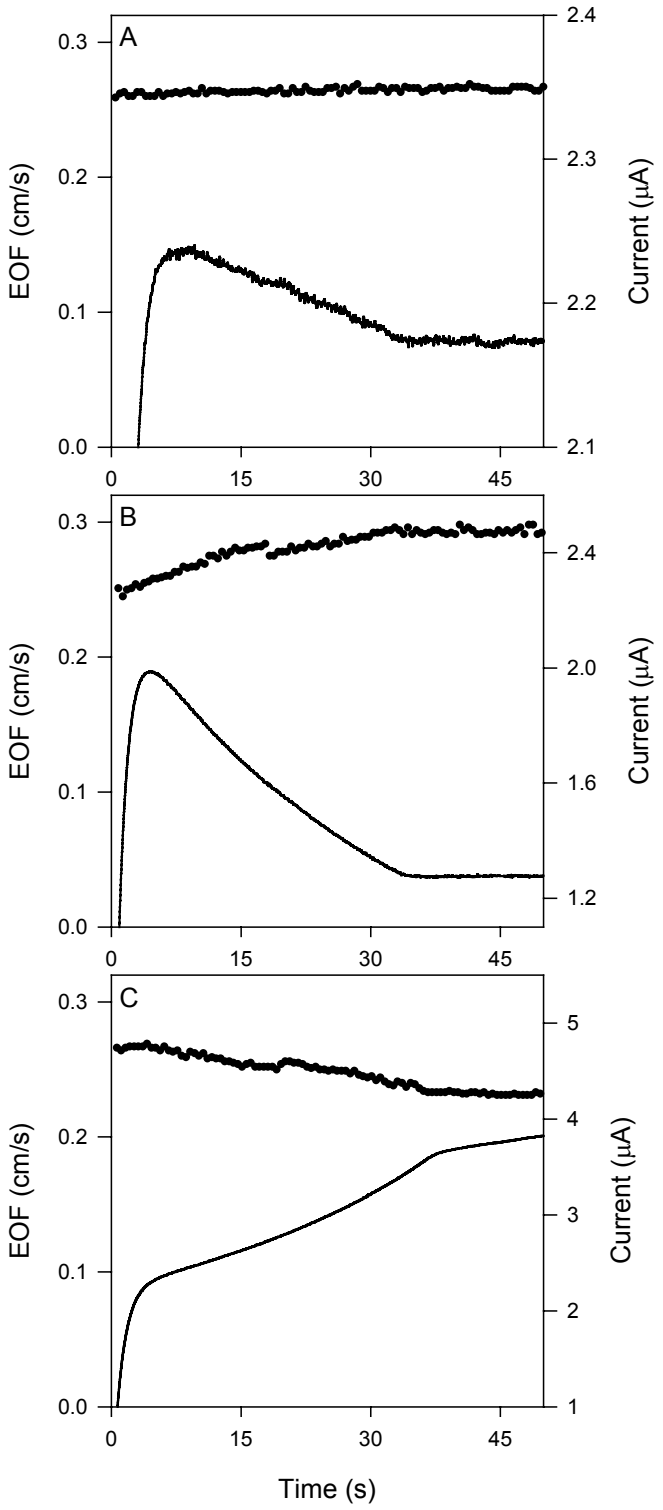

Figure 3-4. EOF (cm/s, top points) and current (μA, bottom curves) measurements versus time as 20 mM borate buffer (pH = 9.0) is replaced by (A) 19 mM, (B) 10 mM, and (C) 40 mM borate buffer (pH = 9.0). The current scales for B and C are exactly 5x and 15x that used in A.

Figure 3-4B shows the change in current and EOF when the replacement buffer is a factor of 2 lower in concentration than the buffer that fills the channel at the beginning of the experiment (10 mM buffer replacing 20 mM buffer). The average EOF measured with the current monitoring method using these solutions is 0.252 ± 0.003 cm/s. The average value of EOF measured using the current monitoring method is effectively identical to the average value measured with the periodic photobleaching method for a channel filled with only 20 mM buffer, but the actual EOF in the channel (Figure 3-4B data) increased from 0.257 ± 0.006 cm/s in the first 8.0 s to 0.290 ± 0.004 cm/s in the last 8.0 s (25.7 - 33.7 s) of the current monitoring experiment. As in the case for 19 mM buffer replacing 20 mM buffer, the average EOF (0.252 ± 0.003 cm/s) measured by current monitoring is lower (10%) than the actual average EOF of 0.278 ± 0.021 cm/s measured by periodic photobleaching. Based on Equation 3-2, as the concentration of the replacement buffer used decreases relative to the 20 mM buffer in the channel, the predicted value for ν_b will increase.

The average EOF measured by the current monitoring for 20 mM buffer in the separation channel being replaced by 5 mM buffer continues the trend of increasing as the concentration of the replacement buffer decreases (Table 3-1). The average EOF (0.273 ± 0.006 cm/s) measured with the current monitoring method is 7.5% greater than the EOF for a separation channel containing only 20 mM buffer and is 9.6% higher than the average EOF measured using 19 mM buffer as the replacement buffer. The average EOF value measured with the current monitoring method continues to be less than the actual average EOF of 0.302 ± 0.040 cm/s measured by the periodic photobleaching method. The EOF increased 20% from 0.269 ± 0.010 in the first 8.0 s to 0.323 ± 0.003 cm/s in the last 8.0 s (23.1 - 31.1 s) of the current monitoring experiment.

While most researchers have used a lower concentration of buffer to replace the buffer filling the channel, some have replaced the buffer in the channel with a buffer of higher concentration.[62,67] The current increases and the EOF rate decreases when the 20 mM buffer is replaced with 40 mM buffer in the separation channel (Figure 3-4C). The current monitoring method gave an average EOF value of 0.231 ± 0.005 cm/s, which is 9% lower than the value obtained by the photobleaching method for a separation channel filled with only 20 mM buffer. The EOF rate decreases by 9.8% from 0.265 ± 0.003 cm/s in the first 8.0 s of the experiment to 0.239 ± 0.004 cm/s in the last 8.0 s (28.8 – 36.8 s). The average EOF (0.254 ± 0.018 cm/s) measured using the periodic photobleaching method is the same as that measured in a separation channel containing 100% 20 mM buffer.

A sudden shift in EOF is observed at an average time of 18 ± 1 s (n = 9) in the data for the current monitoring experiments where 20 mM borate buffer is replaced by 5 mM, 10 mM or 40 mM borate buffer. Figures 3-4B and 3-4C show the shift in EOF for 20 mM borate buffer being replaced by 10 mM and 40 mM borate buffer. A decrease in the peak width of the photobleached zone (12 - 41%) is observed concurrently with the shift in EOF. However, no sudden shift in current occurs at this time. The shift in EOF is reproducible in all experiments where the change in buffer concentration was greater

than 5% but was not observed in experiments where the 20 mM buffer was replaced with 19 mM buffer or in control experiments where only 20 mM buffer was used. In all current monitoring experiments performed here, only the sample reservoir was filled with replacement buffer (Figure 3-5). The shift in EOF is also observed when the replacement buffer is placed in both cross-channel reservoirs and the sample and waste reservoirs (data not shown). We do not yet understand the cause of this EOF shift, but the data in Table 3-1 and Figure 3-4 indicate that EOF dynamics during current monitoring experiments in a simple microfluidic device are more complex than one might anticipate.

One interesting observation about the data in Table 3-1 is that in all cases, the average EOF values determined by the current monitoring method are well below the average EOF values measured by the periodic photobleaching technique. Huang and Zare reported that average EOF values obtained with the current monitoring method and the neutral marker method were identical.[58] The experiments reported in Table 3-1 were repeated, and the same lower EOF values were observed using current monitoring.

In order to explore how EOF was affected by the presence of the cross-channel, EOF was monitored by periodic photobleaching at positions both upstream and downstream from the cross-channel intersection (Figure 3-5). All measurements have been made downstream from the cross-channel intersection for the data in Table 3-1 and Figures 3-2, 3-3 and 3-4. The position where EOF was being monitored in the device was changed by translating the microfabricated device along a single axis of the XY-translation stage that it was mounted to. The positions of the LIF detection beam and the photobleaching beam remained stationary relative to each other, eliminating the need to recalibrate the EOF monitoring instrument as the position of the chip was changed. EOF was monitored for 60 s at a rate of 2 Hz using the periodic photobleaching method.

Figures 3-6 and 3-7 show EOF and photobleached zone width measurements made at points upstream and downstream from the cross-channel intersection during current monitoring experiments where 20 mM borate buffer was replaced by 10 mM (Figure 3-6) and 40 mM buffer (Figure 3-7). The data presented in Figures 3-6 and 3-7 are averages of 10 replicate experiments (1-5 upstream, 6-10 downstream). The data show that the observed effects are reproducible over multiple experiments.

The experiments with low concentration buffer (10 mM) replacing high concentration buffer (20 mM) will be considered first. The upstream EOF rises rapidly from a flow rate of 0.258 cm/s to a maximum of 0.331 cm/s at 2.5 s (Figure 3-6A). Between 2.5 and 32 s, the upstream EOF approaches a stable rate of 0.251 ± 0.001 cm/s. Downstream from the cross-channel intersection, EOF begins at 0.239 cm/s. A slight decrease in EOF to 0.234 cm/s is observed during the first 4.5 s, followed by a steady increase until a flow rate of 0.271 ± 0.001 cm/s is reached after 34.5 s. The average EOF measured by the current monitoring method for 10 mM buffer replacing 20 mM buffer is 0.253 ± 0.005 cm/s (t = 33.5 ± 0.7 s; n = 10), which falls between the values measured on this day in the downstream channel by periodic photobleaching for a separation channel filled with 100% 20 mM buffer (0.241 ± 0.002 cm/s) and 10 mM buffer (0.271 ± 0.003 cm/s). The width (FWHM) of the photobleached zone upstream from the cross-channel intersection, remains close to an average value of 54.4 ± 0.9 ms (Figure 3-6B) as the 20

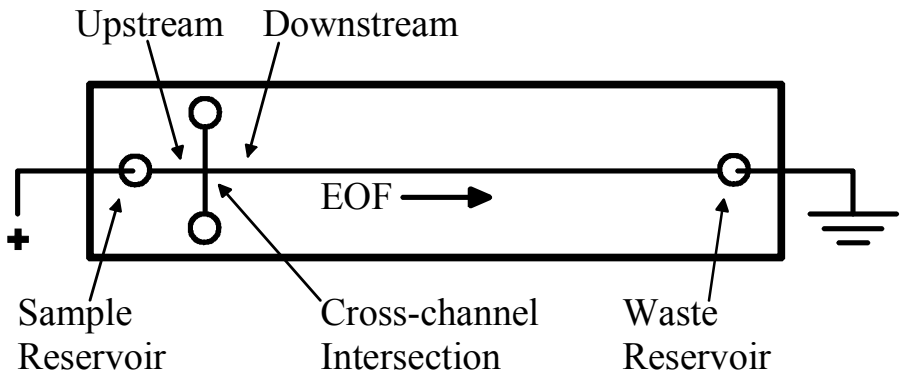

Figure 3-5. Simple schematic of the microfluidic device. The separation channel is defined as the channel between the sample and waste reservoirs. The cross-channel is perpendicular to and intersects the separation channel.

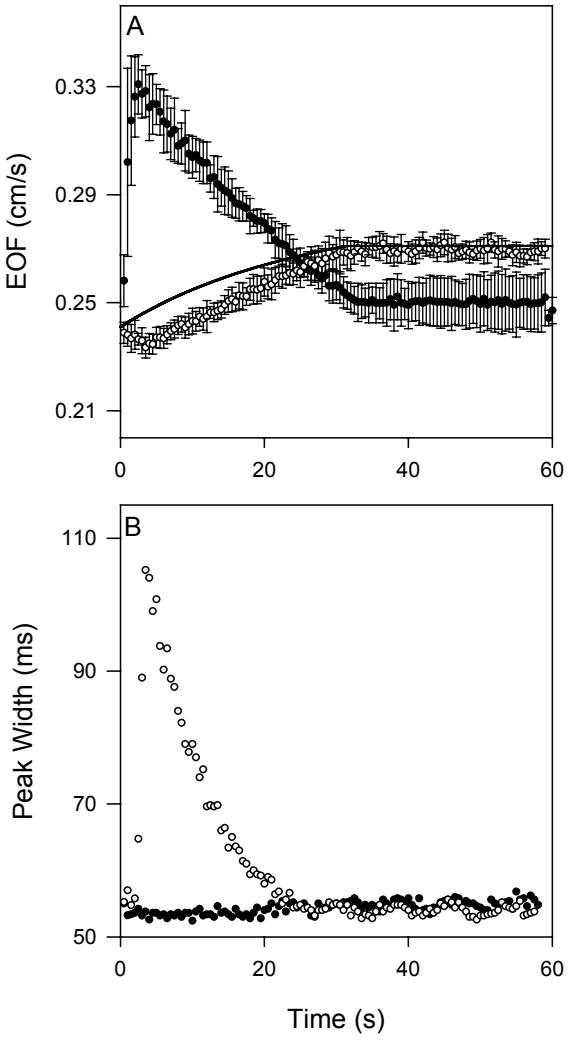

Figure 3-6. The (A) EOF (cm/s) and (B) photobleached zone width (FWHM) upstream from the cross-channel intersection (•) and downstream from the cross-channel intersection (o) versus time as 20 mM borate buffer (pH = 9.0) is replaced by 10 mM borate buffer (pH = 9.0). The experiments were repeated 5 times, and the data were averaged. The solid line shows the calculated EOF as a function of time based on Equation 2. Error bars are ± 1 SD and $d_{F1\text{-}F2}$ = 468 ± 2 μm.

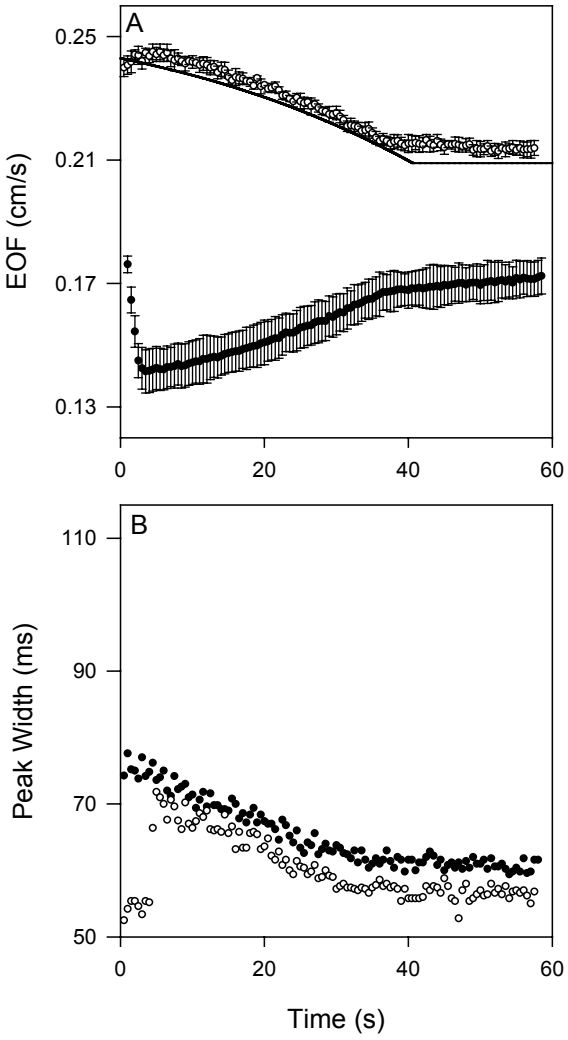

Figure 3-7. The (A) EOF (cm/s) and (B) photobleached zone width (FWHM) upstream from the cross-channel intersection (●) and downstream from the cross-channel intersection (○) versus time as 20 mM borate buffer (pH = 9.0) is replaced by 40 mM borate buffer (pH = 9.0). The experiments were repeated 5 times, and the data were averaged. The solid line shows the calculated EOF as a function of time based on Equation 3-2. Error bars are ± 1 SD and $d_{F1\text{-}F2}$ = 468 ± 2 μm.

mM buffer is replaced by 10 mM buffer. In the downstream channel the width of the photobleached zone begins increasing at 2.0 s from 55.7 ± 0.8 ms and reaches a maximum of 105 ± 18 ms at 3.5 s (89% increase). The width of the photobleached zone gradually returns to 54.0 ± 0.7 ms after 24 s. At the conclusion of the experiment, there is a 7.6% (0.019 cm/s) difference in the EOF rates measured upstream and downstream from the cross-channel intersection.

A model published by Hu *et al.* predicts that when a cross-channel is left floating and a potential is applied across the separation channel, a pressure gradient is established at the intersection of the separation and cross-channels. The solution flow through the cross-channel intersection creates a hydrodynamic flow from the cross-channel into the separation channel. This model further predicts that in a chip filled with a continuous buffer, EOF upstream from the channel intersection will be slower than EOF downstream from the intersection.[137] The average EOF measured in the upstream channel with the glass chip filled with only the 20 mM borate buffer (including 200 nM coumarin 334) was 0.218 ± 0.001 cm/s (n = 5) and the average EOF measured in the downstream channel was 0.229 ± 0.001 cm/s (n = 5). As predicted by Hu *et al.*, the EOF downstream from the channel intersection was greater (5.0%) than the upstream EOF.[137]

In the glass microfabricated device used here, the cross-channel intersects the separation channel 5 mm from the sample reservoir (Figure 3-5). Unlike the closed system of a fused-silica capillary, this cross-channel creates an open system and a path for electrophoretic and pressure gradients to move fluids into or out of the separation channel.[137] The introduction of a second buffer with a different concentration into a microfluidic device not only affects the bulk EOF, but also generates a pressure gradient and laminar flow.[49,50,99,101,138,141,152,153] The presence of a laminar flow profile has not been directly measured here, but is indicated by the observed broadening of the photobleached zones used for EOF monitoring during the current monitoring experiments as shown in Figure 3-6B.

The initial upstream EOF rate indicates that the upstream portion of the separation channel (5 mm) will be filled by the replacement buffer in less than 2 s. The initial increase in electrophoretic current when the potential is applied shows that the rise time (10 to 90%) of the electrophoretic circuit is 2.14 ± 0.03 s (n = 10), and, therefore, interpretation of the flow and peak width data during the first 2 s of the experiment could be clouded by the rising potential field. Future redesign of the electrophoretic circuit and an increase in the EOF monitoring rate will allow for more quantitative and detailed investigation of such early events.[132]

Initially, as the 10 mM buffer replaces the more conductive 20 mM buffer in the upstream separation channel (Figure 3-6), the local potential field increases, resulting in a sharp increase in the upstream EOF. During this same time period the downstream EOF decreases due to the reduced local field strength in this part of the separation channel. As the downstream separation channel fills with the 10 mM buffer, the field strength in the upstream channel decreases and the upstream EOF rate decreases accordingly until the channel is completely filled with the 10 mM buffer. The downstream EOF increases over the same time period. The data in Figure 3-6B show that as the 10 mM replacement

buffer fills the upstream separation channel, the pressure gradient generated at the interface of the two buffer regions is relieved through the arms of the cross-channel. The two halves of the cross-channel are each less than 4 mm in length and provide a path of least resistance for the hydrodynamic pressure gradient generated at the interface of the two buffer regions. Due to this pressure release, minimal hydrodynamic broadening of the photobleached zone is observed in the short upstream portion of the separation channel (5 mm); however, the hydrodynamic broadening of the photobleached zones is pronounced in the downstream channel.

The solid line in Figure 3-6A is a simulation of EOF based on Equation 3-2 and assumes that the upstream and downstream segments of the separation channel are one unbroken channel. The EOF values measured in the downstream channel by periodic photobleaching were used in the simulation. The downstream EOF is close to the simulated EOF, but the upstream flow is far above the EOF predicted by the model and falls rather than rises during the current monitoring experiment. As predicted by Hu *et al.* the final EOF in the upstream channel is lower due to resistance at the channel intersection, but the downstream EOF is unaffected by this intersection.[137] These data still do not explain why the current monitoring method indicates an EOF value lower than the average EOF measured in the downstream channel by periodic photobleaching. The data in Figure 3-6 suggest that the current monitoring method should give a higher value due to relatively fast initial flow in the upstream channel. These data do support the predictions made by Hu *et al.*[137] and suggest that the current monitoring method is not always reliable in microfabricated devices with intersecting channels.

The results for more conductive buffer (40 mM) replacing the 20 mM buffer are strikingly different (Figure 3-7). The upstream EOF begins at 0.176 ± 0.003 cm/s and rapidly decreases to 0.142 ± 0.007 cm/s at 3.5 s while the downstream EOF rises slightly from an initial value of value 0.238 ± 0.001 cm/s to 0.245 ± 0.001 cm/s at 4.5 s. The rise time for the electrophoretic circuit under these conditions was 2.45 ± 0.06 s (n = 10). In this case the potential field in the upstream channel decreases as this channel segment fills with more conductive buffer, and the downstream channel experiences an increased potential field. After reaching its minimum at 3.5 s the upstream EOF gradually increases to 0.168 ± 0.005 cm/s at 39.0 s, and at the same time the downstream EOF decreases to 0.215 ± 0.002 cm/s. The upstream and downstream flow rates at 39.0 s differ by 28% (0.047 cm/s). On this day, an average EOF value of 0.226 ± 0.004 cm/s was measured by the current monitoring method (t = 37.7 ± 0.7 s; n = 10), and the periodic photobleaching method gave an average value of 0.233 ± 0.009 cm/s (n = 5) downstream from the cross-channel intersection. Again, while these data show that EOF dynamics are complicated and interesting during current monitoring experiments, they do not explain why the current monitoring technique and the periodic photobleaching method often give different values for average EOF.

Published data suggest that differences between EOF values measured by the current monitoring method and downstream EOF monitoring by periodic photobleaching could be related to the shape of the interface between high and low concentration buffers.[49,50,58,69,99,152,153] Figure 2 in the manuscript by Huang and Zare[58] and Figure 3 by

Liu *et al.*[69] show electropherograms with conductivity detection during current monitoring experiments. These plots indicate that the boundary between the two zones is much sharper for a 19 mM buffer replacing a 20 mM buffer[58] compared to a 15 mM buffer replacing a 30 mM buffer.[69] This is consistent with broadening of the interface due to laminar flow caused by mismatched EOF in different parts of the capillary or microchannel.[49,50,99,152,153] Conductivity detection and periodic photobleaching take place in short segments of the channel, and conductivity detection directly probes the shape of the interface between the two solution zones. The current monitoring method, in contrast, is based on the resistance down the total length of the microchannel. The electrophoretic current will continue to change after the center of the interface between the solutions has exited the channel, and this will result in measured EOF values that are lower than the actual average EOF during an experiment. The broad interface shown in Figure 3 by Liu *et al.* best illustrates the case for this hypothesis.[69] Conductivity detection was not available for the experiments presented in this paper, and this hypothesis has not been tested here.

The model by Hu *et al.*, predicts that a flow difference will exist in the upstream and downstream parts of the separation channel,[137] but the relatively large difference in the upstream and downstream EOF at the end of the current monitoring measurement at 39.5 s suggests the presence of an additional siphoning contribution to the flow difference as described for capillary gap junctions by Kuhr *et al.*[87] The cross channels are filled with 20 mM borate buffer, and EOF is higher in the downstream channel during current monitoring as it fills with 40 mM buffer. Low concentration buffer (which results in higher EOF) will be siphoned in from the cross channels so that the final buffer concentration in the downstream channel will be lower than 40 mM. This siphoning effect is not indicated by the simulated data in Figure 3-7A because the simulation includes an EOF rate measured with the separation channel filled with 40 mM buffer and the side channels filled with 20 mM buffer. The large difference in final upstream and downstream EOF values does support a siphoning contribution in these experiments. It is also important to note that at 39.5 s, the EOF rate both upstream and downstream of the cross-channel intersection still appear to be changing slowly although both parts of the separation channel should be completely filled with the replacement buffer by this time. This suggests that the extent of siphoning of 20 mM buffer from the cross-channels still may be increasing.[87]

Peak broadening starts immediately in the upstream channel (77.6 ± 10.0 ms at 1.0 s) because of the pressure gradient created due to faster EOF in the downstream channel (Figure 3-7B). As the separation channel fills with 40 mM buffer, the peak widths gradually decline to an average of 61.1 ± 0.8 ms in the 10 s following the end of the current monitoring experiment. Initial peak broadening is lower in the downstream channel, presumably until 40 mM buffer enters this part of the separation channel, creating a pressure gradient in the downstream channel that can't be relieved through the side channels. The downstream peak width reaches a maximum of 71.8 ± 4.0 ms at 5.0 s and gradually declines to an average value of 56.6 ± 1.3 ms in the 10 s following the conclusion of the current monitoring experiment. The difference between upstream and downstream final peak widths in Figure 3-7B (4.0 ± 0.9 ms) is greater than that in Figure

3-6B and is consistent with the larger final difference in upstream and downstream EOF rates. Hydrodynamic effects should be minimal at this point of the experiment, but the longer migration time for photobleached zones at lower flow rates will lead to increased diffusional broadening of these peaks.[107,146]

Conclusions

We have demonstrated monitoring of EOF in glass microfluidic channels at rates up to 2 Hz with a precision of better than 1%. The direct comparison of this new technique to the current monitoring method demonstrates the ability of our method to quantitatively study EOF dynamics in microfluidic devices. It also shows that the current monitoring technique must be applied with caution in microfluidic systems since the measurement technique itself will alter EOF, and the effects of intersecting channels in even simple devices can lead to misleading flow measurements. We have also demonstrated the ability of our technique to measure EOF in different intersecting channels to study the differences in EOF dynamics between these channels. The initial failure of this technique for EOF measurements in PDMS-glass microfluidic channels illustrates the major limitation of this technique. To accurately measure EOF, neutral, fluorescent dyes are required that do not interact with the channel surface or buffer components such as micelles. Despite these limitations, this technique can be used successfully to study EOF dynamics in microfabrciated devices over a wide range of experimental conditions where these requirements can be met. Future simplification, optimization and miniaturization of the optical system could lead to a device capable of improving the analytical performance in microfluidic devices by providing a record of fluid flow in the device during an experiment for data correction or feedback control.

Acknowledgements

The authors thank Jasna Vellovic for her assistance with programming in MatLAB. Financial support for this work was provided by the University of Tennessee.

CHAPTER IV

Experimental Studies of Electroosmotic Flow Dynamics During Sample Stacking For Capillary Electrophoresis

This chapter is a slightly revised version of a paper by the same title submitted for publication in the journal *Analytical Chemistry* in 2003 by Jason L. Pittman, Herman J. Gessner, Kimberley F. Schrum, Eloise M. Raby, Joseph B. Batts and S. Douglass Gilman:

Pittman, J. L.; Gessner, H. J.; Schrum, K. F.; Raby, E. M.; Batts, J. B.; Gilman S. D. *Anal. Chem.* **2003,** *Submitted for Publication.*

Abstract

Electroosmotic flow dynamics during a field-amplified sample stacking experiment have been studied experimentally using the periodic photobleaching of a dilute, neutral fluorophore added to the separation buffer. Changes in electroosmotic flow during a separation of arsenic compounds with field-amplified sample stacking have been monitored at a rate of 1 Hz. The effects of hydrodynamically injecting different sample plug lengths of analyte dissolved in 0.125 mM (120, 240, and 600 s) and 41.7 μM (27, 45, and 74 s) phosphate buffer with a separation buffer concentration of 12.5 mM phosphate buffer were examined. The observed effects of increasing the sample plug length on electroosmotic flow and electrophoretic current agreed qualitatively with predictions by theoretical models presented in the literature. Electroosmotic flow changes greater than 100% (1.6 – 3.3 mm/s) have been observed. Broadening of the flow monitoring peaks has been used to examine laminar flow due to the discontinuous buffer systems used for sample stacking.

Introduction

Poor concentration detection limits are a significant disadvantage of capillary electrophoresis (CE) relative to larger scale separation techniques like HPLC. For example, detection limits for CE with UV/VIS absorbance are typically 10^{-6} M or higher due to the short optical pathlength defined by a CE capillary.[49,154] Electrophoretic sample stacking is an experimentally simple approach for oncolumn sample preconcentration and has been applied extensively to overcome detection limitations of CE.[49,154-157] Concentration factors of 5- to over 2000-fold have been achieved using electrophoretic sample stacking.[49,154-157] Several variations of this approach to sample preconcentration have been reported in the literature such as field-amplified sample stacking (FASS),

large-volume sample stacking (LVSS), pH-mediated stacking and isotachophoresis.[49,154-157] Of these methods, FASS is the simplest to perform experimentally and has been applied most frequently.[155-157]

The sample for FASS is prepared in a very dilute buffer or in pure water.[49,154-157] Typically, a long plug of the sample is injected hydrodynamically into a capillary, which is filled with a more concentrated separation buffer. After the sample plug is injected, the injection end of the capillary is placed back into a reservoir containing the more concentrated separation buffer, and a separation potential is applied. The electroosmotic flow (EOF) in the capillary moves the sample plug through the capillary, drawing the more concentrated separation buffer in behind it and creating a zone of dilute buffer with the more concentrated buffer to either side. The analytes in the sample plug will experience an increased electrophoretic velocity due to the increase in the potential field across the lower conductivity sample plug. This will cause the analytes to migrate rapidly toward the interface of the sample plug and the more concentrated separation buffer, where a rapid decrease in the local electric field occurs, resulting in a decrease of the analytes' electrophoretic velocities. This causes a zone of concentrated or "stacked" analyte to form at this interface. As the stacked zone of analyte molecules migrates down the capillary in the more concentrated separation buffer, the electrophoretic separation proceeds normally.

The dynamics of EOF in a capillary during a sample stacking experiment must be understood in order to take full advantage of FASS. The migration times and quantitation of analytes are greatly affected by changes in EOF.[43,50,51,118,158,159] The mismatch of EOF between segments of the capillary containing different solutions will also create pressure gradients resulting in hydrodynamic flow. This laminar flow will cause broadening of analyte zones and of the interface between different solutions. Models describing the behavior of the EOF in a capillary during a FASS experiment have been reported.[49-51] Chien and Helmer developed a model describing the behavior of EOF due to the introduction of a discontinuous buffer system into the separation capillary.[50] This model calculates a bulk EOF value by summing the contributions of each section of the capillary containing a different solution. As the length of dilute sample buffer zone in the capillary is increased, its contribution to the bulk EOF increases. The magnitude of the contribution of the dilute sample plug on the bulk EOF is also dependent on the ratio of conductivities between the two buffers in the discontinuous system. Chien and Helmer further discuss the impact of hydrodynamic flow generated due to the mismatch of local EOF rates between the sample plug and more concentrated separation buffer. Both the length of the injected sample plug and broadening of the analyte peaks due to hydrodynamic flow generated by FASS counteract the effects of sample stacking.[49,50,155,156,158,160,161] Chien and Helmer's model predicts that EOF will be constant for a FASS experiment until the dilute buffer zone begins to elute from the end of the capillary. Their model does not account for the effects of diffusional and hydrodynamic broadening on the shape, concentration and ionic strength of the sample plug and its impact on the bulk EOF as the changing sample plug migrates through the capillary.[50]

The model reported by Thormann *et al.* predicts that EOF will change throughout a FASS separation due primarily to changes in ionic strength in the sample zone as it migrates through the capillary.[51] Their model predicts that EOF will decrease from the beginning of a FASS experiment until the dilute sample buffer zone has completely eluted from the end of the capillary.[51] The addition of ionic strength as a factor affecting EOF to a previously published dynamic capillary zone electrophoresis model allows the description of the effects of a continually changing dilute sample plug on the EOF, current and analyte peaks. As the sample plug migrates through the capillary, its broadening results in a dynamically changing local electric field in both the sample zone and the more concentrated separation buffer. The model calculates the effects of ionic strength in both the sample zone and the more concentrated separation buffer on the electric double layer formed at the internal capillary surface-solution interface. The simulated results of a model separation were presented and included the prediction of changes in EOF and current occurring during the separation. The separation results and predicted changes in electrophoretic current matched well with data obtained experimentally. Thormann *et al.* did not monitor the predicted dynamic changes in EOF to confirm this aspect of their model, and they state that EOF is "difficult to monitor accurately."[51]

In this paper, EOF dynamics during a FASS experiment are studied experimentally using a technique based on periodic photobleaching of a dilute, neutral fluorophore added to the separation buffer.[86,146,162] The effects of increasing injection times and decreasing sample buffer concentrations on EOF dynamics during FASS are examined. The experimental results are compared to the predicted changes in EOF described by Thormann *et al.*[51]

Experimental Section

Chemicals

Laser grade coumarin 334, (4-amino-phenyl)-arsonic acid (PABA), dimethyl-arsinic acid (DMA) and citric acid were obtained from Acrōs (Pittsburgh, PA). Phenylarsonic acid (PAA) was purchased from Alfa Aesar (Ward Hill, MA), and dibasic sodium phosphate was purchased from Mallinckrodt (Phillipsburg, NJ). Boric acid was obtained from J.T. Baker Chemical Co. (Phillipsburg, NJ). Mesityl oxide was purchased from Sigma Chemical Co. (St. Louis, MO). Sodium hydroxide and hydrochloric acid were obtained from Fisher Scientific (Fair Lawn, NJ). All solutions were prepared in doubly distilled water.

EOF Monitoring

The instrument used for monitoring EOF has been described in detail previously.[146] Figure 4-1 illustrates the technique for measuring EOF using this instrument and presents a sample of flow-monitoring data. Flow is measured by determining the time (t_{F1-F2}) required for a photobleached zone of a neutral fluorophore to

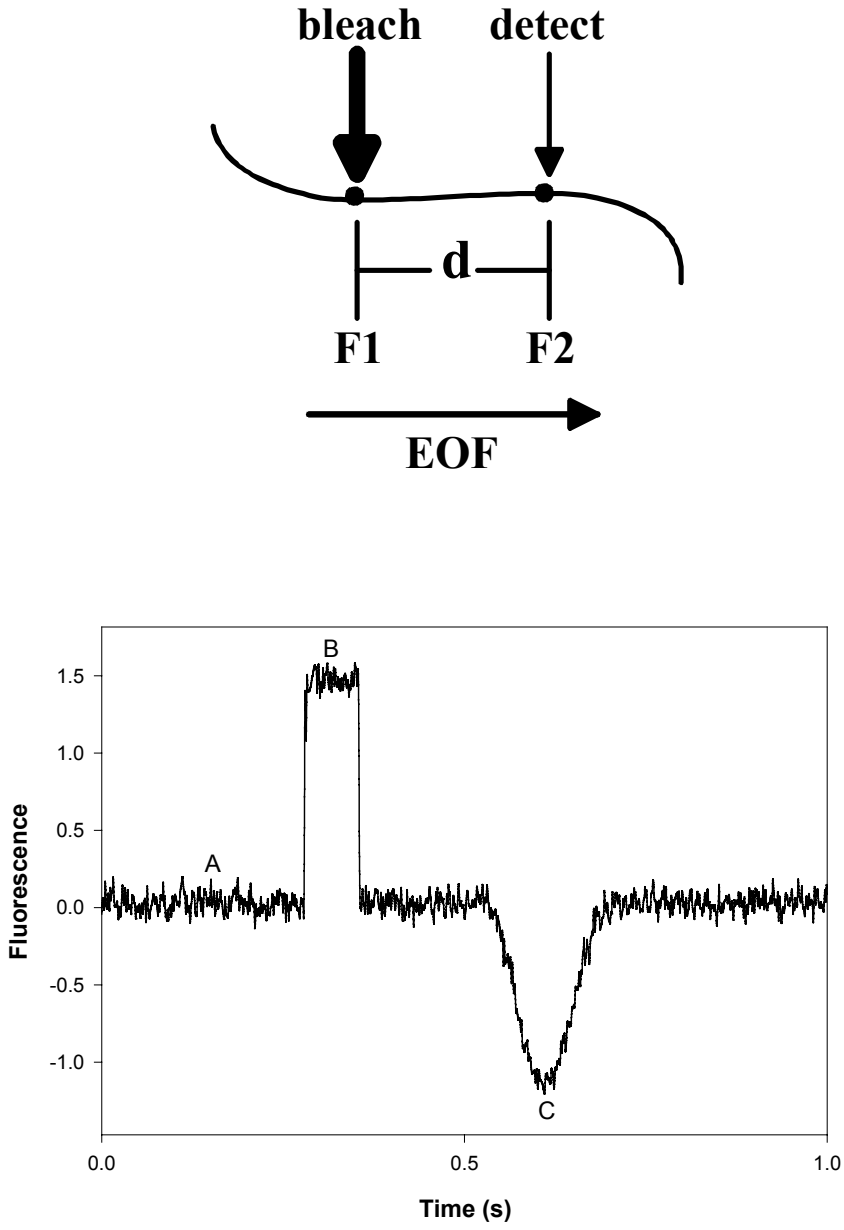

Figure 4-1. Schematic and data illustrating the EOF monitoring technique. F1, bleaching beam focal point; F2, detection beam focal point; d, distance separating F1 and F2 (1.03 mm). The solution flowing through the capillary was a 12.5 mM phosphate buffer (pH = 6.5) containing 15 nM coumarin 334. The photobleached zone was generated using a 75-ms bleaching pulse from an Ar^+ laser. The photobleaching and LIF detection beams were 50.0 and 12.6 mW, respectively at a wavelength of 457.9 nm. (Applied potential = 333 V/cm; flow rate = 0.161 cm/s).

migrate through the capillary from position F1 (bleaching beam focal point) to position F2 (detection beam focal point) over a distance d_{F1-F2}. Measurement of d_{F1-F2} was carried out as described previously.[86,146] A computer-controlled shutter (Uniblitz 310 B; Vincent Associates, Rochester, NY) blocks the bleaching portion of the laser beam from an Ar^+ laser (Coherent Innova 90C-5; Santa Clara, CA) at position F1 on the capillary. When the shutter is closed, blocking the bleaching beam at F1, a constant fluorescence signal is observed (A, Figure 4-1) at the laser-induced fluorescence (LIF) detector at position F2. The shutter is then opened for a brief period of time, exposing the fluorophore in the capillary to the bleaching beam and generating a photobleached zone at F1. A positive peak is observed (B, Figure 4-1) due to light from the bleaching beam that is redirected by an optical fiber to the photomultiplier tube (PMT) for LIF detection, indicating the opening of the shutter and marking the beginning of the flow measurement. After the shutter has closed, the signal returns to the baseline value. The photobleached zone then flows from F1 to F2, and a negative peak is observed as the photobleached zone travels past the LIF detector at position F2 (C, Figure 4-1). This process is repeated to make subsequent EOF measurements.

Capillary Electrophoresis

The CE instrument used in this work has been described previously.[86] Briefly, fused-silica capillary (50 μm i.d., 220 μm o.d.) was obtained from SGE (Austin, TX) and used for all experiments. The electrophoretic potential was applied using a Spellman CZE1000R high voltage power supply (Hauppauge, NY). A Linear UVIS 204 detector with an on-column capillary cell was used for absorbance detection.

Coumarin 334 Neutrality Studies

The pH range over which coumarin 334 is neutral was determined based on coelution with a neutral marker. A solution of coumarin 334 in 10 mM citric acid buffer was spiked with a neutral marker, mesityl oxide, and was electrophoretically injected into a capillary for 3.0 s. The elution of these compounds was detected by UV/VIS absorbance at 215 nm. The pH of the citric acid buffer was adjusted as needed with HCl and NaOH. The injection and separation potentials were adjusted from 15-19 kV (247 to 313 V/cm) in order to maintain an operating current between 20-30 μA as the ionic strength of the buffer changed with pH. The separation was performed in a 60.7 cm capillary (48.0 cm to the detector).

Coumarin 334 Detection Limit Studies

The capillary was filled with 50 mM phosphate buffer (pH = 9.0) containing coumarin 334 at concentrations from 0.66 to 33 nM. At each concentration of coumarin 334, a series of 75-ms bleaching pulses was applied to the running buffer as it flowed through the capillary. Signal was determined at each coumarin 334 concentration by measuring the difference between the fluorescence signal with the shutter closed (A, Figure 4-1) and the minimum value of the photobleached zone (C, Figure 4-1). The LOD was defined as the concentration of coumarin 334 at which the signal was 3 times greater

than the rms noise of the fluorescence intensity from unbleached coumarin 334. The 457.9-nm laser line was used for bleaching (34.8 mW) and LIF detection (13.5 mW). An electrophoretic potential of 20.0 kV (312 V/cm) was applied across a capillary 64.0 cm in length with a detection window 54.0 cm (F2, Figure 4-1A) from the injection end of the capillary.

Sample Stacking Studies.

Solutions of 156 μM DMA, 33.0 μM PAA and 23.0 μM PABA were prepared in 12.5 mM, 0.125 mM and 41.7 μM phosphate buffer (pH = 6.5). Blank solutions containing no arsenic compounds at the same buffer concentrations were also prepared for experiments without analytes. All solutions contained 15.0 nM coumarin 334. Sample injections were performed hydrodynamically by raising the injection end of the capillary 14.0 cm above the detection end. The effects of increasingly large sample plugs on EOF dynamics were examined by making injections of 120, 240 and 600 s from the sample solutions in 12.5 mM and 0.125 mM phosphate buffer.

The volume of analyte solution injected into the capillary at each injection time was calculated using the Hagen-Poiseuille equation.[163] The calculated volume injected was then divided by the total capillary volume to determine the percentage of the capillary filled by sample solution.

The bulk EOF (V_b) in the capillary for each sample volume injected into the capillary in 12.5 and 0.125 mM buffer was calculated using the following equation:[49,50]

$$V_b = \frac{\left[\gamma x V_{eo1} + V_{eo2}(1-x)\right]}{\left[\gamma x + (1-x)\right]} \tag{4-1}$$

where x is the percentage of the capillary filled with the dilute buffer plug, V_{eo1} and V_{eo2} are the EOF values for a capillary filled only with dilute and concentrated buffers, respectively, and γ is the ratio of the resistivity of the dilute buffer to the resistivity of the concentrated buffer ($\gamma = \rho_1/\rho_2$).[49,50] The resulting values of V_b were then used to calculate values of x for injections of sample dissolved in 41.7 μM buffer that would produce V_b values identical to those for longer injections made for a sample in 0.125 mM buffer.

Sample solutions in 41.7 μM phosphate buffer were injected for 27, 45 and 74 s. A separation potential of 30.0 kV (333 V/cm) was applied across the capillary for all sample stacking experiments. The fused-silica capillary was 90.0 cm in length with the UV/VIS and LIF detectors located 40.0 and 75.0 cm from the injection end of the capillary, respectively. The CE running buffer was 12.5 mM phosphate buffer (pH = 6.5) for all experiments. Absorbance detection at 200 nm was used to detect the analytes during the separation. The 457.9-nm laser line from an Ar^+ laser was used for bleaching and LIF detection at powers of 50.0 and 12.6 mW, respectively. Bleaching pulses 75-ms in duration were used for EOF monitoring. EOF was monitored at a rate of 1 Hz.

Instrument Control, Data Acquisition and Data Analysis

A program written in LabVIEW (National Instruments, Austin, TX) was used for data acquisition and instrument control. All data were acquired with a National Instruments PCI-6024E data acquisition board at an acquisition rate of 1000 Hz. All signals were filtered with a 500-Hz low-pass RC filter prior to acquisition. A program written in MatLAB (The MathWorks, Natick, MA) was used for baseline subtraction and measurement of time values of the peak maxima, minima and fwhm for each EOF measurement. The output from the MatLAB program was imported into Peak Fit 4.0 (SPSS Science, Chicago, IL) or Microsoft Excel (Microsoft Corp., Redmond, WA) for further analysis.

Results and Discussion

Coumarin 334

The overall goal of this work is to experimentally measure EOF dynamics during sample stacking. In previous studies using our EOF monitoring technique based on periodic photobleaching, the neutral fluorophore added to the CE running buffer was rhodamine B.[86,146] Ideally, the fluorophore used for monitoring EOF will be neutral over a wide pH range, easily photobleached and detectable at low concentrations. Rhodamine B satisfies the requirements of being neutral over a wide pH range and detectable at concentrations that do not interfere with other methods of analyte detection, but it also requires high laser powers for photobleaching (230 mW at 514.5 nM, 30% photobleached).[146]

Coumarin 334 has been identified as an alternative neutral fluorophore that can be photobleached more easily than rhodamine B.[94] Based on the structure of coumarin 334 (Figure 4-2A), it is expected to be neutral over a wide pH range, and this was confirmed experimentally from a pH of 3.5 to 11.0. This is an improvement over the pH range where rhodamine B is in the zwitterionic form (Figure 4-2B) (pH = 6.0-10.8).[86] The LOD for EOF monitoring with coumarin 334 was 0.66 nM, ~11 times lower than the LOD for rhodamine B (7 nM).[146] This detection limit means that lower concentrations of neutral fluorophore additive can be used for monitoring EOF, decreasing the likelihood of the dye affecting EOF or interfering with a concurrent analyte detection method such as UV/VIS absorbance.

Electroosmotic Flow Dynamics During Sample Stacking

The separation of three arsenic species was chosen to examine EOF dynamics during a sample stacking experiment. The separation procedure was adapted from the work of Gil *et al.* and did not require any buffer additives or a polarity reversal step for the removal of the sample plug.[52] In order to achieve sample stacking, Gil *et al.* decreased the conductivity of the sample buffer by the addition of methanol or other organic solvents.[52] In this work, dilutions of the 12.5 mM phosphate separation buffer at

A)

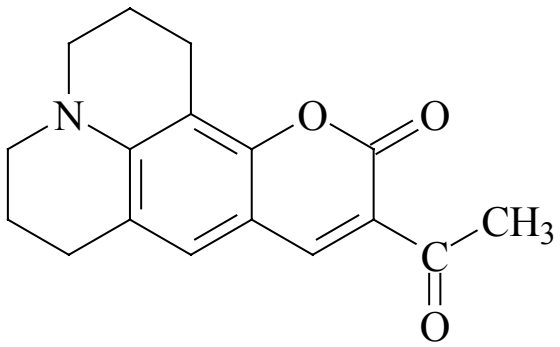

B)

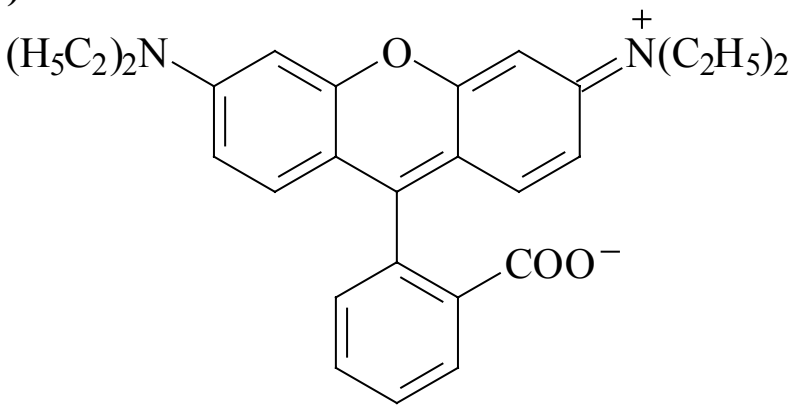

Figure 4-2. Structures of (A) coumarin 334 and (B) the zwitterionic form of rhodamine B.

pH 6.5 (0.125 mM and 41.7 μM phosphate) were used to achieve a region of decreased conductivity instead of adding methanol.

Figure 4-3A shows an electropherogram with UV/VIS absorbance detection following a 2.0-min hydrodynamic injection of the three arsenic containing compounds dissolved in the running buffer (12.5 mM phosphate). Under these conditions, there was no discontinuity between the sample and separation buffers, and no sample stacking occurred. Figure 4-3B shows an electropherogram for a 2.0-min hydrodynamic injection of the sample dissolved in a 1:100 dilution of the running buffer (0.125 mM phosphate). The three peaks in Figure 4-3B are clearly sharper and higher than the peaks in Figure 4-3A, indicating that sample stacking has occurred. The 2.0-min injection time was optimized to produce the best resolution of the three compounds for injection in the 0.125 mM phosphate buffer.

During the separation shown in Figure 4-3B, EOF and current through the capillary were monitored (Figure 4-3C). The length of the dilute sample plug after a 2.0-min injection (1.9% of the total capillary length) was not large enough to cause changes in EOF that could clearly be measured. The plot of current versus time qualitatively resembles what is predicted by the model of Thormann and coworkers.[51] A region where no EOF data was recorded is also indicated in Figure 4-3C (443-469 s). This region corresponds to the migration past the LIF detector of the dilute sample plug. During this time, the fluorescence dropped and not photobleached peaks were observed at F2. It is not clear what the cause of this is. One possible explanation is that temperature increases in the sample zone during stacking causes thermal degradation of the coumarin 334.[164,165] While current is measured across the total length of the capillary, the UV/VIS and EOF detectors make measurements at different points along the capillary. As the analytes and dilute sample plug migrate through the capillary, the time at which the analyte and sample plug pass each of these positions is different. It is important to keep the different times at which an electrophoretic zone is observed in mind when examining.

The hydrodynamic injection time was increased to 4.0 min (3.8% of the capillary) in an attempt to increase the magnitude of the EOF changes during the FASS experiment. As shown in Figure 4-4A, the three arsenic containing compounds are still baseline resolved, but the resolution is slightly less than for a 2.0-min injection (Figure 4-3B). Equation 4-1 predicts that the increased length of the injection (4.0 min) will result in an increased effect of the dilute sample plug on the bulk EOF.[49,50] The EOF dynamics measured during the FASS experiment are much more defined for the 4.0-min injection (Figure 4-4B). The most remarkable aspect of this result is the qualitative similarity to the EOF changes during a FASS experiment predicted by the computer model of Thormann and coworkers (Figure 5A in Ref. 51).[51] This close qualitative resemblance is despite substantial differences in the experimental conditions used here and the conditions used for the modeling experiments (buffer, pH, dilution factor and applied potential field). The model of Chien and Burgi (Equation 4-1) would predict constant EOF until elution of the dilute sample plug begins at ~510 s.[49,50]

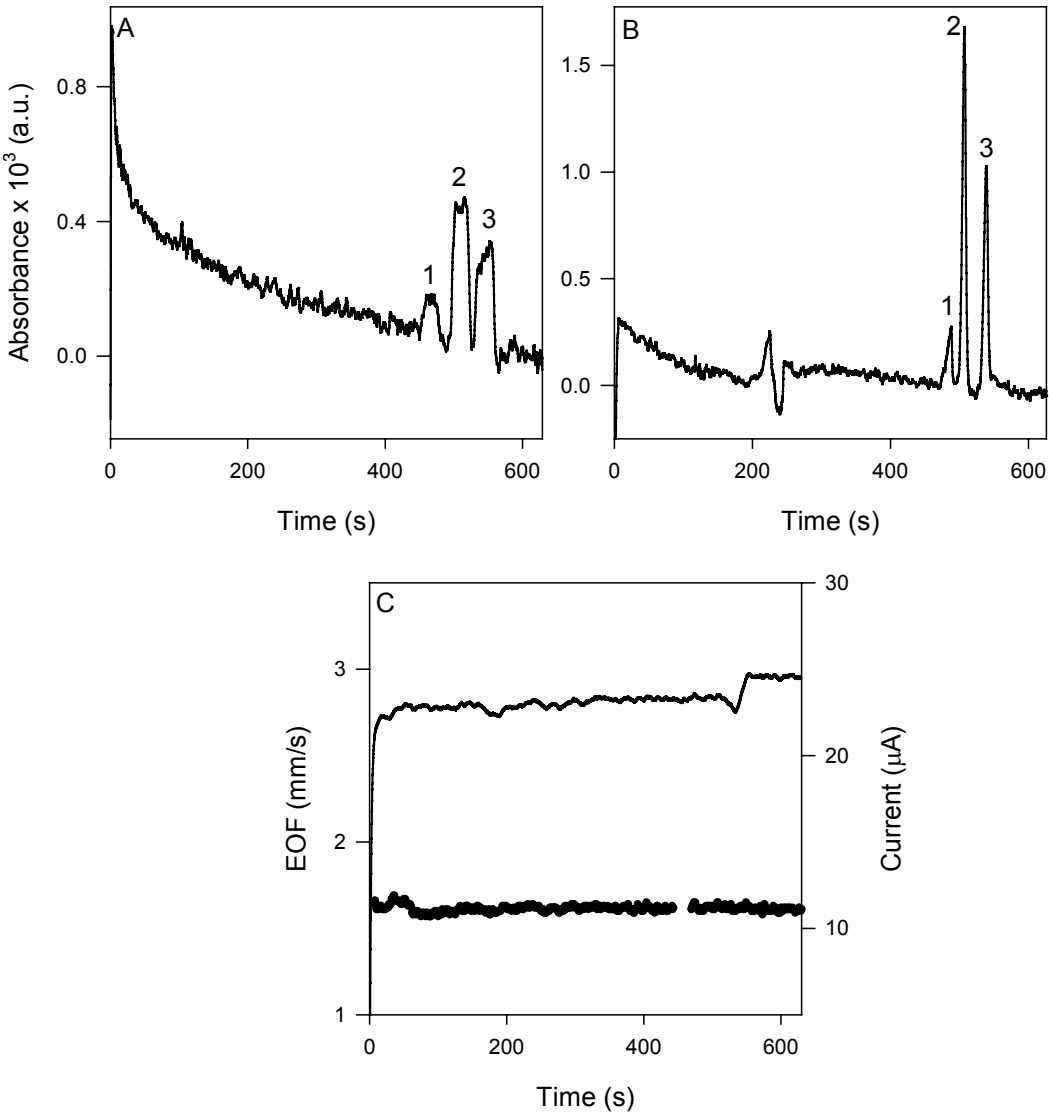

Figure 4-3. Electropherogram of a separation of arsenic compounds dissolved in (A) 12.5 mM phosphate buffer and (B) 0.125 mM phosphate buffer. The samples were hydrodynamically injected for 2.0 min (height = 14.0 cm). The running buffer was 12.5 mM phosphate buffer (pH = 6.5). The peaks in the electropherograms in (A) and (B) are: 1) DMA ; 2) PABA; 3) PAA. (C) EOF rate (•) and current (solid line) vs. time for the electropherogram presented in (B). All solutions contained 15 nM coumarin 334. (Applied potential = 333 V/cm; UV/VIS detection, λ = 200 nm; bleaching power = 50.0 mW; LIF detection power = 12.6 mW; bleaching pulse duration = 75 ms; d_{F1-F2} = 1.03 mm).

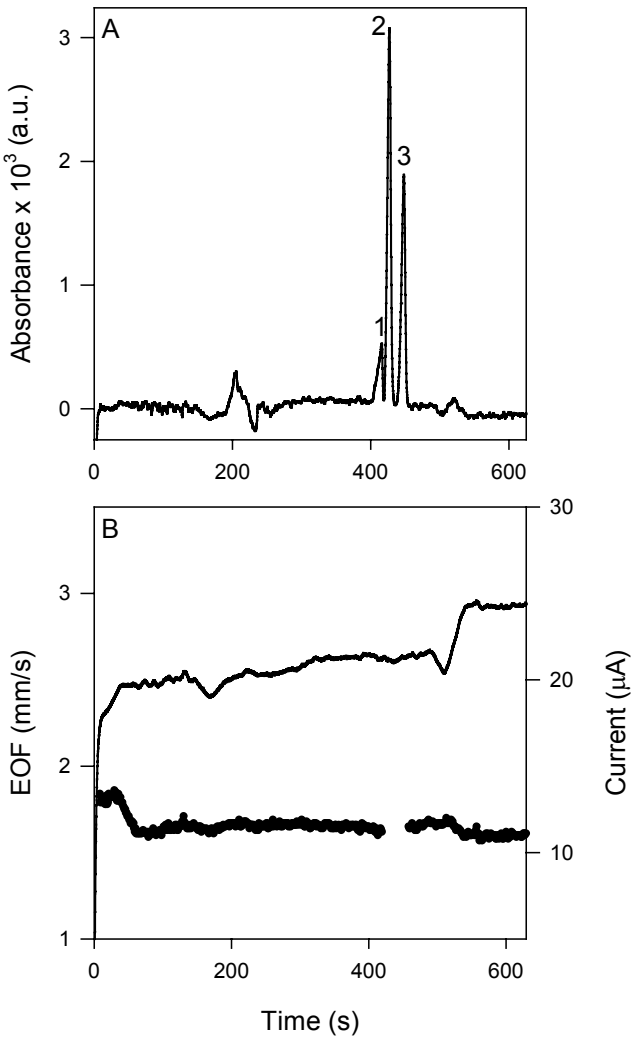

Figure 4-4. An (A) electropherogram with (B) EOF (•) and current (solid line) for a separation of three arsenic containing compounds after a 4.0-min hydrodynamic injection of sample dissolved in 0.125 mM phosphate buffer. Peak identities and other experimental conditions are the same as in Figure 4-3.

The measured EOF begins at 1.8 mm/s from 8-38 s and then rapidly decreases to 1.6 mm/s at ~61 s. From 61 s to 520 s the EOF remains fairly constant at 1.65 mm/s. The EOF then drops to 1.60 mm/s by 537 s when the dilute sample plug has eluted from the capillary. During the course of the separation, there is a gradual increase in the current through the capillary (solid line, Figure 4-4B) as expected.[51]

Figure 4-5A shows an electropherogram of a separation following a 10.0-min sample injection (9.5% of the capillary). Under optimized conditions (2.0-min injection), the analytes are well resolved, as seen in Figure 4-3B. Following a 10.0-min injection, a single peak is observed with no separation of the three compounds. This phenomenon has been described previously in the literature.[155,158-160] The loss of resolution results from both an increase in EOF and a decrease in the potential field in the running buffer (12.5 mM). The longer sample plug results in higher overall EOF, and the analyte zones migrate to the detector in less time, resulting in a loss of resolution. Additionally, the enhanced field strength in the large sample zone, which causes sample stacking, lowers the field strength in the running buffer (12.5 mM) where the separation takes place. For the long 10.0 min injection these two effects result in a complete loss of resolution of the three analytes.

Figure 4-5B shows the EOF and current for the 10.0 min injection. At 23 s the EOF is at a maximum value of ~3.3 mm/s and then decreases to ~2 mm/s at 42 s. Following the elution of the dilute sample plug (~380 s), the EOF decreases to 1.64 ± 0.02 mm/s. The effect of the sample plug on the current through the capillary was also larger than that for the experiments shown in Figures 4-3 and 4-4, starting at 6 μA and gradually rising to 12.2 μA over 380 s. At 380 s, the current increases sharply to 24.6 μA. The EOF data in Figure 4-5B from 0-380 s is noisy due primarily to poor S/N of the EOF monitoring peaks. This poor S/N is caused by broadening of the peaks due to laminar flow as discussed in the following section. There could also be a contribution from real variability in the EOF since the electrophoretic current is relatively unstable during this time.

FASS Induced Pressure Gradients

The presence of zones of sample and solution buffers in a capillary at different concentrations with different potential field strengths will lead to mismatches in local electroosmotic velocities. This will create pressure gradients and laminar flow which counteract peak narrowing by FASS.[49,50,155,158,160,161] Figure 4-6 shows the width of the photobleached peaks (fwhm) following 4.0 and 10.0-min injections of the analyte mixture in 0.125 mM buffer. In Figure 4-6A (4.0-min injection), the peak widths start at a maximum value of 0.21 s before decreasing to 0.11 at 55 s. The peak widths have an average value of 0.111 ± 0.009 s from 55 to 510 s. The peak widths are 0.085 ± 0.003 s from 530 s to the end of the experiment. Following a 10.0-min injection (Figure 4-6B), the broadening of the photobleached zones due to laminar flow is increased. The peak width begins at 0.31 s (average value, 0-20 s) and decreases to 0.23 s by 390 s. A sharp decrease in peak width is observed from 390 to 430 s before they stabilize at 0.086 ± 0.002 s. The broad peaks before the elution of the sample zone for the 10.0 min

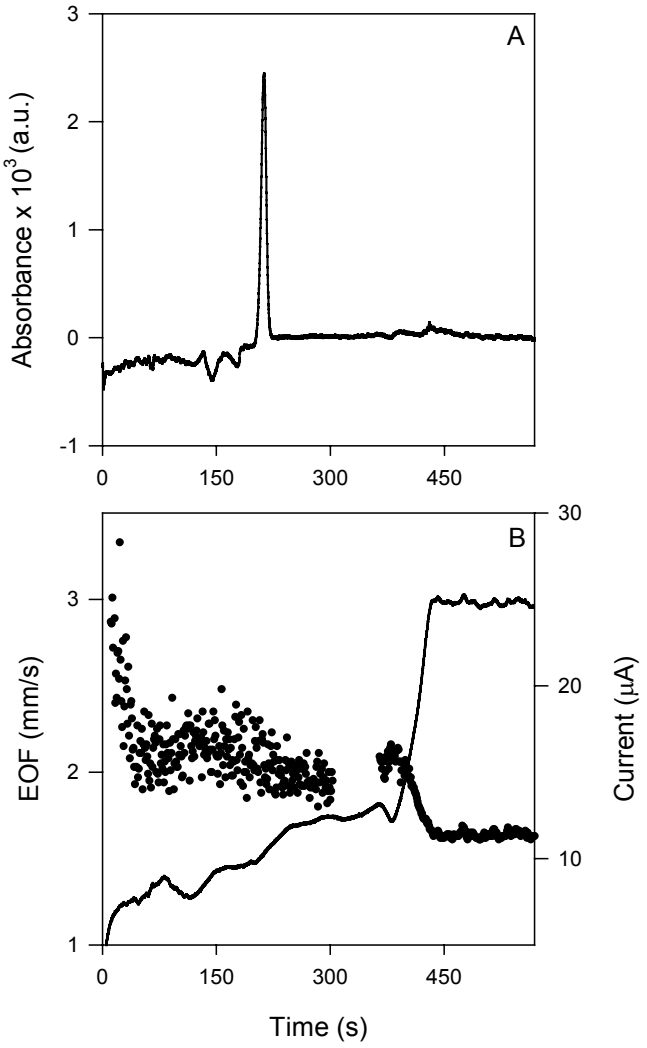

Figure 4-5. An (A) electropherogram with (B) EOF (•) and current (solid line) for a separation of three arsenic containing compounds after a 10.0-min hydrodynamic injection of sample dissolved in 0.125 mM phosphate buffer. All other experimental conditions are the same as those in Figure 4-3.

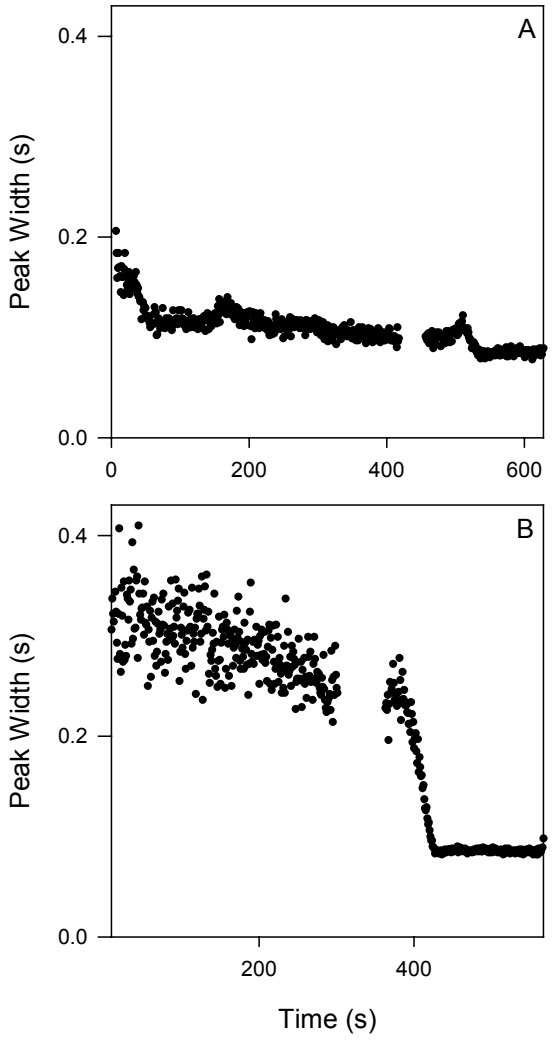

Figure 4-6. Peak widths of the photobleached zones (fwhm) during FASS experiments. Sample was injected hydrodynamically for (A) 4.0 min and (B) 10.0 min. Experimental conditions are identical to those for Figure 4-3.

injection also result in poor S/N as indicated by the scatter in the data in Figure 4-6B and Figure 4-5B.

It is interesting that the changes in peak width during FASS experiments (Figure 4-6) appear to correspond to the changes in EOF (Figures 4-4B, 4-5B). This occurs because both the changes in peak width and EOF reflect changes in the sample plug as it migrates through the capillary. As the sample plug degrades due to diffusion and laminar flow, its impact on EOF and the generation of laminar flow decrease. When the sample plug elutes from the end of the capillary, EOF and peak widths return to values characteristic of the higher concentration running buffer.

The presence of laminar flow and its effects on the shape of the photobleached zones must be kept in mind when analyzing EOF monitoring data from the periodic photobleaching technique. During the calibration, the buffer inside the capillary is homogeneous and no electrophoretic mismatch or laminar flow is present when measuring $d_{F1\text{-}F2}$. If the front or rear of the photobleached zone is used to measure migration times ($t_{F1\text{-}F2}$) in the presence of laminar flow, a flow rate which is greater or less than the actual value will be measured, respectively. Broadening of the photobleached zone will not affect the migration time of the peak center, but will result in a decrease in peak depth and S/N.

Impact of Shorter, More Dilute Sample Plug Injections

Samples were prepared in 41.7 μM phosphate buffer to examine EOF dynamics for FASS experiments with more dilute sample solutions. Injection times (27, 45 and 74 s) were selected to produce EOF values equivalent to 2.0, 4.0 and 10.0 min injections from 0.125 mM buffer according to Equation 4-1. Although there was evidence of sample stacking, significant changes in EOF and electrophoretic current were not observed. Figure 4-7 shows an electropherogram, EOF and current data from a 74-s injection (1.2% of the capillary) in 41.7 μM buffer. All three analyte peaks are baseline resolved in the electropherogram (Figure 4-7A) and exhibit peak widths (fwhm) of 6.75, 6.75 and 7.59 s (peaks 1, 2 and 3, respectively). In the absence of sample stacking and ignoring the effects of longitudinal diffusion, a 74-s injection would result in peak widths of 9.07, 9.66 and 10.3 s. Clearly sample stacking has occurred. In Figure 4-7B, EOF begins at 1.69 mm/s and decreases to 1.62 mm/s in the first 30 s of the separation. An average value of 1.62 ± 0.01 mm/s is observed for the remainder of the experiment.

These changes in EOF and electrophoretic current are much smaller than what was expected based on Equation 4-1. Although the EOF and current data do not suggest that significant sample stacking has occurred, the peak widths in Figure 4-7A do suggest sample stacking has taken place. Analysis of the peak widths for the EOF monitoring data did not indicated the presence of laminar flow. All the FASS experiments presented in this paper, including those in Figure 4-7, were repeated without the three arsenic compounds to determine the impact of the sample ions on the experiments. The absence of the arsenic compounds did not significantly change the results for the experiments presented in Figure 4-7 or Figures 4-3, 4-4, 4-5 and 4-6 (data not shown).

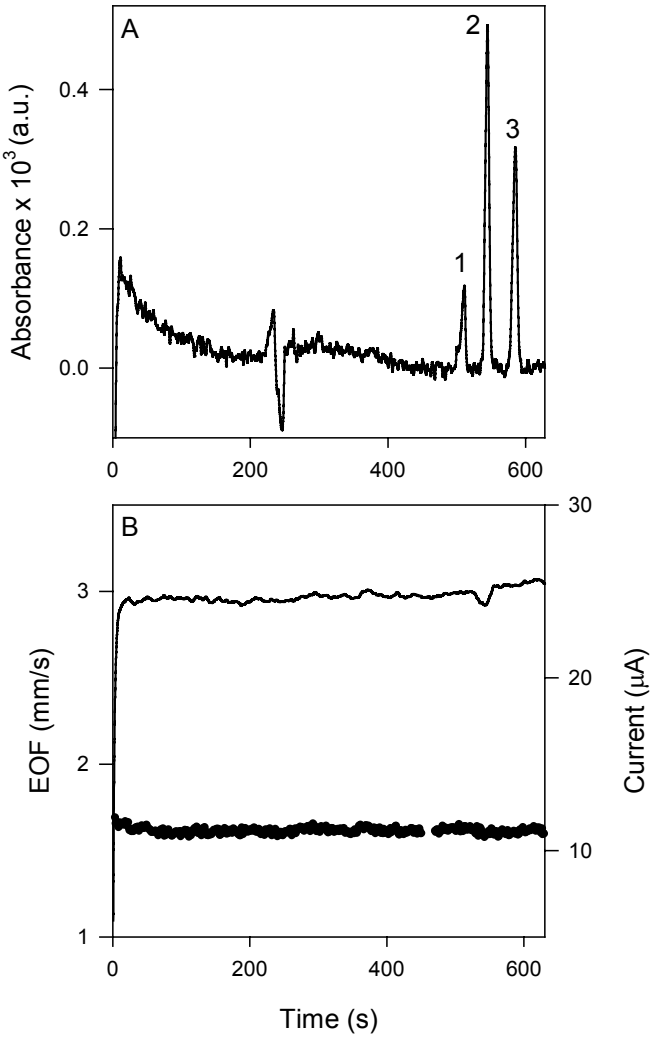

Figure 4-7. An (A) Electropherogram with (B) EOF (•) and current (solid line) for a separation of three arsenic containing compounds after a 74-s hydrodynamic injection of sample dissolved in 41.7 μM phosphate buffer. Peak identities and all other experimental conditions are identical to those for Figure 4-3.

One possible explanation for the data in Figure 4-7 is that sample stacking took place vary rapidly at the beginning of the experiment, but the short, dilute sample buffer zone rapidly degraded due to laminar flow and extreme thermal effects before the effects on EOF could be detected. The short, dilute sample zone will experience a very high potential field, which will result in extreme Joule heating. Temperature increases as high as several hundred °C have been suggested for FASS experiments.[165] This heating would rapidly degraded the sample solution zone by thermal convection. In addition, the EOF mismatch between the sample zone and running buffer would be very high, which would contribute to the rapid degradation of the sample solution zone. Experimental artifacts did not allow very early effects on electrophoretic current and EOF to be observed. First, the measured time constant for the electrophoretic current is 4.8 s, so early changes in current would be severely dampened. Second, EOF was only measured at 1 Hz, and no EOF data were obtained during the first 3 to 10 s of each experiment. Much of the coumarin 334 near the LIF detector was photobleached during the hydrodynamic injection, so no fluorescence was detected until a few seconds after the separation potential was applied.

Conclusions

Changes in EOF occurring during a sample stacking separation of three arsenic species have been monitored at a rate of 1 Hz using a technique based on periodic photobleaching of a dilute, neutral fluorophore added to the separation buffer. Injections of a sample prepared in the separation buffer (12.5 mM phosphate buffer) were confirmed to have no effect on EOF during a separation. However, injections of analyte dissolved in a 1:100 dilution of separation buffer (0.125 mM phosphate buffer) caused changes in EOF that are qualitatively consistent with the predictions by Thormann *et al.*[51] The presence of FASS-induced laminar flow has been monitored by observing broadening of the negative photobleached zones used for EOF monitoring. The ability to monitor EOF during an electrophoretic experiment will enable researchers to better understand and optimize electrophoretic experiments that result in changing EOF. This approach is also important for quantitatively testing theoretical models describing EOF dynamics.

Acknowledgments

Financial support for this work was provided by the University of Tennessee. K.F.S. was supported by the NSF RSEC Program at UT (9974734).

CHAPTER V

Optically Gated Vacancy Electrophoresis in Microfluidic Devices

This chapter is a slightly revised version of a paper by the same title accepted for publication in the journal *Analytica Chimica Acta* in 2003 by Jason L. Pittman, Anton I. Terekhov, Steven W. Suljak and S. Douglass Gilman:

Pittman, J. L.; Terekhov, A. I.; Suljak, S. W.; Gilman, S. D. *Anal. Chim. Acta* **2003,** *Accepted for Publication.*

Abstract

Electrophoretic vacancy separations with optically gated injections are presented as an alternative method of performing separations in microfluidic devices. Vacancy electrophoretic separations of FITC-labeled amino acids have been performed over a separation distance of 0.9 cm at a field strength of 353 V/cm, with an injection every 8.0 s. For a series of 10 vacancy electrophoretic separations with 100-ms (177 pL) optically gated injections, the RSD for retention times was 0.17% and the RSD for peak height was 1.6%. The performance of optically gated vacancy electrophoresis has been quantitatively compared to the performance of standard optically gated electrophoresis for the same separation using the same microfluidic device and identical experimental conditions. For these separations, the overall performance of the two optically gated injection methods is similar. The resolution obtained with the electrophoretic vacancy separations was slightly lower (6-14%) than with the standard electrophoretic separations due to the larger injection volume for optically gated vacancy injection, using the same injection time.

Introduction

Reproducible injection of discrete sample plugs into separation channels in microfluidic devices is a current topic of intensive investigation.[14,18,38,88,111,134,135,166-178] In capillary electrophoresis, a sample injection can be made by placing the injection end of the capillary in a vial containing the sample and using either hydrodynamic or electroosmotic flow to inject a plug of sample into the capillary. The injection end of the capillary is returned to a vial containing the background electrolyte. This straightforward injection strategy cannot be practically applied to microfluidic devices. A variety of methods for making discrete injections from a sample channel that intersects the separation channel in a microfluidic device have been reported in the literature.[14,18,38,88,135,166-173,177]

One common form of sample introduction from a channel crossing the separation channel in a microfluidic device is a "floating" injection.[18,88,134,135,170,177] In a floating injection, a potential is applied to one of the cross channel reservoirs (1, Figure 5-1), and the second reservoir (2, Figure 5-1) is connected to ground. During the injection process, the sample and waste reservoirs (S and W, Figure 5-1) are allowed to float electrically. The volume of analyte injected using this technique increases with increasing injection time due to leaking of the injected analyte plug into the separation channel.[88] In order to reduce the amount of sample leaking into the separation channel from the injection channel during a floating injection, the "double-T" injector was developed to physically limit the amount of analyte injected to the volume of the channel intersection.[18,38,134,170,171] Two related approaches, the pinched injection and the gated-valve injection, have been described.[14,18,88,134,135,166,168-173] Electrophoretic injection bias is reduced for these two methods by controlling the applied potentials at 3-4 reservoirs to spatially confine the sample stream to the intersection of the sample channel and the separation channel. By strictly confining the sample plug to the channel intersection, a representative amount of all analytes is injected. All of these methods require a cross channel that intersects the separation channel and application of a potential across at least two buffer reservoirs in order to perform an injection. These methods allow discrete injections of analyte into the separation channel, but require the interruption of the electrophoretic potential to make an injection. Interfacing of microfluidic chips to continuously flowing sample streams external to the microfluidic device has been reported. Discrete injections of analyte into the separation channel of the microfluidic device from the channel interfaced to the external sample stream still use the same injection methods discussed above and require significant modification of the microfluidic device in order to be coupled with the external sample source.[174,175,178]

Optically gated injections have been demonstrated in microfluidic devices as an alternative approach to sample injection for electrophoretic separations.[111] This approach does not require construction of intersecting channels or rapid, coordinated switching of applied potentials in multiple wells on the device. Optically gated injections were originally developed in capillaries to perform rapid electrophoretic separations (0.5 s - 3 s).[106-110,170] To perform an optically gated injection, the separation channel is filled with the sample mixture. A laser beam is disproportionately split into two beams. The more intense split beam acts as the gating beam and is directed to a point on the separation channel where the optically gated injection takes place. The gating beam continuously irradiates the sample solution, photobleaching the fluorophore-labeled analyte molecules. The less intense portion of the split beam is directed to another point on the separation channel and is used for laser-induced fluorescence (LIF) detection. When the gating beam is briefly blocked, a plug of unbleached, fluorescent sample is left behind in the channel. The analytes in the sample plug are separated and detected as fluorescence peaks at the downstream LIF detector.

Lapos and Ewing adapted optically gated injections from capillaries to microfluidic chips and were able to perform six separations in less than 30 s. The separations showed less than a 1% RSD for retention times and a 2.6% RSD for peak areas. The volume of analyte injected can be changed by simply increasing or decreasing

the length of the injection time (shutter closed) and is not limited by the dimensions of the channel intersection on the microfluidic device.[111]

We recently reported a method for continuous monitoring of electroosmotic flow in capillaries.[86,146] This technique is based on repeated measurement of the migration rate of a photobleached zone generated by optical gating in a capillary filled with a neutral fluorescent dye at nanomolar concentrations. This flow monitoring technique is experimentally similar to optically gated electrophoresis,[106] except that for flow monitoring, the gating beam is unblocked during injection and is blocked during migration of the injected zone. A constant fluorescence signal from the neutral fluorophore is observed at the LIF detector, and opening the shutter that blocks the bleaching beam generates photobleached zones, which are detected as negative peaks at the LIF detector. This flow monitoring method can also be described as an optically gated vacancy electrophoretic separation of a neutral compound. Vacancy electrophoretic separations have been studied in capillaries.[179-181] In these studies, a capillary was filled with a sample mixture, and a vacancy injection was performed by introducing a short zone of running buffer, which did not contain the analytes to be separated. These experiments result in an electropherogram with negative, vacancy peaks, which migrate at the same rate as the corresponding chemical components of the sample mixture.

In this paper we present a study of optical gating as an injection method for performing vacancy electrophoretic separations in microfluidic devices. The reproducibility of this injection method has been examined, and the effect of the duration of the optically gated injection on the resolution, efficiency and peak heights for vacancy separations has been explored. The analytical performance of optically gated vacancy electrophoresis has been directly compared to standard optically gated electrophoresis[106,111] using the same separation channel and optical system, identical sample mixtures and electrophoretic conditions, the same injection times, and the same gating and detection beam powers.

Experimental Section

Chemicals

L-(+)-aspartic acid (Asp), L-(+)-arginine hydrochloride (Arg) and 5-fluorescein isothiocyanate (FITC) were obtained from Acrōs Organics (Pittsburgh, PA). L-phenylalanine (Phe) was purchased from Aldrich (Milwaukee, WI), and boric acid was purchased from Mallinckrodt (Phillipsburg, NJ). All solutions were prepared in doubly distilled water.

Microfluidic chip

A simple cross-T microfluidic chip manufactured from low fluorescence Borofloat glass was purchased from Micralyne (Edmonton, Alberta, Canada). The channels in the chip were 50 μm wide and 20 μm deep. The main separation channel was

8.5 cm in length with an 8.0-mm long injection channel located perpendicular to the separation channel, 5.0 mm from the sample reservoir (S in Figure 5-1). The injection channel was not used for these experiments. Buffer reservoirs were fashioned from pieces of micropipette tips (1000 μL Fisher*brand* Redi-Tip; Fisher Scientific; Phillipsburg, NJ) and attached to the microchip with 5 Minute epoxy (Devcon, Danvers, MA). Electrical connections to the microfluidic chip were made with platinum wire electrodes inserted into the sample and waste reservoirs (W in Figure 5-1). The electrophoretic potential (+3000 V) was applied to the sample reservoir with a Bertan Associates Model 215, 3000 V power supply (Hicksville, NY), and the waste reservoir was connected to ground. The remaining two buffer reservoirs (1 and 2 in Figure 5-1) were allowed to float electrically. (***Danger:*** *Extreme caution must be used when working around the exposed high-voltage connections present in this apparatus.*) Filling of the channels was achieved by filling three reservoirs (S, 1 & 2, Figure 5-1) with buffer solution and applying a mild vacuum to the waste reservoir until no air-bubbles were observed in the channels.

Optical Gating and LIF Instrument

The instrument used for optical gating and LIF detection was a modified version of an instrument described previously for measuring electroosmotic flow in capillaries.[86,146] For this work, the microfluidic chip was mounted horizontally on an XY-translation stage (TSX-10; Newport, Irvine, CA) so that the separation channel could be easily aligned underneath the LIF detection and optical gating optics. An Argon-ion (Ar^+) laser beam (488.0-nm line; Coherent Innova 90C-5; Santa Clara, CA) was split with a broadband, cubic beam-splitter. One split beam was used for LIF detection and the other was used for optical gating. The gating and detection beams for both optically gated vacancy injections and optically gated injections were 130 and 6 mW, respectively. The detection beam was attenuated to 6 mW with neutral density filters to prior to being turned 90° by a dichroic mirror (505DRLP; Omega Optical; Brattleboro, VT). The detection beam was then reflected down with a mirror and passed through a 5× microscope objective (N.A. = 0.12). The microscope objective was mounted at 90° relative to the microchip on an XYZ-mount (LP-1-XYZ; Newport, Irvine, CA) to facilitate alignment and focusing. The detection beam was focused onto the separation channel at D (Figure 5-1) by the microscope objective, and the fluorescence was collected by the same microscope objective at 180° relative to the source. The fluorescence passed through the dichroic mirror and was then spectrally and spatially filtered. A 510 nm cut on long-pass glass filter (03FCG483; Melles Griot; Irvine, CA) was used to remove scattered light at the source wavelength, and a 560 nm cut off short-pass filter (35-5347; Coherent Auburn Group; Auburn, CA) was used to reduce Raman scattering from water. The fluorescence was spatially filtered with a 1.4-mm diameter pinhole prior to being detected by a PMT (Hamamatsu HC120; Bridgewater, NJ).

The gating beam was directed through a computer-controlled shutter (Uniblitz LS6Z2; Vincent Associates; Rochester, NY), which was either opened or closed by a +5 V TTL signal from the data-acquisition and instrument control program. Once the gating

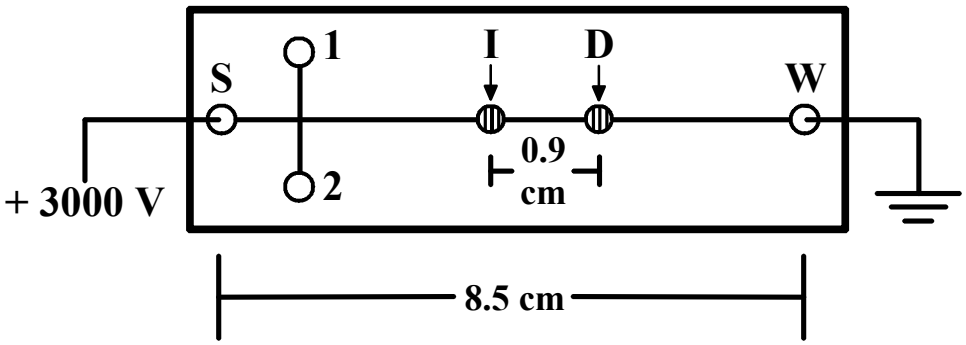

Figure 5-1. Diagram of the microfluidic device. The electrophoretic potential (+3000 V) is applied at the sample reservoir (S) with the waste reservoir (W) at ground. The distance between the injection (I) and LIF detection (D) points is 0.9 cm. The cross-channel reservoirs (1 & 2) are filled with buffer and left to float electrically. The total channel length (S to W) is 8.5 cm.

beam passed through the shutter, it was directed downward through a plano-convex lens (f = 100 mm) and focused onto the injection point on the separation channel (I, Figure 5-1). The focusing lens was mounted on an XYZ-translation stage to aid in the positioning and focusing of the gating beam.

Derivatization of Amino Acids with FITC

The amino acids were derivatized with FITC by adding a stoichiometric excess of amino acid in 20 mM borate buffer (pH = 8.5) so that the concentration of detectable, FITC-labeled amino acids was equal to the FITC concentration. Individual samples were prepared by combining 12.6 mM FITC with Arg (23 mM), Asp (19.8 mM) or Phe (18.9 mM) in a total volume of 1.25 mL. The solutions were then allowed to incubate in a darkened drawer at room temperature for four hours in sealed micro-centrifuge tubes.[182] These stock solutions were then stored in the dark at 4 °C until diluted for use. Each of the three FITC-labeled amino acids was diluted to a final concentration of 500 nM for experiments.

Optically Gated Injections and Electrophoretic Separations

Optically gated *vacancy* injections were carried out by leaving the shutter blocking the gating beam closed, and then opening it briefly to make an injection by photobleaching.[86,146] The shutter was opened for 25, 50, 100, 250, 500 or 750 ms every 8.00 s. The corresponding injection volumes for vacancy injections were 74.3, 109, 177, 383, 725 and 1070 pL. Optically gated injections were carried out by leaving the shutter open and then closing it briefly to inject a plug of sample into the separation channel.[106,111] The injection volumes for optically gated injections were 0, 28.5, 97.0, 303, 645 and 988 pL. Prior to filling with the mixture of amino acids, the channels were rinsed with 0.1 M NaOH followed by methanol. The channels of the microchip were then filled with 20 mM borate buffer (pH = 8.5) containing 500 nM concentrations of FITC-labeled Arg, Asp and Phe and allowed to electrophorese (3000 V, 353 V/cm) until a stable current was observed (1.0 μA).

Instrument Control, Data Acquisition and Analysis

A program was written in LabVIEW (National Instruments; Austin, TX) to control the shutter and acquire all data. All data were filtered with a 50 Hz RC low-pass filter prior to being acquired at 250 Hz with a National Instruments PCI-6024E data acquisition board. After acquisition, data were imported into Peak Fit (SPSS Science; Chicago, IL) and digitally filtered at 10 Hz with a FFT low-pass filter. All other data analysis was conducted in Microsoft Excel (Microsoft Corp.; Redmond, WA). The signal to noise ratio (S/N) was calculated by dividing the peak height (positive or negative) by the standard deviation of the baseline signal.

Results & Discussion

Optically Gated Vacancy Electrophoresis

We have demonstrated a series of reproducible vacancy electrophoretic separations using optically gated injections in a microfluidic device. Vacancy electropherograms for a series of three successive optically gated injections are presented in Figure 5-2. The separation channel is filled with a solution containing a mixture of three amino acids at 500 nM each, and an electrophoretic potential is applied (353 V/cm). A constant fluorescence signal from all three analytes is observed at the LIF detector. The shutter is opened for 100 ms, exposing the FITC-labeled amino acids to the gating beam (130 mW) at the injection point on the separation channel (I, Figure 5-1) to create a photobleached zone. The TTL pulses applied to open the shutter are also shown in Figure 5-2. The vacancy zones, created by photobleaching the three labeled amino acids, separate as they migrate 0.9 cm down the separation channel to the LIF detector at D in Figure 5-1. The individual analyte peaks for the first injection (Arg 1, Phe 1 and Asp 1; Figure 5-2) are detected as vacancies (decreased fluorescence against a constant fluorescence background). The next sample injection (Inj 2, Figure 5-2) is performed prior to the completion of the first separation, and vacancy peaks are detected later as Arg 2, Phe 2 and Asp 2.

Optical gating at position I (Figure 5-1) can be used to perform a subsequent vacancy injection without interruption of the electrophoretic potential as the previously injected sample is still being detected downstream at position D (Figure 5-1).[108,111] For the work presented here, a separation was conducted every 8.00 s although the total separation time was approximately 13 s. The serial injections were reproducible, with a series of ten 100-ms (177-pL) injections producing Arg peak heights with a RSD of 1.6%. The Arg retention times exhibited a RSD of 0.17%, which is consistent with the < 1% injection-to-injection variation observed by Lapos and Ewing.[111]

The duration of the optically gated vacancy injection was varied from 25 ms to 750 ms (74.3 to 1070 pL) in order to examine the effects of injection time on the vacancy electrophoretic separations. Figure 5-3 illustrates the effect of injection time on peak height for Arg. In previously published work, it has been shown that under conditions of constant flow rate and laser power, the percentage of fluorophore photobleached increases as the injection time is increased, until a plateau is reached.[146] The data shown in Figure 5-3 are consistent with this earlier observation. The maximum peak height is reached when two conditions are met: 1) the volume of flow during the time that the shutter is open exceeds the volume irradiated by the bleaching beam and 2) the attenuation of the analyte peak due to diffusional broadening is negligible.[146] The reproducibility of injections based on peak height improves with increasing injection time. The RSD of the peak height for Arg decreases from 2.9% for a 25-ms (74.3-pL) injection to 0.5% and 0.6% for 500-ms (725-pL) and 750-ms (1070-pL) injections, respectively. This is due to an improvement of the S/N, from 24 for a 25-ms (74.3-pL) injection to 156 for a 500-ms (1070-pL) injection. The fluorescence baseline, which determines the detection noise, is not affected by the injection time.

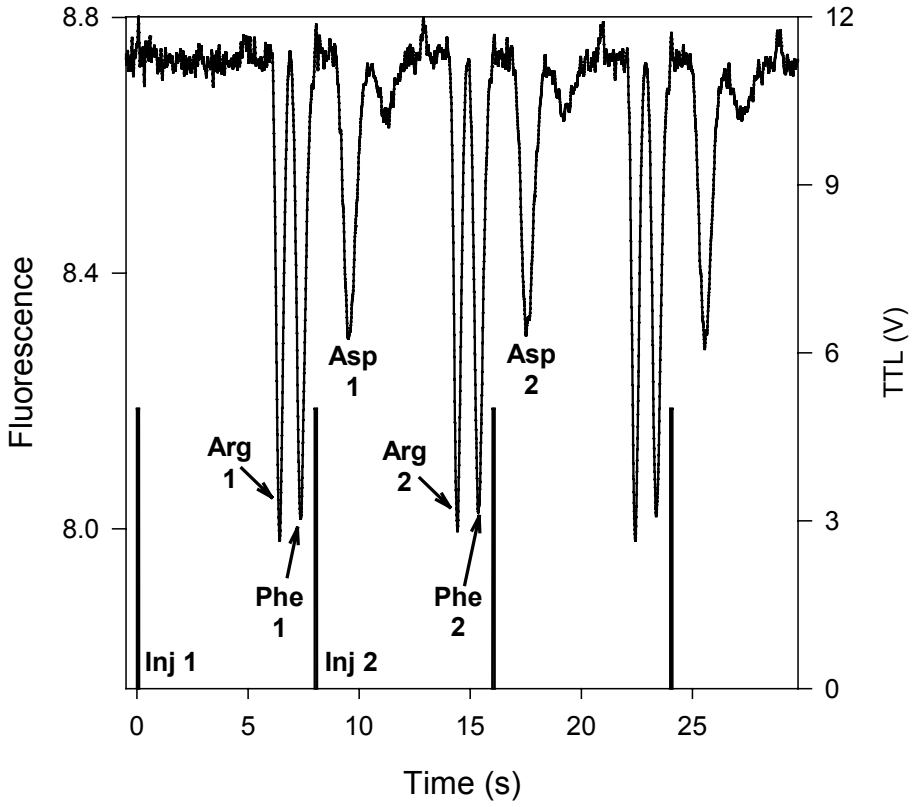

Figure 5-2. Series of 3 vacancy electrophoretic separations. The injections are 100-ms long and are indicated by the TTL trace at the bottom of the figure. Peaks for arginine, phenylalanine and aspartic acid (Arg 1, Phe 1 and Asp 1) correspond to analytes injected at Inj 1. Arg 2, Phe 2 and Asp 2 correspond to Inj 2. All analytes were at a concentration of 500 nM FITC-labeled amino acid. The applied potential field was 353 V/cm. The power of the gating and LIF detection beams were 130 and 6 mW, respectively.

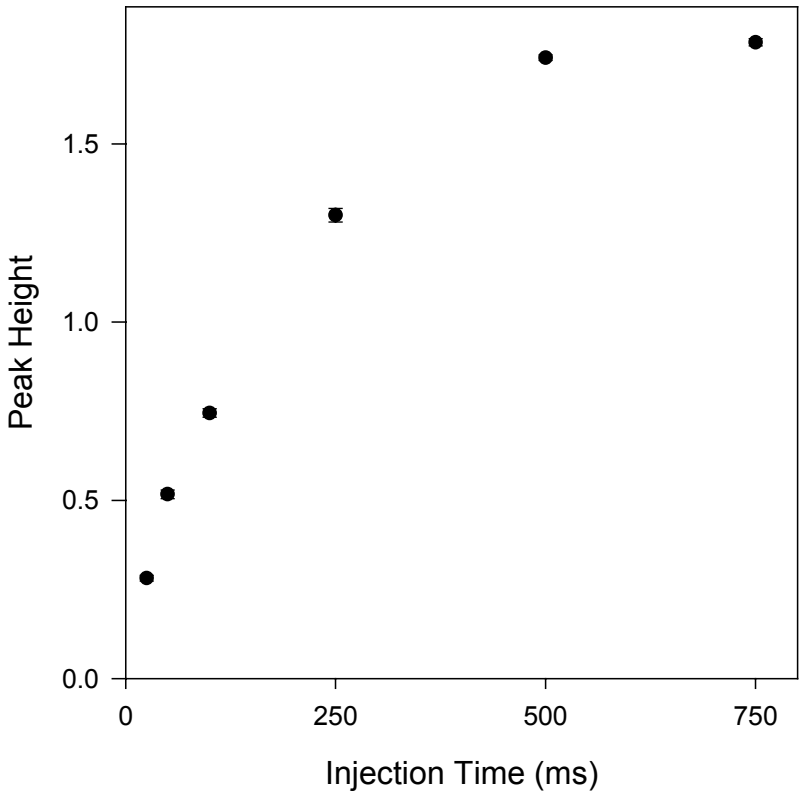

Figure 5-3. Peak height for Arg versus optically gated vacancy injection time. Error bars are ± 1 S.D.

As the injection time is increased, a decrease in separation efficiency for the Arg peak (Table 5-1) and a decrease in resolution of the Arg and Phe peaks (Figure 5-4) are observed. At very short injection times, separation efficiency and resolution are limited primarily by longitudinal diffusion of the short photobleached zone as it migrates to the detector.[107,146] The data in Table 5-1 and Figure 5-4 show that the separation efficiency and resolution are reduced only slightly as the duration of the optically gated vacancy injection is increased from 25 ms to 100 ms. As the injection time is increased beyond 100 ms, the duration of the optically gated vacancy injection begins to dominate the observed separation efficiency and resolution, which both decrease.

These results indicate that a careful compromise must be made between separation efficiency and detectability. A 5-fold decrease in injection time from 500 ms to 100 ms results in a 57% decrease in Arg peak height and a 48% increase in resolution. A 4-fold decrease in injection time from 100 ms to 25 ms results in a 62% decrease in Arg peak height and a negligible (4.5%) increase in resolution. An injection time of 100-ms provides a resolution of 1.4 with a S/N of 53 for the Arg peak. An increase in S/N can also be achieved by increasing the laser power to the gating beam, resulting in a larger percentage of the fluorescently labeled analyte being photobleached during the injection.[106,109,146]

Optically Gated Vacancy Electrophoresis Versus Standard Optically Gated Electrophoresis

We have compared the performance of optically gated vacancy and standard optically gated electrophoretic separations. Standard optically gated electrophoretic separations [106,111] were performed using optics, solutions and separation conditions identical to those used for the optically gated vacancy electrophoretic separations. In order to perform the standard optically gated separations, the response of the shutter blocking the gating beam to a TTL pulse was reversed from that used for the optically gated vacancy separations.

Figure 5-5 shows the injection process for optically gated vacancy electrophoresis (A, C, E) and standard optically gated electrophoresis (B, D, F). For the purpose of this discussion, it is assumed that photobleaching of the fluorescent analyte is instantaneous and that the intensity of the focused gating beam is uniform across its diameter. Figures 5-5A and 5-5B represent the concentration of the fluorescent analyte at the instant the shutter is opened to start an optically gated vacancy injection (5-5A) or closed to start a standard optically gated injection (5-5B). At this instant, no change in analyte concentration has taken place for the standard injection, but a photobleached zone the same width as the gating beam diameter has been created for the vacancy injection. The two injections are illustrated in Figures 5-5C and 5-5D after the analyte has migrated a distance 1.25 times the width of the gating beam. The photobleached zone for the vacancy injection is now 2.25 times the gating beam width (5-5C), but an unbleached zone only 1.25 times the gating beam width has passed under the shuttered gating beam for the standard injection (5-5D). Figures 5-5E and 5-5F show the two injections after the shutter has returned to its original state just after the point in time represented by

Table 5-1. Theoretical plates for Arg with optically gated vacancy and standard optically gated electrophoretic separations.[a]

Injection Time (ms)	Vacancy Theoretical Plates (Arg)	Standard Theoretical Plates (Arg)
25	2160 ± 250	-
50	1960 ± 90	2150 ± 350
100	1860 ± 80	2040 ± 230
250	1490 ± 30	1700 ± 30
500	800 ± 10	980 ± 20
750	330 ± 20	450 ± 10

[a] n = 10

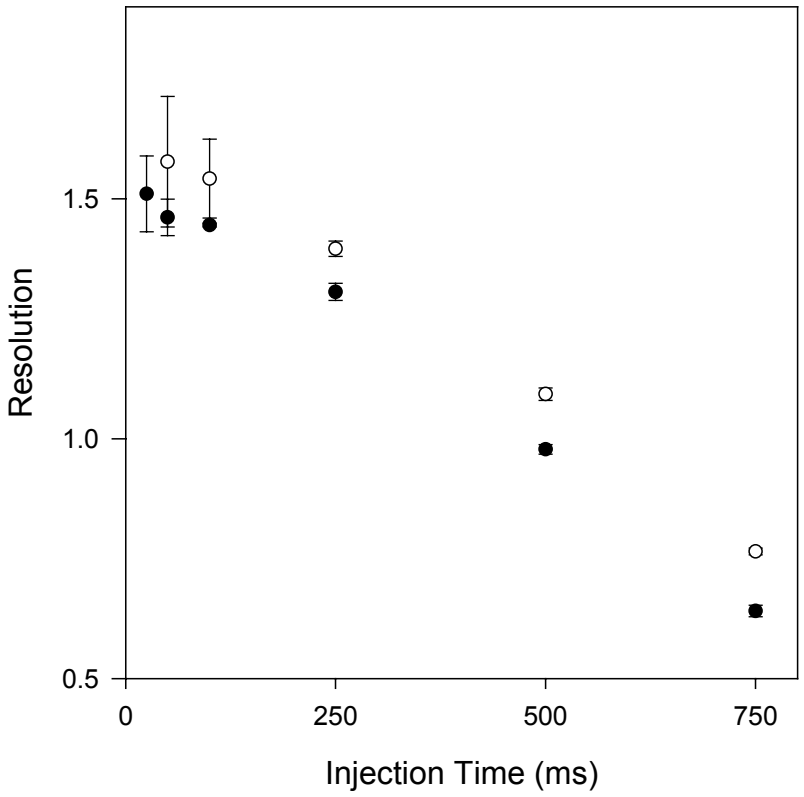

Figure 5-4. Resolution of Arg/Phe peaks as a function of injection time for optically gated vacancy (•) and standard optically gated (o) separations. A peak was not detected for the standard optically gated separation with a 25-ms injection. Error bars are ± 1 S.D.

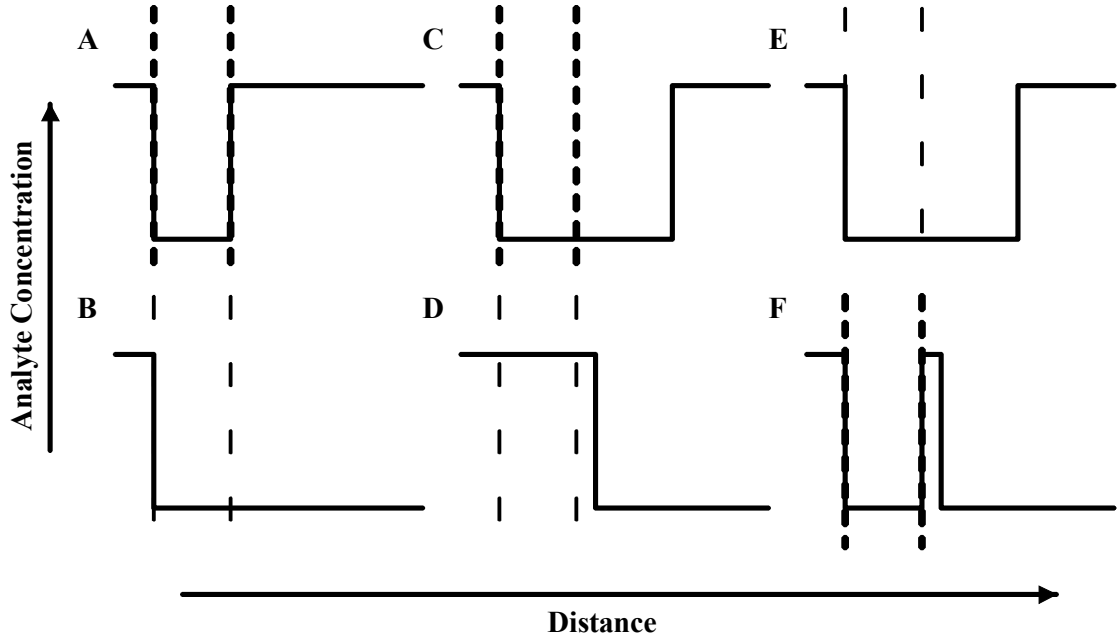

Figure 5-5. Schematic of the injection process for optically gated vacancy electrophoresis (A, C, E) and standard optically gated electrophoresis (B, D, F). The dark dashed lines indicate an open gating beam, and light dashed lines indicate a shuttered gating beam. The fluorescent species are migrating from left to right in the figure.

Figures 5-5C and 5-5D. The optically gated vacancy injection zone is still 2.25 times the width of the gating beam. However, the standard optically gated injection zone is only 0.25 times the width of the gating beam because the unbleached material in the path of the shuttered gating beam in Figure 5-5D has now been photobleached. The concentration profiles for real optically gated injections will be more complex due to photobleaching kinetics for real analytes and the Gaussian profile of the gating beam intensity, but Figure 5-5 illustrates important, general differences between the two injection techniques. Vacancy injections will always be wider than standard injections by two times the gating beam width, and the two injections will be centered at the same position as shown in Figures 5-5E and 5-5F. The minimum width for an optically gated vacancy injection is equal to the width of the gating beam; however, for a standard optically gated injection, the injection width can be 0 if the gating beam is shuttered for a time less than or equal to the time required for the analyte to migrate across the width of the gating beam. Injection volumes calculated for this paper take into account this difference between the two optically gated injection methods.

Figures 5-6A and 5-6B show electropherograms for optically gated vacancy (A) and standard optically gated (B) separations with 50-ms injections. The span of the y-axis in both plots is identical. The mean peak heights for Arg are 0.52 ± 0.01 and 0.09 ± 0.01 ($n = 10$) for vacancy and standard separations, respectively. The Asp peak is not detected in the Figure 5-6B, and no peaks were observed for 25-ms standard optically gated injections. These results are consistent with the injection models illustrated in Figure 5-5. The calculated diameter of the gating beam at its focal point is 40 μm. For the standard optically gated injection, if individual analytes migrate a distance less than the gating beam width during the time the shutter is closed, no analyte will be injected. Migration rates can be calculated for all three analytes from separations with longer injection times (e.g. Figure 5-2). During a 50-ms injection, the Arg zone will migrate 69 μm, the Phe zone will migrate 60 μm, and the Asp zone will migrate 46 μm. The injection model predicts that for a standard optically gated injection, small peaks will be observed for Arg, Phe, and Asp although no Asp peak was actually observed. The migration distance of 46 μm is very close to the *calculated* size of the gating beam (40 μm), and it is likely that either the real, effective size of the gating beam is larger than 46 μm or the size of the Asp zone injected is so small that it is undetectable. This simple analysis correctly predicts that no peaks will be observed for a 25-ms standard optically gated injection since the migration distances during injection for Arg, Phe and Asp will be 34, 30 and 23 μm, respectively.

Figures 5-6C and 5-6D show optically gated vacancy (C) and standard optically gated (D) separations with 500-ms injections. The mean Arg peak height is 1.742 ± 0.008 for the vacancy separation and 1.566 ± 0.011 for the gated separation ($n = 10$). At long injection times, the difference between the amount of analyte injected using the two optically gated injection methods is diminished. The standard optically gated separation has a S/N 21% greater than the optically gated vacancy separation for a 500-ms injection. The higher S/N for the standard optically gated separation is due to lower baseline noise compared to the vacancy separation. The baseline signal of the optically gated vacancy

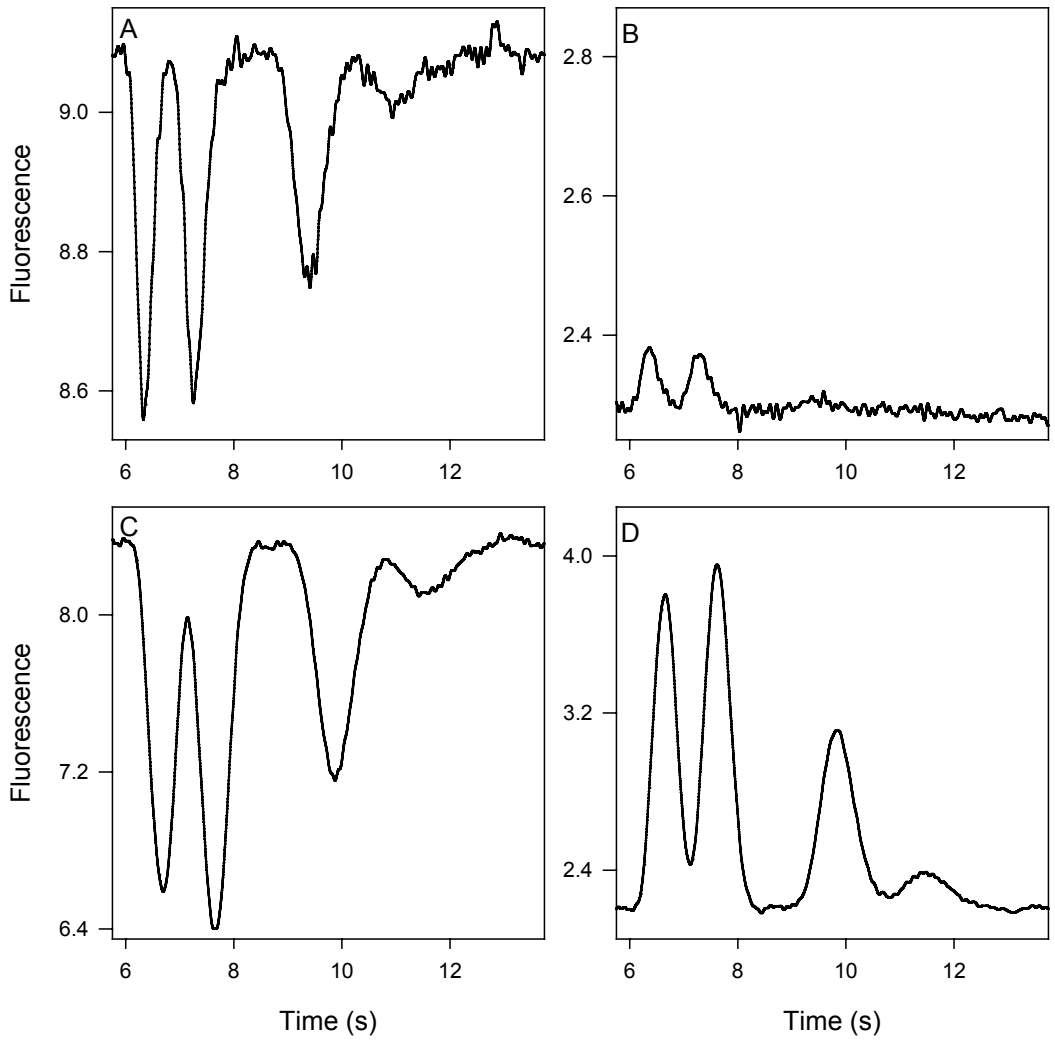

Figure 5-6. Electrophoretic separations following a 50-ms (A) optically gated vacancy and (B) standard optically gated injection of 3 FITC-labeled amino acids. Electrophoretic separations after a 500-ms (C) optically gated vacancy and (D) standard optically gated injection. All analytes were present at a concentration of 500 nM FITC-labeled amino acid (Peak identities are shown in Figure 5-2).

separation is composed of fluorescence from all labeled analytes while the standard optically gated separation baseline signal is due to the lower, residual fluorescence after photobleaching of the analytes.

The injection model shown in Figure 5-5 indicates that the two optically gated injection methods will produce injection zones centered at the same position, and it predicts that the two injection methods should produce analyte peaks with identical migration times. The observed migration times with optically gated vacancy and standard optically gated injections are nearly identical for the range of injection lengths studied (0.04 - 1.0 % difference for all experiments). However, the observed error is systematic. In every case, with the exception of the Asp peak with a 100-ms injection, the migration times are longer for optically gated vacancy experiments. The cause of this is not yet understood. Heating of the solution by the gating beam would lead to the opposite result. The gating beam is irradiating the separation channel more during the standard optically gated separations. The resulting heating of the solution would reduce the solution viscosity and the migration rates would be faster compared to the vacancy experiments. This is the opposite of what is observed.

Figure 5-4 shows the resolution for both separation methods at multiple injection times. The separation efficiency for Arg with both separation methods is presented in Table 5-1. As expected, the resolution and separation efficiency of both methods decreases with increasing injection time.[106,111] The observed resolution of the standard gated separations is consistently higher (6-14%) than that obtained with the vacancy separations. The decreased resolution obtained with vacancy separations at a given injection time is expected because the zone width of analyte injected is larger than that injected for a standard optically gated injection under the same injection conditions as illustrated in Figure 5-5. Earlier studies of vacancy electrophoresis in capillaries reported slightly poorer efficiency compared to standard electrophoresis.[180,181] The reports did not quantify these observations, and they did not use optically gated injection methods.

Conclusions

Optically gated vacancy electrophoretic separations in microfluidic devices offer the advantage of sample injection without interruption of the electrophoretic potential or the need for sample channels intersecting the separation channel and control of the applied potential in these channels. The amount of sample injected can be controlled by changing the amount of time that the gating beam is opened during injection. For the experiments presented here, separation resolution and signal-to-noise ratios for individual peaks are similar to what are obtained using standard optically gated electrophoresis.[111] Standard optically gated electrophoresis ultimately can provide better signal-to-noise and dynamic range than the equivalent optically gated vacancy electrophoretic separation because peaks are detected on top of a lower background signal using this approach; however, very high gating beam intensities may be required to realize this advantage depending on the photochemical stability of the fluorescent analytes.[106,109,146] Optically

gated vacancy electrophoretic separations offer additional interesting possibilities such as the use of pulsed lasers with extremely high peak powers to perform optically gated injections.

Acknowledgements

Financial support for this work was provided by the University of Tennessee and the National Science Foundation RSEC Program at UT (CHE-9974734).

CHAPTER VI

Conclusions

The research detailed in this dissertation describes the development of instrumentation and methodologies for monitoring electroosmotic flow during capillary electrophoretic separations performed in both fused-silica capillaries and glass microfluidic devices. This optical flow monitoring method does not require any complex modifications to be made to either a capillary or a microfluidic device although nanomolar concentrations of a neutral, fluorescent dye must be added to the solutions used. The research focuses on experimentally monitoring electroosmotic flow during field-amplified sample stacking experiments and during current monitoring experiments so that direct comparisons to theories describing flow dynamics in discontinuous buffer systems can be made. The techniques developed are further applied to performing rapid, optically gated, vacancy separations of analytes in microfluidic devices as an alternative to traditional optically gated separations.

In fused silica capillaries, EOF can be monitored at up to 1 Hz with precision better than 1%. The addition of nanomolar concentrations of a neutral fluorophore does not interfere with other detection methods such as UV/VIS absorbance, allowing flow dynamics to be studied while an absorbance electropherogram of a separation is being recorded. During a separation where the sample and running buffers are of the same composition, no changes in flow rate are observed. In future work, the integration of the EOF monitoring instrument into a commercial CE device would allow active control of EOF during CE separations. This will improve the precision in peak migration times, peak areas and peak heights, making them comparable to those obtained with HPLC.

In glass microfluidic devices, EOF can be monitored at rates of up to 2 Hz with precision better than 1%. The traditional method of measuring EOF in microfluidic devices, the current monitoring method, alters EOF and cannot be used to measure accurate EOF rates in microfluidic devices. The current monitoring method however, cannot yet be replaced by the periodic photobleaching technique for measuring flow rates in PDMS microfluidic devices. Absorption of the neutral fluorophore into the walls of the PDMS device prevents flow monitoring from being performed. To overcome this limitation of the periodic photobleaching technique, a neutral dye that is less hydrophobic must be found or a technique that does not require any buffer additives must be developed.

In microfluidic devices, the presence of channel intersections causes changes in EOF rates in different parts of a single channel. These cross-channel intersections provide a source of fluid flow into or out of the channel that the potential is applied across. When EOF is monitored both upstream and downstream from the cross-channel intersection, the effect of the cross-channel intersection can be measured. This effect is substantial during a current monitoring experiment and is less pronounced when the

channel is filled with a single buffer concentration. Broadening of the photobleached zones indicates the presence of hydrodynamic flow and the EOF monitoring technique can be used to monitor both EOF rates and the magnitude of hydrodynamic flow. Monitoring EOF at various positions in a microfluidic device allows the complete mapping of flow dynamics in a microfluidic network rather than across single channels as in the current monitoring method.

The flow dynamics of FASS experiments are qualitatively similar to those predicted by theory. The introduction of a buffer of different concentration results in changes in EOF and the generation of laminar flow. Dynamic changes in the concentration and length of the dilute sample plug as it migrates through the capillary are reflected in changes of the EOF and broadening of the photobleached zones. At short injection lengths of a very dilute buffer plug, theory does not accurately predict the impact of the dilute plug on the bulk EOF through the capillary. Sample stacking does occur, but the change in EOF and current predicted by theory are not observed.

Optically gated vacancy injections are an alternative to traditional optically gated injections. The injection process of each of these two techniques depends on the size of the gating beam, however the dependence is not the same. In optically gated vacancy injections the spot size of the gating beam defines a minimum injection width and the analyte injected during the injection time is added to this minimum injection value. In optically gated injections the minimum injection is determined by a combination of injection time and flow rate, therefore, it is possible to inject some but not all analytes using this injection method. Optically gated injections allow simple, single channel microfluidic devices to be used to perform rapid separations and do not require the rapid switching of injection and separation potentials.

LIST OF REFERENCES

(1) Jorgenson, J. W.; Lukacs, K. D. *Anal. Chem.* **1981**, *53*, 1298-1302.

(2) Hjerten, S. *Chromatogr. Rev.* **1967**, *9*, 122-219.

(3) Mikkers, F. E. P.; Everaerts, F. M.; Verheggen, T. P. E. M. *J. Chromatogr.* **1979**, *169*, 11-20.

(4) Harris, D. C. *Exploring Chemical Analysis*; W. H. Freeman and Co.: New York, 1996.

(5) Skoog, D. A.; West, D. M.; Holler, F. J.; Crouch, S. R. *Analytical Chemistry: An Introduction*, 7th ed.; Saunders College Publishing: Fort Worth, 1999.

(6) Harvey, D. *Modern Analytical Chemistry*; McGraw-Hill Higher Education: Boston, 2000.

(7) Karger, B. L.; Foret, F. In *Capillary Electrophoresis Technology*; Guzman, N. A., Ed.; Marcel Dekker, Inc.: New York, 1993, pp 3-64.

(8) Harrison, D. J.; Manz, A.; Fan, Z.; Ludi, H.; Widmer, H. M. *Anal. Chem.* **1992**, *64*, 1926-1932.

(9) Gravesen, P.; Branebjerg, J.; Jensen, O. S. *J. Micromech. Microeng.* **1993**, *3*, 168-182.

(10) Manz, A.; Effenhauser, C. S.; Burggraf, N.; Harrison, D. J.; Seiler, K.; Fluri, K. *J. Micromech. Microeng.* **1994**, *4*, 257-265.

(11) Regnier, F. E.; He, B.; Lin, S.; Busse, J. *Tr. Biotech.* **1999**, *17*, 101-106.

(12) Arulanandam, S.; Li, D. *Coll. Surf. A* **2000**, *161*, 89-102.

(13) Bousse, L.; Cohen, C.; Nikiforov, T.; Chow, A.; Kopf-Sill, A. R.; Dubrow, R.; Parce, J. W. *Annu. Rev. Biophys. Biomol. Struct.* **2000**, *29*, 155-181.

(14) Bruin, G. J. M. *Electrophoresis* **2000**, *21*, 3931-3951.

(15) Culbertson, C. T.; Jacobson, S. C.; Ramsey, J. M. *Anal. Chem.* **2000**, *72*, 5814-5819.

(16) Figeys, D.; Pinto, D. *Anal. Chem.* **2000**, *72*, 330A-335A.

(17) Morf, W. E.; Guenat, O. T.; deRooij, N. F. *Sens. Actuat. B* **2001**, *72*, 266-272.

(18) Polson, N. A.; Hayes, M. A. *Anal. Chem.* **2001**, *73*, 312A-319A.

(19) Backofen, U.; Matysik, F.-M.; Lunte, C. E. *Anal. Chem.* **2002**, *74*, 4054-4059.

(20) Bharadwaj, R.; Santiago, J. G.; Mohammadi, B. *Electrophoresis* **2002**, *23*, 2729-2744.

(21) Rice, C. L.; Whitehead, R. *J. Phys. Chem.* **1965**, *69*, 4017-4024.

(22) Schwer, C.; Kenndler, E. *Anal. Chem.* **1991**, *63*, 1801-1807.

(23) Dougherty, A. M.; Cooke, N.; Shieh, P. In *Handbook of Capillary Electrophoresis,* 2nd ed.; Landers, J. P., Ed.; CRC Press: Boca Raton, 1996, pp 675-715.

(24) Bard, A. J.; Faulkner, L. R. *Electrochemical Methods: Fundamentals and Applications*; John Wiley & Sons: New York, 1980.

(25) Salomon, K.; Burgi, D. S.; Helmer, J. C. *J. Chromatogr.* **1991**, *559*, 69-80.

(26) Tavares, M. F. M.; McGuffin, V. L. *Anal. Chem.* **1995**, *67*, 3687-3696.

(27) Arulanandam, S.; Li, D. *J. Coll. Int. Sci.* **2000**, *225*, 421-428.

(28) Freund, J. B. *J. Chem. Phys.* **2002**, *116*, 2194-2200.

(29) Jorgenson, J. W.; Lukacs, K. D. *Science* **1983**, *222*, 266-272.

(30) Taylor, J. A.; Yeung, E. S. *Anal. Chem.* **1993**, *65*, 2928-2932.

(31) Tsuda, T.; Ikedo, M.; Jones, G.; Dadoo, R.; Zare, R. N. *J. Chromatogr.* **1993**, *632*, 201-207.

(32) Paul, P. H.; Garguilo, M. G.; Rakestraw, D. J. *Anal. Chem.* **1998**, *70*, 2459-2467.

(33) Mosier, B. P.; Mikkelsen, J. C., Jr.; Santiago, J. G. *MEMS* **2000**, *2*, 455-459.

(34) Ross, D.; Johnson, T. J.; Locascio, L. E. *Anal. Chem.* **2001**, *73*, 2509-2515.

(35) van de Goor, A. A. A. M.; Wanders, B. J.; Everaerts, F. M. *J. Chromatogr.* **1989**, *470*, 95-104.

(36) Hayes, M. A.; Ewing, A. G. *Anal. Chem.* **1992**, *64*, 512-516.

(37) Bello, M. S.; Capeilli, L.; Righetti, P. G. *J. Chromatogr. A* **1994**, *684*, 311-322.

(38) Vazquez, M.; McKinley, G.; Mitnik, L.; Desmarais, S.; Matsudaira, P.; Ehrlich, D. *Anal. Chem.* **2002**, *74*, 1952-1961.

(39) Guiochon, G. *Amer. Lab.* **1998**, *30*, 14-15.

(40) Ghosal, S. *Anal. Chem.* **2002**, *74*, 771-775.

(41) Yang, J.; Bose, S.; Hage, D. S. *J. Chromatogr. A* **1996**, *735*, 209-220.

(42) Lukacs, K. D.; Jorgenson, J. W. *J. High Res. Chromatogr. Commun.* **1985**, *8*, 407-411.

(43) Schaeper, J. P.; Sepaniak, M. J. *Electrophoresis* **2000**, *21*, 1421-1429.

(44) Mayer, B. X. *J. Chromatogr. A* **2001**, *907*, 21-37.

(45) Cohen, N.; Gruska, E. *J. Chromatogr. A* **1994**, *678*, 167-175.

(46) Dose, E. V.; Guiochon, G. *Anal. Chem.* **1991**, *63*, 1154-1158.

(47) Jumppanen, J. H.; Riekkola, M.-L. *Anal. Chem.* **1995**, *67*, 1060-1066.

(48) Crabtree, H. J.; Cheong, E. C. S.; Tilroe, D. A.; Backhouse, C. J. *Anal. Chem.* **2001**, *73*, 4079-4086.

(49) Chien, R.-L.; Burgi, D. S. *Anal. Chem.* **1992**, *64*, 489A-496A.

(50) Chien, R.-L.; Helmer, J. C. *Anal. Chem.* **1991**, *63*, 1354-1361.

(51) Thormann, W.; Zhang, C.-X.; Caslavska, J.; Gebauer, P.; Mosher, R. A. *Anal. Chem.* **1998**, *70*, 549-562.

(52) Gil, E. P.; Ostapczuk, P.; Emons, H. *Anal. Chim. Acta* **1999**, *389*, 9-19.

(53) Terabe, S.; Otsuka, K.; Ichikawa, J.; Tsuchiya, A.; Ando, T. *Anal. Chem.* **1984**, *56*, 111-113.

(54) Kenndler, E. In *High-Performance Capillary Electrophoresis*; Khaledi, M. G., Ed.; John Wiley & Sons, Inc.: New York, 1998; Vol. 146, pp 25-76.

(55) Sandoval, J. E.; Chen, S.-M. *Anal. Chem.* **1996**, *68*, 2771-2775.

(56) Ermakov, S. V.; Capelli, L.; Righetti, P. G. *J. Chromatogr. A* **1996**, *744*, 55-61.

(57) Williams, B. A.; Vigh, G. *Anal. Chem.* **1996**, *68*, 1174-1180.

(58) Huang, X.; Gordon, M. J.; Zare, R. N. *Anal. Chem.* **1988**, *60*, 1837-1838.

(59) Lee, C. S.; Blanchard, W. C.; Wu, C.-T. *Anal. Chem.* **1990**, *62*, 1550-1552.

(60) Lee, C. S.; McManigill, D.; Wu, C.-T.; Patel, B. *Anal. Chem.* **1991**, *63*, 1519-1523.

(61) Locascio, L. E.; Perso, C. E.; Lee, C. S. *J. Chromatogr. A* **1999**, *857*, 275-284.

(62) Liu, Y.; Fanguy, J. C.; Bledsoe, J. M.; Henry, C. S. *Anal. Chem.* **2000**, *72*, 5939-5944.

(63) Ocvirk, G.; Munroe, M.; Tang, T.; Oleschuk, R.; Westra, K.; Harrison, D. J. *Electrophoresis* **2000**, *21*, 107-115.

(64) Wang, S.-C.; Perso, C. E.; Morris, M. D. *Anal. Chem.* **2000**, *72*, 1704-1706.

(65) Bianchi, F.; Wagner, F.; Hoffmann, P.; Girault, H. H. *Anal. Chem.* **2001**, *73*, 829-836.

(66) Bianchi, F.; Chevolot, Y.; Mathieu, H. J.; Girault, H. H. *Anal. Chem.* **2001**, *73*, 3845-3853.

(67) Buch, J. S.; Wang, P.-C.; DeVoe, D. L.; Lee, C. S. *Electrophoresis* **2001**, *22*, 3902-3907.

(68) Li, Q.-F.; Zhang, X.-Y.; Zhang, H.-Y.; Chen, X.-G.; Liu, M.-C.; Hu, Z.-D. *Chin. J. Chem.* **2001**, *19*, 581-587.

(69) Liu, Y.; Wipf, D. O.; Henry, C. S. *Analyst* **2001**, *126*, 1248-1251.

(70) Ren, X.; Bachman, M.; Sims, C.; Li, G. P.; Allbritton, N. *J. Chromatogr. B* **2001**, *762*, 117-125.

(71) Xu, W.; Uchiyama, K.; Shimosaka, T.; Hobo, T. *J. Chromatogr. A* **2001**, *907*, 279-289.

(72) Pugmire, D. L.; Waddell, E. A.; Haasch, R.; Tarlov, M. J.; Locascio, L. E. *Anal. Chem.* **2002**, *74*, 871-878.

(73) Wanders, B. J.; van de Goor, T. A. A. M.; Everaerts, F. M. *J. Chromatogr. A* **1993**, *652*, 291-294.

(74) Rainey, P. V.; Mitchell, N. S. J.; Gamble, H. S. *Proc. SPIE Opt. Eng.* **2000**, *4177*, 185-193.

(75) Altria, K. D.; Simpson, C. F. *Anal. Proc.* **1986**, *23*, 453-454.

(76) Altria, K. D.; Simpson, C. F. *Chromatographia* **1987**, *24*, 527-532.

(77) Sugarman, J. H.; Prud'homme, R. K. *Ind. Eng. Chem. Res.* **1987**, *26*, 1449-1454.

(78) Mathies, R. A.; Peck, K.; Stryer, L. *Anal. Chem.* **1990**, *62*, 1786-1791.

(79) Eggeling, C.; Widengren, J.; Rigler, R.; Seidel, C. A. M. *Anal. Chem.* **1998**, *70*, 2651-2659.

(80) Ricka, J. *Exp. Fluid.* **1987**, *5*, 381-384.

(81) Crimaldi, J. P. *Exp. Fluid.* **1997**, *23*, 325-330.

(82) Lee, T. T.; Dadoo, R.; Zare, R. N. *Anal. Chem.* **1994**, *66*, 2694-2700.

(83) Weimer, W. A.; Dovichi, N. J. *Appl. Optics* **1985**, *24*, 2981-2986.

(84) StClaire, J. C.; Hayes, M. A. *Anal. Chem.* **2000**, *72*, 4726-4730.

(85) Markov, D. A.; Bornhop, D. J. *Fresenius J. Anal. Chem.* **2001**, *371*, 234-237.

(86) Schrum, K. F.; Lancaster, J. M.; Johnston, S. E.; Gilman, S. D. *Anal. Chem.* **2000**, *72*, 4317-4321.

(87) Kuhr, W. G.; Licklider, L.; Amankwa, L. *Anal. Chem.* **1993**, *65*, 277-282.

(88) Jacobson, S. C.; Hergenroder, R.; Koutny, L. B.; Warmack, R. J.; Ramsey, J. M. *Anal. Chem.* **1994**, *66*, 1107-1113.

(89) Seiler, K.; Fan, Z. H.; Fluri, K.; Harrison, D. J. *Anal. Chem.* **1994**, *66*, 3485-3491.

(90) Clark, B. K.; Sepaniak, M. J. *J. Microcol. Sep.* **1995**, *7*, 593-601.

(91) Manz, B.; Stilbs, P.; Jonsson, B.; Soderman, O.; Callaghan, P. T. *J. Phys. Chem.* **1995**, *99*, 11297-11301.

(92) Wu, D.; Chen, A.; Johnson, C. S., Jr. *J. Magn. Res. A* **1995**, *115*, 123-126.

(93) Johansson, J.; Witte, D. T.; Larsson, M.; Nilsson, S. *Anal. Chem.* **1996**, *68*, 2766-2770.

(94) Preisler, J.; Yeung, E. S. *Anal. Chem.* **1996**, *68*, 2885-2889.

(95) Ermakov, S. V.; Jacobson, S. C.; Ramsey, J. M. *Anal. Chem.* **1998**, *70*, 4494-4504.

(96) Barker, S. L. R.; Ross, D.; Tarlov, M. J.; Gaitan, M.; Locascio, L. E. *Anal. Chem.* **2000**, *72*, 5925-5929.

(97) Culbertson, C. T.; Ramsey, R. S.; Ramsey, J. M. *Anal. Chem.* **2000**, *72*, 2285-2291.

(98) Hanning, A.; Lindberg, P.; Westberg, J.; Roeraade, J. *Anal. Chem.* **2000**, *72*, 3423-3430.

(99) Herr, A. E.; Molho, J. I.; Santiago, J. G.; Mungal, M. G.; Kenny, T. W.; Garguilo, M. G. *Anal. Chem.* **2000**, *72*, 1053-1057.

(100) Alarie, J. P.; Jacobson, S. C.; Ramsey, J. M. *Electrophoresis* **2001**, *22*, 312-317.

(101) Lichtenberg, J.; Verpoorte, E.; de Rooij, N. F. *Electrophoresis* **2001**, *22*, 258-271.

(102) Dovichi, N. J.; Martin, J. C.; Jett, J. H.; Trkula, M.; Keller, R. A. *Anal. Chem.* **1984**, *56*, 348-354.

(103) MacTaylor, C. E.; Ewing, A. G. *Electrophoresis* **1997**, *18*, 2279-2290.

(104) Beale, S. C. *Anal. Chem.* **1998**, *70*, 279R-300R.

(105) Tao, L.; Kennedy, R. T. *Tr. Anal. Chem.* **1998**, *17*, 484-491.

(106) Monnig, C. A.; Jorgenson, J. W. *Analytical Chemistry* **1991**, *63*, 802-807.

(107) Moore, A. W., Jr.; Jorgenson, J. W. *Analytical Chemistry* **1993**, *65*, 3550-3560.

(108) Moore, A. W., Jr.; Jorgenson, J. W. *Anal. Chem.* **1995**, *67*, 3448-3455.

(109) Tao, L.; Thompson, J. E.; Kennedy, R. T. *Analytical Chemistry* **1998**, *70*, 4015-4022.

(110) Thompson, J. E.; Vickroy, T. W.; Kennedy, R. T. *Anal. Chem.* **1999**, *71*, 2379-2384.

(111) Lapos, J. A.; Ewing, A. G. *Anal. Chem.* **2000**, *72*, 4598-4602.

(112) Gordon, M. J.; Shear, J. B. *J. Amer. Chem. Soc.* **2001**, *123*, 1790-1791.

(113) Kaneta, T. *Anal. Chem.* **2001**, *73*, 540A-547A.

(114) Yamashita, M.; Kashiwagi, H. *IEEE J. Quant. Elect.* **1976**, *QE-12*, 90-95.

(115) Korobov, V. E.; Shubin, V. V.; Chibisov, A. K. *Chem. Phys. Lett.* **1977**, *45*, 498-501.

(116) Yamashita, M.; Kuniyasu, A.; Hashiwagi, H. *J. Chem. Phys.* **1977**, *66*, 986-988.

(117) Beer, D.; Weber, J. *Opt. Commun.* **1972**, *5*, 307-309.

(118) Wielgos, T.; Turner, P.; Havel, K. *J. Cap. Electrophor.* **1997**, *4*, 273-278.

(119) Tsuda, T.; Kitagawa, S.; Dadoo, R.; Zare, R. N. *Bunseki Kagaku* **1997**, *46*, 409-414.

(120) Tallarek, U.; Rapp, E.; Scheenen, T.; Bayer, E.; As, H. V. *Anal. Chem.* **2000**, *72*, 2292-2301.

(121) Kennedy, R. T.; German, I.; Thompson, J. E.; Witowski, S. R. *Chem. Rev.* **1999**, *99*, 3081-3131.

(122) Cartoni, G.; Coccioli, F.; Jasionowska, R. *J. Chromatogr. A* **1995**, *709*, 209-214.

(123) Korobov, V. E.; Chibisov, A. K. *J. Photochem.* **1978**, *9*, 411-424.

(124) Jones, G. In *Dye Laser Principles with Applications*; Duarte, F. J., Hillman, L. W., Eds.; Academic Press, Inc.: Boston, 1990, pp 287-343.

(125) Becker, I. S.; Gregor, E. T. *Chem. Phys. Lett.* **1998**, *283*, 350-356.

(126) Hinckley, D. A.; Seybold, P. G.; Borris, D. P. *Spectrochim. Acta* **1986**, *42A*, 747-754.

(127) Selwyn, J. E.; Steinfeld, J. I. *J. Phys. Chem.* **1972**, *76*, 762-774.

(128) Arbeloa, I. L.; Ojeda, P. R. *Chem. Phys. Lett.* **1981**, *79*, 347-350.

(129) Hinckley, D. A.; Seybold, P. G. *Spectrochim. Acta* **1988**, *44A*, 1053-1059.

(130) Arbeloa, F. L.; Ojeda, P. R.; Arbeloa, I. L. *J. Luminesc.* **1989**, *44*, 105-112.

(131) Arbeloa, F. L.; Arbeloa, T. L.; Estevez, M. J. T.; Arbeloa, I. L. *J. Phys. Chem.* **1991**, *95*, 2203-2208.

(132) Huang, X.; Coleman, W. F.; Zare, R. N. *J. Chromatogr.* **1989**, *480*, 95-110.

(133) Weinberger, R. *Practical Capillary Electrophoresis*, 2nd ed.; Academic Press: San Diego, 2000.

(134) Harrison, D. J.; Fluri, K.; Seiler, K.; Fan, Z.; Effenhauser, C. S.; Manz, A. *Science* **1993**, *261*, 895-897.

(135) Patankar, N. A.; Hu, H. H. *Anal. Chem.* **1998**, *70*, 1870-1881.

(136) Fletcher, P. D. I.; Haswell, S. J.; Paunov, V. N. *Analyst* **1999**, *124*, 1273-1282.

(137) Hu, L.; Harrison, J. D.; Masliyah, J. H. *J. Coll. Int. Sci.* **1999**, *215*, 300-312.

(138) Bianchi, F.; Ferrigno, R.; Girault, H. H. *Anal. Chem.* **2000**, *72*, 1987-1993.

(139) Henry, A. C.; Tutt, T. J.; Galloway, M.; Davidson, Y. Y.; McWhorter, C. S.; Soper, S. A.; McCarley, R. L. *Anal. Chem.* **2000**, *72*, 5331-5337.

(140) Polson, N. A.; Hayes, M. A. *Anal. Chem.* **2000**, *72*, 1088-1092.

(141) Dutta, P.; Beskok, A. *Anal. Chem.* **2001**, *73*, 1979-1986.

(142) Chien, R.-L.; Bousse, L. *Electrophoresis* **2002**, *23*, 1862-1869.

(143) Conlisk, A. T.; McFerran, J.; Zheng, Z.; Hansford, D. *Anal. Chem.* **2002**, *74*, 2139-2150.

(144) Dittrich, P. S.; Schwille, P. *Anal. Chem.* **2002**, *74*, 4472-4479.

(145) Martin, R. S.; Gawron, A. J.; Lunte, S. M.; Henry, C. S. *Anal. Chem.* **2000**, *72*, 3196-3202.

(146) Pittman, J. L.; Schrum, K. F.; Gilman, S. D. *Analyst* **2001**, *126*, 1240-1247.

(147) Cardot, P. J. P.; Trolliard, P.; Guernet-Nivaud, E. *Chromatographia* **1992**, *33*, 361-368.

(148) Terabe, S.; Otsuka, K.; Ando, T. *Anal. Chem.* **1985**, *57*, 834-841.

(149) Knox, J. H.; McCormack, K. A. *Chromatographia* **1994**, *38*, 207-214.

(150) Fan, Z. H.; Harrison, D. J. *Anal. Chem.* **1994**, *66*, 177-184.

(151) Swinney, K.; Bornhop, D. J. *Electrophoresis* **2002**, *23*, 613-620.

(152) Potocek, B.; Gas, B.; Kenndler, E.; Stedry, M. *J. Chromatogr. A* **1995**, *709*, 51-62.

(153) Ghosal, S. *Anal. Chem.* **2002**, *74*, 4198-4203.

(154) Albin, M.; Grossman, P. D.; Moring, S. E. *Anal. Chem.* **1993**, *65*, 489A-497A.

(155) Beckers, J. L.; Bocek, P. *Electrophoresis* **2000**, *21*, 2747-2767.

(156) Osbourn, D. M.; Weiss, D. J.; Lunte, C. E. *Electrophoresis* **2000**, *21*, 2768-2779.

(157) Quirino, J. P.; Terabe, S. *J. Chromatogr. A* **2000**, *902*, 119-135.

(158) Beckers, J. L.; Ackermans, M. T. *J. Chromatogr.* **1993**, *629*, 371-378.

(159) Hirokawa, T.; Ikuta, N.; Yoshiyama, T.; Okamoto, H. *Electrophoresis* **2001**, *22*, 3444-3448.

(160) Burgi, D. S.; Chien, R.-L. *Anal. Chem.* **1991**, *63*, 2042-2047.

(161) Vinther, A.; Soeberg, H. *J. Chromatogr.* **1991**, *559*, 3-26.

(162) Pittman, J. L.; Henry, C. S.; Gilman, S. D. *Anal. Chem.* **2003**, *Accepted for publication*.

(163) Baker, D. R. In *Handbook of Instrumental Techniques for Analytical Chemistry*; Settle, F., Ed., 1997.

(164) Vinther, A.; Soeberg, H. *J. Chromatogr.* **1991**, *559*, 27-42.

(165) Zhang, C.-X.; Thormann, W. *Anal. Chem.* **1996**, *68*, 2523-2532.

(166) Jacobson, S. C.; Hergenroder, R.; Moore, A. W., Jr.; Ramsey, J. M. *Anal. Chem.* **1994**, *66*, 4127-4132.

(167) Jacobson, S. C.; Ramsey, J. M. *Electrophoresis* **1995**, *16*, 481-486.

(168) von Heeren, F.; Verpoorte, E.; Manz, A.; Thormann, W. *Anal. Chem.* **1996**, *68*, 2044-2053.

(169) Jacobson, S. C.; Ermakov, S. V.; Ramsey, J. M. *Anal. Chem.* **1999**, *71*, 3273-3276.

(170) Kennedy, R. T. *Analytica Chimica Acta* **1999**, *400*, 163-180.

(171) Shultz-Lockyear, L. L.; Colyer, C. L.; Fan, Z. H.; Roy, K. I.; Harrison, D. J. *Electrophoresis* **1999**, *20*, 529-538.

(172) Alarie, J. P.; Jacobson, S. C.; Culbertson, C. T.; Ramsey, J. M. *Electrophoresis* **2000**, *21*, 100-106.

(173) Ermakov, S. V.; Jacobson, S. C.; Ramsey, J. M. *Anal. Chem.* **2000**, *72*, 3512-3517.

(174) Attiya, S.; Jemere, A. B.; Tang, T.; Fitzpatrick, G.; Seiler, K.; Chiem, N.; Harrison, D. J. *Electrophoresis* **2001**, *22*, 318-327.

(175) Lin, Y.-H.; Lee, G.-B.; Li, C.-W.; Huang, G.-R.; Chen, S.-H. *J. Chromatogr. A* **2001**, *937*, 115-125.

(176) Palmer, J.; Burgi, D. S.; Munro, N. J.; Landers, J. P. *Anal. Chem.* **2001**, *73*, 725-731.

(177) Zhang, C.-X.; Manz, A. *Anal. Chem.* **2001**, *73*, 2656-2662.

(178) Fang, Q.; Xu, G.-M.; Fang, Z.-L. *Anal. Chem.* **2002**, *74*, 1223-1231.

(179) Desiderio, C.; Fanali, S.; Gebauer, P.; Bocek, P. *J. Chromatogr. A* **1997**, *772*, 81-89.

(180) Gebauer, P.; Bocek, P. *J. Chromatogr. A* **1997**, *772*, 73-79.

(181) Mikkers, F. E. P. *Anal. Chem.* **1997**, *69*, 333-337.

(182) Howard, G. C. In *Methods in Nonradioactive Detection*; Howard, G. C., Ed.; Appleton & Lange: Norwalk, 1993, pp 40-46.

APPENDIX

APPENDIX I

Data Acquisition and Analysis Programs

The data acquisition and instrument control program and hardware perform two main functions. A +5 V transistor-to-transistor logic (TTL) signal is output from one of the timing circuits of the data acquisition board and used to control the electronic shutter blocking the bleaching/gating beam. All data (i.e. PMT, current, UV/Vis etc.) are converted from analog to digital signals and then collected and saved to file.

Data Acquisition and Flow Monitoring Instrument Control

The data acquisition and instrument control program used for the work presented in this thesis is written in the graphical programming language LabVIEW (National Instruments; Austin, TX). The data acquisition and instrument control are performed using a PCI-6024E DAQ board with a BNC-2080 board used to make connections to the instrument (National Instruments; Austin, TX). Once the data acquisition program is opened, the front panel or user interface is displayed. Prior to beginning an experiment, the data acquisition rate (Scan Rate), shutter opening time (Time Open) and shutter cycle time (Pulse Delay) must be entered. The *Continuous Pulse Generator Config.vi* used to generate the TTL signal that controls the opening and closing of the shutter requires that two values, repetition frequency and duty cycle, be input prior to starting the experiment. These values, however, are not the same as shutter cycle time and shutter opening time. The inverse of the user entered shutter cycle time is used as the repetition frequency and the user entered shutter opening time divided by the shutter cycle time is used as the duty cycle. Figure A1-1 illustrates the relationship between the TTL signal and the functioning of the shutter. In this illustration, the shutter starts in the closed position and is opened by the input of a +5 V square wave. If the shutter is initially open, the +5 V signal will close the shutter for the input time period. The initial state of the shutter is controlled from the front panel of the Uniblitz Model VMM-D1 shutter driver with the N.O./N.C. (open/closed) switch. It is also important to note that there is a delay between the delivery of the +5 V TTL signal and the actual opening of the shutter of approximately 1-2 ms.

The default voltage input range for the PCI-6024E is ± 10 V, but this value can be changed to ± 10 V, 5 V, 0.5 V or 0.05 V if desired. The voltage range can be set independently for each of the data acquisition channels being used. Using a 12-bit analog-to-digital (A/D) converter, the PCI-6024E has a voltage resolution of 4.9 and 0.02 mV for the ± 10 V and ± 0.05 V ranges, respectively.

Each of the data channels to be acquired must also be entered into the program before starting the data acquisition. The typical channel assignment is as follows: Ch0) PMT; Ch1) Current; Ch2) UV/Vis; Ch3) Shutter TTL. Using the PCI-6024E and the BNC-2080, it is possible to acquire data from up to 16 channels at a maximum acquisition rate of 12.5 kHz per channel. While it is unnecessary to monitor all channels

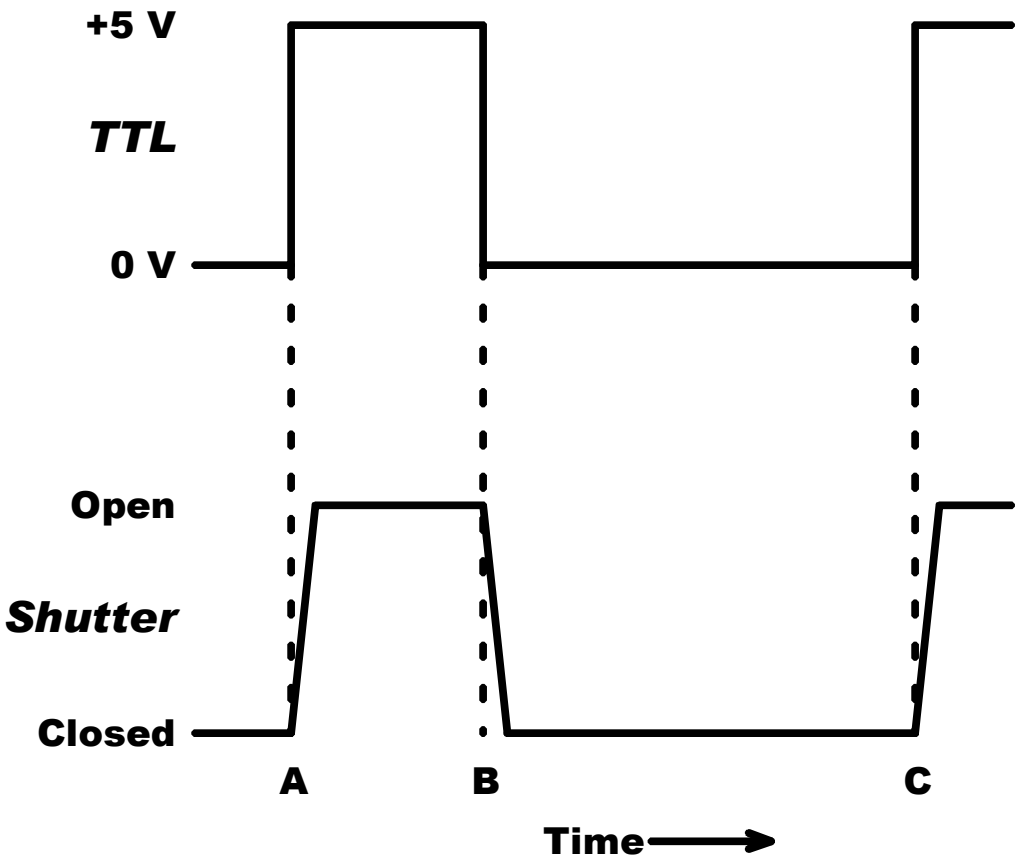

Figure A1-1. Relationship between TTL output by LabVIEW data acquisition and instrument control and shutter function. A-B indicates the total shutter open time per cycle and A-C indicates the total cycle time, which are input into the program by the user prior to starting the experiment.

(i.e. current or UV/Vis) at the same acquisition rate as the PMT channel, it is necessary to acquire the same number of data points from each channel due to only one timing circuit being available to control the data acquisition rate. Once the program is started, the user is prompted to select a file name for the data to be collected to. The data are saved as a tab-delimited *.txt* file. Data files can reach sizes of up to 15 MB, approximately 900,000 data points per channel, when data is acquired from three channels at a rate of 1500 Hz over 10 minutes.

Flow Monitoring Data Analysis

A program for the post-acquisition analysis of flow monitoring data (*Analysis.m*) has been written in MatLAB MatLAB (The MathWorks; Natick, MA). This program has two main sections. The first section is a baseline subtraction routine adapted from the work of Dietrich, Rudel and Neumann.[1] The second portion of the program analyzes the individual flow rate measurements and returns values for the 10%- and 50%-peak heights and the peak maximum or minimum of each negative and positive peak detected. The peak detection and analysis section was adapted from the work of Cardot and coworkers.[2]

In order to begin analyzing flow monitoring data using the *Analysis.m* program, the operating directory in MatLAB must first be changed to the directory containing the data files to be analyzed. Once in the correct directory, typing "analysis" at the prompt in the MatLAB Command Window will start the program. A prompt will appear requesting the name of the data file to be analyzed. It is important that the file name, including the file suffix, if used, be entered. At this point, the data file is loaded into memory as the variable "*data*." The program then requests that the column of the data file containing the data from the PMT channel, be identified. If using the above LabVIEW data acquisition program, this will be the first column of the data file. The program then generates the variable "*rPMT*" containing only the data acquired from the PMT channel. The program then generates prompts requesting that the data acquisition rate (*Fs*), shutter open time (*pulse_width*) and shutter cycle time (*cycle*) be entered. Using the data acquisition rate entered, the program will then generate a time axis (*rtime*) for the flow monitoring data set and a xy-plot of the raw data file.

The program next asks if there is any region of the data file that does not contain any useful flow monitoring information. This portion of the program is designed to remove segments of the data file where there is no flow monitoring data to be analyzed. Under certain experimental conditions, the negative photobleached zone will be obscured by the elution of the buffer or solvent from the sample plug past the LIF detector. If the entire data set contains data that provides useable flow measurements, this step is skipped and the baseline subtraction algorithm is entered into directly.

Baseline Subtraction

In order to decrease the amount of computing resources necessary for determining baseline data points, the first step in the subtraction algorithm is to decrease the number of data points in the file. This step does not permanently alter the raw data file, but it will

affect the outcome of the baseline determination. The value entered here is dependent upon acquisition rate as well as the signal-to-noise ratio of each individual data file. Unfortunately, there is no set rule to guide the choice of a value to be entered here. Once a value is entered, MatLAB simply takes every n-th data point and creates a smaller array (*PMT*) from the original data set. This array (*PMT*) will be used throughout the baseline subtraction portion of the program.

The reduced data set is then filtered (*fPMT*) to remove high frequency noise so that picking of the baseline points is made easier. There are four filtering options available: 1) a moving average; 2) a Savitzky-Golay filter; 3) a median filter; and 4) no filtering. The moving average results in the greatest amount of data smoothing and produces the best baseline detection results. Again, there is no hard rule for determining the best filtering window. The Savitzky-Golay filter is used to reduce high frequency noise while maintaining the shape of the peaks in the data set. The median filter is also useful for removing high frequency noise, but will affect the shape of the peaks in the data. The overall goal of this data filter is not to preserve the accuracy of the flow monitoring data. The goal is to enhance the determination of which data points are in peaks and which data points are in the baseline. If the level of filtering selected is not large enough and new filtering conditions are desired, by answering no when asked if the filtering results are adequate, the filtering step will be repeated.

Following the filtering step, the program takes the first derivative of the now-filtered PMT data set and then generates a power spectrum of the data. A power spectrum is simply the first derivative of the flow monitoring data, squared. Using the power spectrum, the data points belonging to peaks in the data set are identified. (Note: It has also been noted that if the negative flow monitoring peaks are broad and the baseline program identifies data points within the negative peak as baseline data, increasing the power spectrum to a power of four will help to alleviate this problem.)

In order to identify the location of peaks in the data set, a threshold value is determined by taking the mean of the power spectrum plus three times the standard deviation. Any data points that have values greater than this threshold value are identified as peaks and are removed from the data set. The positions of these data points are noted by writing a value of one for a peak and a value of zero for baseline to an array (*peaks*). Once the data points that have been identified as belonging to peaks are removed from the data set, a new threshold value is determined and the process repeated. This process is repeated until there are no data points having values greater than the threshold value. Once this process of identifying data points that belong to peaks or baseline is completed, the presence of single point peaks or "spikes" is detected and eliminated.

Spike detection and elimination is accomplished using a three-point window which starts with the first three data points of the *peaks* array. The spike correction routine first looks to see if the middle data point of the three-point window is a zero or a one. Once this is determined, the values of the two data points to either side are determined. If the center value is equal to either one or both of the other two values, no change is made. If the first and third data points in the window are equal, and the value

of the middle data point is not equal to the value of the first and third data points, the middle data point is considered a spike and is made equal to the other two values. This process continues through the entire *peaks* array until the end of the array is reached.

The *peaks* array is then used to identify the baseline data points in the *PMT* array and display the results for approval. A plot is presented that superimposes the baseline on the PMT data. If data points in peaks are detected as baseline, answering no when asked whether or not the identified baseline points are acceptable repeats the above process. It will be necessary to enter a new value for the filter window during this step. Again, this is an empirical process that has no hard rules for determining the ideal filtering window to be used.

Once a set of baseline data points is accepted, the program will display the number of data points that have been identified as baseline data points. It is important to remember that this value is a portion of the reduced data set and not the whole. The program then asks if the number of baseline data points should be reduced. This option was initially included to decrease processing time. However, it has been found that this does not impact the amount of time needed to subtract a baseline from the data set. Answering zero to this question will cause the program to use all the identified baseline data points and will result in an improved fit of the baseline to the original data. A cubic spline curve is then used to connect all the identified baseline points together so that an equation defining the baseline can be generated. The results of this spline curve generation are then displayed superimposed on top of the PMT data so that the final fit of the baseline can be approved. Once approved, the baseline is subtracted from the original PMT data (*rPMT*) and the baseline subtracted data are displayed.

Flow Monitoring Data Analysis

The first step of the data analysis routine is to remove regions of the data file that contain no EOF information. It is at this point that the program removes the segment of data identified at the beginning of the analysis as well as asking where the flow monitoring data begins. Identification of the beginning of the flow data allows for data accumulated prior to the beginning of the experiment to be removed prior to analysis. The program next uses the values for shutter cycle time and data acquisition rate entered previously to determine whether or not there are incomplete flow measurements at the end of the data set that can be removed. Once the data set has been trimmed of portions that do not require analysis, a choice of filters is presented once more.

The filtering options presented for use on the baseline corrected PMT data are identical to those provided previously. It is important, however, that careful selection of filtering parameters be performed at this step. A moving average filter using a window size of no more than 5 data points is typically adequate for removing some high frequency noise from the data set without altering the shape of the peaks to be analyzed. If the data are over filtered at this stage, the results of the EOF monitoring experiment will be altered due to changes in the width and height/depth of the peaks in the data set. Once the data set is filtered, it is divided into an array using the cycle times input at the beginning of the program, where each row of the array is one EOF measurement. The

beginning of the first EOF measurement is identified manually by inputting a time value that occurs before the first positive peak of the data set. This array is then used for the remaining analysis. A second array, which is the PMT data cubed, is also generated at this point for the purpose of detecting errors in the identification of peak values.

The next step is to identify the beginning and ending points of both the positive and negative peaks in each window. The program will request that a value less than or equal to one be entered at this time, which will be used in establishing the positive and negative threshold values. These values will be used as a multiplier for the standard deviation calculated for each window of the data set. The values resulting from the product of the standard deviation and the supplied multiplier is then used as the threshold value for each respective data set. Any data points greater than the positive threshold are considered to be part of the positive peak and any data points less than the negative threshold part of the negative peak. Once two data points, indicating the beginning and ending, for both a positive and negative peak have been identified at the threshold value, the program follows the data until the first and last data points of each peak at the median value are found. This process is then repeated for the cubed data set for error analysis.

The error analysis compares the values determined for the start and end of both the positive and negative peaks as measured using the cubed data set and the normal data set. In most cases, there will be a small difference of approximately ± 2-3 data points observed between these two columns. As long as this difference remains relatively constant within a given data set, the time values measured for each of the flow rate measurements are accurate. If the difference presented in the error columns is large (e.g. ± 50 or more data points), the data point is unreliable and should be examined further. This discrepancy is typically caused by random events that result in a change to the shape of either the positive or negative peaks (i.e. spikes due to dust particles, baseline fluctuation, etc.).

The magnitude and time of the photobleached zone minimum is determined next. The center of each photobleached zone is first approximated by finding the minimum value of each flow measurement. The peak of the photobleached zone is next fit with a second-order polynomial in order to better identify the peak time and peak magnitude. The values from the polynomial fit are then saved to two arrays, *neg_height* and *neg_peak_time*. The median value of each data set in combination with the values in *neg_height* are used to determine the time values for the 10% and 50% peak heights of the photobleached zones. These values are saved to the arrays *neg_ten_percent* and *neg-_half_height*. This process, excluding the use of the polynomial fit, is then used to determine the same values for the positive peak for each flow measurement.

Once the program is completed, a prompt requesting a name to which the completed analysis is to be saved to is displayed. This will save the analysis results to a space-delimited *txt* file. The columns in this file are in the following order: 1) Measurement Index Number; 2) Error TTL Peak Start; 3) Error TTL Peak End; 4) Error Negative Peak Start; 5) Error Negative Peak End; 6) TTL Peak Time; 7) TTL Time Start; 8) TTL Time End; 9) TTL 10% Start; 10) TTL 10% End; 11) TTL 50% Start; 12) TTL 50% End; 13) Negative Peak Time; 14) Negative Peak Start; 15) Negative Peak End; 16)

Negative 10% Start; 17) Negative 10% End; 18) Negative 50% Start; 19) Negative 50% End.

Appendix I References

(1) Dietrich, W.; Rudel, C.; Neumann, M. *J. Magn. Res.* **1991**, *91*, 1-11.

(2) Cardot, P. J. P.; Trolliard, P.; Guernet-Nivaud, E. *Chromatographia* **1992**, *33*, 361-368.

APPENDIX II

Electroosmotic Flow Monitoring Using a Refractive Index Detector

Abstract

A refractive index detection system for capillary electrophoresis was constructed for monitoring electroosmotic flow and hydrodynamic flow rates. Small plugs of solution were heated using an Argon-ion laser to cause a change in the local refractive index upstream from a refractive index detector. This change in refractive index was detected and examined as a means for monitoring flow rates through a fused-silica capillary with a 50 μm i.d. Flow rates from 0.021 to 73.4 cm/s were studied to determine the effectiveness of this method. Phenol red, rhodamine-B and fluorescein were tested as additives to the running buffer to achieve heating of the solution by absorption of the Argon-ion laser beam.

Introduction

The ideal measurement method measures the desired property of the native experimental system and does not require the addition of any foreign compound or the introduction of any additional devices into the system being measured. The measurement of flow rates in microfabricated and capillary electrophoretic devices often requires the modification of the running buffer or the experimental system for the measurement of a flow rate. Methods for measuring a flow rate in capillaries and microfluidic devices include the neutral marker method, the current monitoring method and the periodic photobleaching of a dilute fluorophore.[1-6] Weighing the effluent from a capillary column does not require the modification of the experimental system or addition of any compounds; however, it is impractical for use in microfabricated devices and capillaries.[7,8]

Micro-interferometric back-scatter detection (MIBD) is a detection method that measures changes in the refractive index (RI) of the running buffer filling a capillary or microfabricated device.[9-19] MIBD is a non-invasive detector that does not require any modification of the sample or of the separation buffer. It is also relatively simple and inexpensive to assemble.[15] The RI of an aqueous solution is dependent upon both solute composition as well as temperature.[12,20,21] Using the thermal dependence of RI, it is possible to detect microdegree changes in temperature by MIBD.[12] In order to use MIBD to measure flow rates, a signal must be generated which can be used to determine the amount of time required for a well-defined plug of solution to travel between two points along the length of the capillary or microfluidic channel.

Weimer and Dovichi used crossed-beam thermal lens measurements to determine flow rates through a 1 mm path-length flow cell.[22] In this technique iron-1,10-phenanthroline (0.5 μM), a chromophore, was added to a 50/50 water/methanol mixture. The solution was heated by a 4-mW HeCd pump laser and probed by a 5-mW HeNe laser. Absorption of the pump beam by the chromophore heated the solution flowing through the focal point of the beam, creating a thermal lens. The path of the probe beam was deflected by the magnitude of the thermal gradient created at the intersection of the two beams. As the flow rate changed, the magnitude of the thermal gradient changed as well. This was used to measure flow rates of 0.2-30 mm/s.[22] In this report, only hydrodynamic flow was studied, eliminating the concern that the chromophore would have a migration rate different from the bulk solution, which could occur during an electrophoretic separation.

StClaire and Hayes later reported using a resistive heating element to generate a well-defined region of heated solution in a 184 μm i.d. fused-silica capillary.[15] The solution in the capillary was heated by applying current to a NiChrome wire wrapped around the outer diameter of the capillary. The heated zone of solution was then detected 9 mm downstream by MIBD. Flow rates of 2-25 cm/s were measured with an accuracy of 1%. This method did not require the addition of any additives to the running solution and is easily scalable to microfabricated devices.

Markov and Bornhop improved upon the technique reported by StClaire and Hayes by replacing the resistive heating element with an IR diode laser (λ = 960 nm).[18] Using the laser, the aqueous solution in the capillary was heated directly, and no chromophore additives were required. The heated zone of solution was detected 1-2 mm downstream from the heating region by MIBD at flow rates of 0.034 to 0.34 cm/s. To measure the time delay between application of the heating beam and detection of the heated zone at the MIBD, signals from both the MIBD and the computer controlling the IR laser were recorded. A Fourier transform of these two signals was taken and the phase shift between the IR laser triggering signal and the MIBD signal was used to determine the time difference between the application of the heating beam and detection of the heated zone of solution.

In each of the techniques using refractive index detection, only hydrodynamic flow was examined and the ability to monitor flow rates on a continuous basis was not demonstrated.[15,18] In this appendix, laser heating of the solution flowing through a capillary under conditions of both hydrodynamic and electroosmotic flow is examined. The use of a chromophore additive was necessary since an IR laser of the appropriate wavelength was not readily available.

Experimental

Chemicals

Boric acid and phenol red were acquired from Fisher Scientific (Fair Lawn, NJ). Rhodamine-B and disodium fluorescein were purchased from Acrōs (Pittsburgh, PA) and Sigma Chemical (St. Louis, MO), respectively. Mesityl oxide was obtained from Aldrich (Milwaukee, WI). All solutions were made in doubly-distilled water.

Refractive Index Detector

The refractive index (RI) detector (Figure A2-1) was constructed by focusing the output from a HeNe laser beam (Model 145-02; Spectra-Physics, Inc.; Mt. View, CA) on a fused-silica capillary. The output wavelength of the laser was 632 nm with an output power of ~2.3 mW. The laser beam was focused on to the capillary by a plano-convex lens (f = 100 mm). In order to optimize the appearance of the interference pattern, the laser head was simply rotated in its holder until any secondary interference patterns were reduced in magnitude or eliminated. To simplify this process, a $\lambda/2$ or $\lambda/4$ plate can be placed in the HeNe beam path in front of the capillary to adjust the polarity of the laser beam.[18,19,23] The interference pattern resulting from the light scattered by the fused-silica capillary was directed to a PMT (Hamamatsu HC120; Bridgewater, NJ), located underneath the incoming HeNe laser beam by placing the fused-silica capillary at a ~5° angle relative to the HeNe laser beam. Prior to reaching the PMT, the interference pattern was passed through two cut-on filters with cut-on wavelengths of 550 and 560 nm (CG-OG-550-1.00-2 and LP-560-1.00; CVI Laser Corporation; Albuquerque, NM) and a variable-width slit. The cut-on filters were used to limit the amount of light detected from sources other than the HeNe laser. The adjustable slit was used to limit the portion of the interference pattern fringe that is detected at the PMT.

The PMT and the adjustable slit were mounted to a single-axis translation stage (TSX-1D; Newport, Corp.; Irvine, CA) so that the PMT and slit could be placed at the desired position on a single interference fringe (Figure A2-2). The PMT and slit were positioned so that when a change in RI occurred, the shift in the position of the interference pattern resulted in an increase in the intensity of the light detected at the PMT. Initially, the width of the slit opening was equal to the i.d. of the capillary. To increase the resolution of the detector, the width of the slit was made smaller than the capillary i.d.

Heating of the Running Buffer

The running buffer was heated by irradiating the buffer-filled capillary with an Argon-ion (Ar^+) laser beam (Coherent Innova 90C-5; Santa Clara, CA). The Ar^+ laser beam was blocked by an electronic shutter (Uniblitz 310B; Vincent Associates; Rochester, NY) and was opened to allow the laser to irradiate the buffer solution for a desired amount of time at pre-determined intervals. The Ar^+ laser beam was focused onto the capillary using a plano-convex lens (f = 38 mm). For flow monitoring using

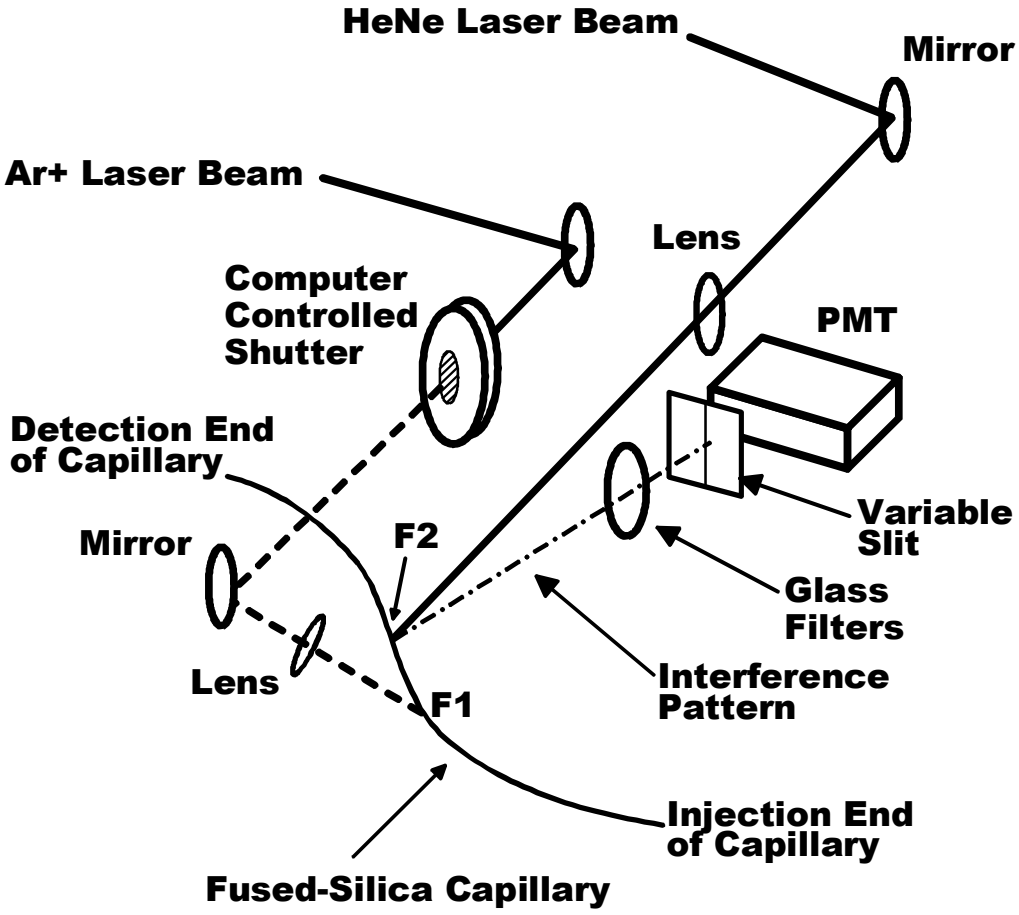

Figure A2-1. Refractive index flow monitoring instrument. The heating beam is focused on to the capillary at F1 and the RI detector is focused at position F2.

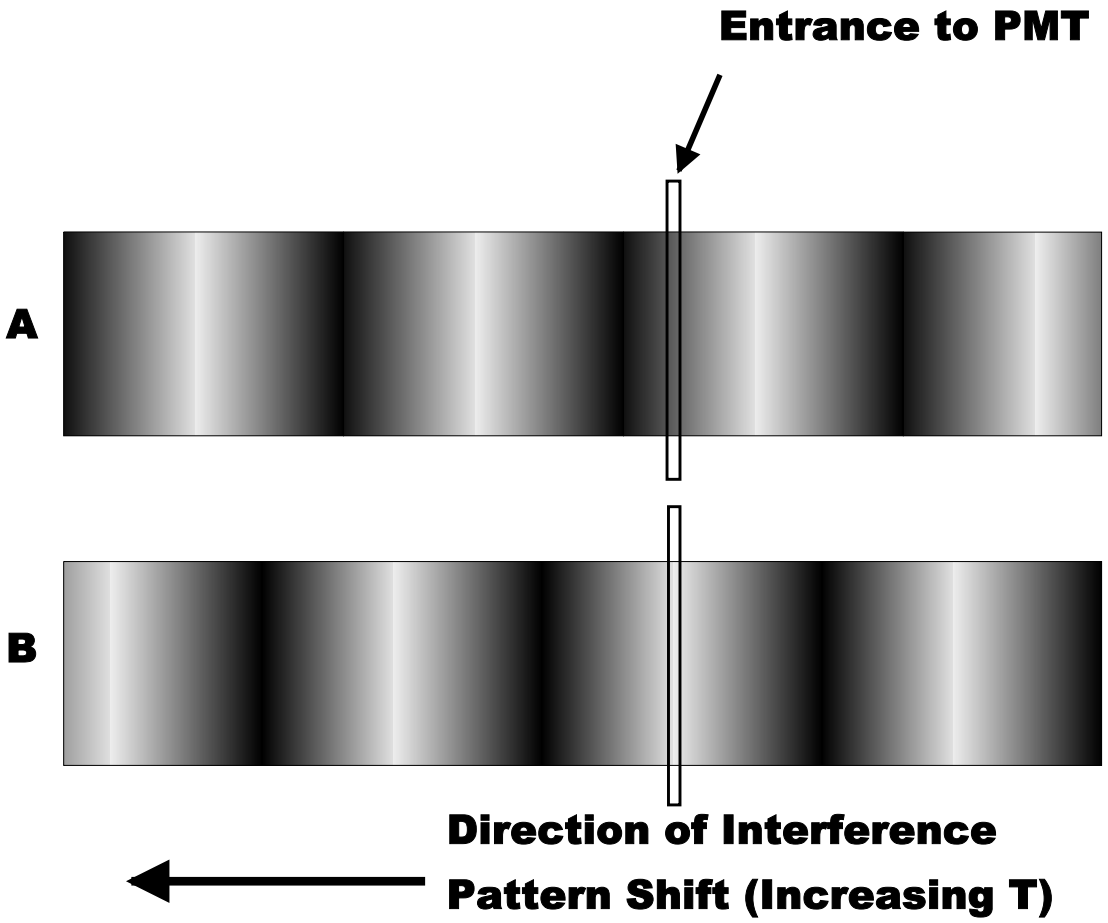

Figure A2-2. Illustration of the interference pattern as observed at the PMT (A) before heating and (B) after heating the solution filling the fused-silica capillary.

rhodamine-B and phenol red dissolved in the running buffer, the 514.5 nm laser-line was selected. For experiments with disodium fluorescein, the 457.9 nm laser-line was used.

Capillary System and Flow Experiments

The fused-silica capillary (50 μm i.d./220 μm o.d. and 100 μm i.d./360 μm o.d.; SGE; Austin, TX) was mounted in a holder at an angle (~5°) relative to the HeNe laser beam. The position of the capillary at the focal point of the HeNe laser was adjusted to optimize the intensity and position of the interference pattern at the PMT. The capillary was filled with 10 mM borate buffer (pH = 9.0) containing 0.5 mM phenol red, rhodamine B or fluorescein. Electroosmotic flow was generated by applying an electrical potential across the capillary using a high-voltage power supply (Spellman CZE1000R; Hauppauge, NY). Hydrodynamic flow was generated by applying up to 250 psig at the injection end of the capillary. The end of the capillary was immersed in a vial containing running buffer inside a pressure chamber. The desired pressure was then applied using helium gas.

Electroosmotic flow rates were calibrated using the neutral marker method.[1,2,24] Hydrodynamic flow rates were calibrated by collecting and weighing column effluent for a pre-determined period of time.[8,25,26]

Instrument Control and Data Acquisition

A program written in LabVIEW (National Instruments; Austin, TX) was used for data acquisition and instrument control. All data were acquired with a National Instruments PCI-6024E data acquisition board at an acquisition rate of 250 Hz. All signals were filtered with a 50-Hz low-pass RC filter prior to acquisition. All data were analyzed with MatLAB (The Math Works; Natick, MA), Peak Fit 4.0 (SPSS Science; Chicago, IL) or Microsoft Excel (Microsoft Corp.; Redmond, WA).

Results and Discussion

Electroosmotic Flow Monitoring

A capillary was filled with a solution of phenol red and the response of the RI detector was observed under conditions of electroosmotic flow. Figure A2-3 shows an example of data from the RI detector where a small secondary peak is observed on the trailing edge of the larger primary peak (d = ~7 mm). It is believed that the large peak is due to heating of the solution that occurs due to absorption of the heating beam by the phenol red dissolved in the running buffer. When a negative electric potential was applied across the capillary, the main peak was still observed at the detector downstream from the heating beam. This indicates that the region of solution heated by the Ar^+ laser beam expands along the capillary by propagation of the thermal gradient through the nearby solution faster than the bulk EOF rate. The migration of the primary peak at a rate faster than that of the EOF eliminates the possibility for using it to monitor EOF.

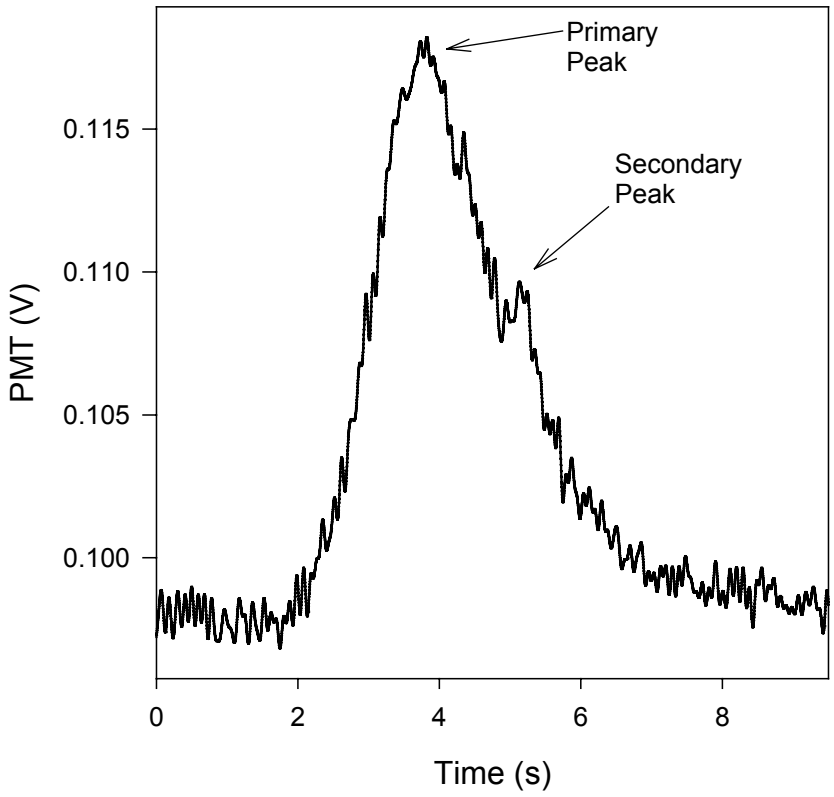

Figure A2-3. Primary (3.8 s) and secondary (5.7 s) peaks observed during a flow monitoring experiment using a RI detector and laser heating of the running buffer (10 mM borate buffer; pH = 9.0) containing 0.5 mM phenol red. (Applied potential = 294 V/cm; flow rate = 0.253 cm/s; slit width = 50 μm).

The second, smaller peak in Figure A2-3 is possibly a photoproduct of the phenol red that is generated when it is irradiated by the Ar^+ laser. This photoproduct then migrates to the detector downstream from the heating beam. If the secondary peak is a photoproduct of the phenol red that migrates under the influence of an applied potential, then under conditions of a negative applied electric potential, the peak will not be observed at the trailing edge of the main peak shown in Figure A2-3. This hypothesis was tested and confirmed that the secondary peak is a possible photoproduct which migrates independent of the main peak.

The electrophoretic migration time of the secondary peak on the trailing edge of the primary peak has been found to change as a function of applied potential (Figure A2-4). This was confirmed over an applied potential range of 67-400 V/cm with corresponding EOF rates of 0.045 – 0.333 cm/s. However, as the data in Figure A2-4 illustrate, the EOF rates measured by using the RI data do not exactly match the EOF rates measured by the neutral marker method with mesityl oxide. Figure A2-4 shows two sets of flow rate measurements for the phenol red secondary peak calculated using two values of d (d = 0.365 and 0.718 cm). Under ideal circumstances, the distance between the heating and probe beams could be calibrated with the marker compound at any applied potential and EOF rate, and this calibration should be valid for other applied fields and EOF rates. If the slowest measured flow rate is used to determine a value for d, a value of 0.365 cm is measured which results in EOF rates that are lower than those measured by the neutral marker method. This indicates that the small secondary peak migrates faster than the slowest flow rate, resulting in a value of d that is smaller than expected. However, if d is calibrated at the highest EOF value, d = 0.718 cm, the values measured with phenol red are close to those of mesityl oxide, with the exception of the data point at 67 V/cm.

To examine the effects of the chromophore's charge on the EOF rates measured, both rhodamine B (Figure A2-5) and fluorescein (Figure A2-6) were examined as buffer additives for RI flow monitoring. As shown previously, rhodamine B is a neutral, zwitterionic species at pH=9.0.[4] Therefore, the behavior of the secondary RI peak observed with rhodamine B should indicate whether or not the behavior of the secondary peak is due to the electrophoretic mobility of the phenol red. Figure A2-5 shows data from the same experiment as that conducted to obtain the data in Figure A2-4, but with rhodamine B as the buffer additive. The secondary RI peak for rhodamine B was only observed at flow rates ranging from 0.021 to 0.168 cm/s. At flow rates greater than 0.168 cm/s, the rhodamine B peak was not observed. The two values obtained for d when calibrated versus mesityl oxide using the slowest and fastest flow rates were 0.384 and 0.341 cm, respectively. The flow rates measured using rhodamine B (Figure A2-5) did not deviate as far from the true values measured with mesityl oxide compared to those measured using phenol red (Figure A2-4).

The same experiment was repeated with fluorescein added to the running buffer (Figure A2-6). Under the experimental conditions used, fluorescein is negatively charged. The calibrated values of d were 0.442 and 0.526 cm when using the fastest and

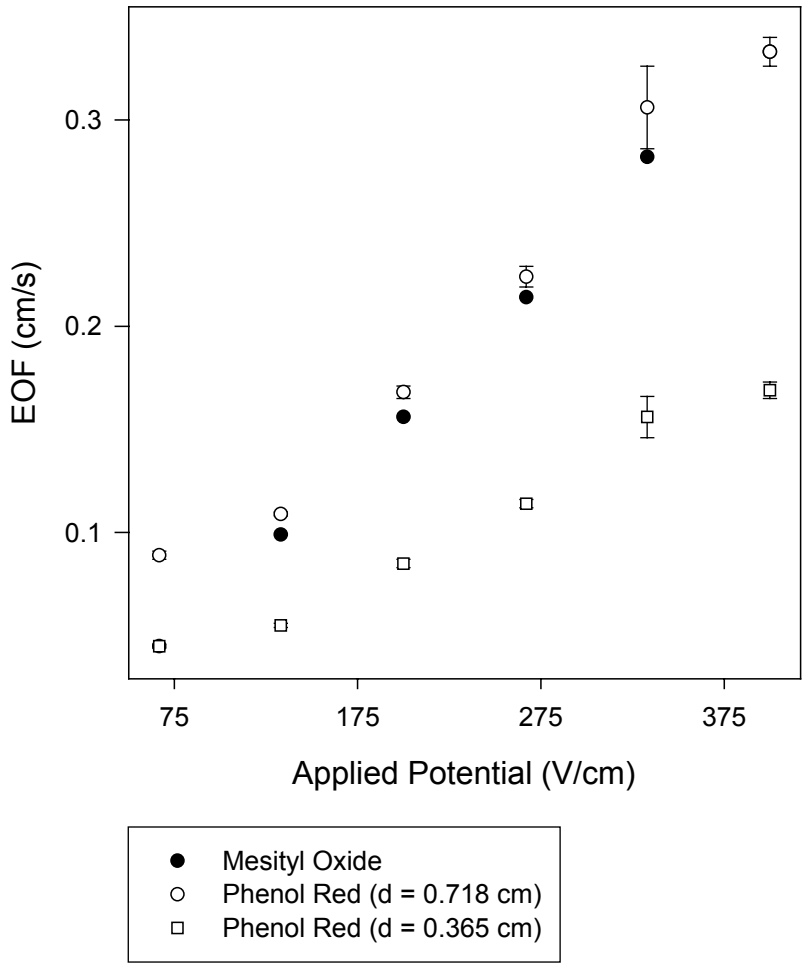

Figure A2-4. Flow rates measured using the secondary peak observed with 0.5 mM phenol red in 10 mM borate buffer (pH = 9.0). The distance between the heating beam (F1) and the detection beam (F2) was calibrated with both the slowest and fastest flow rates measured with mesityl oxide. (Heating beam λ = 514.5 nm; Slit width = 25 μm; Error bars are ± 1 SD).

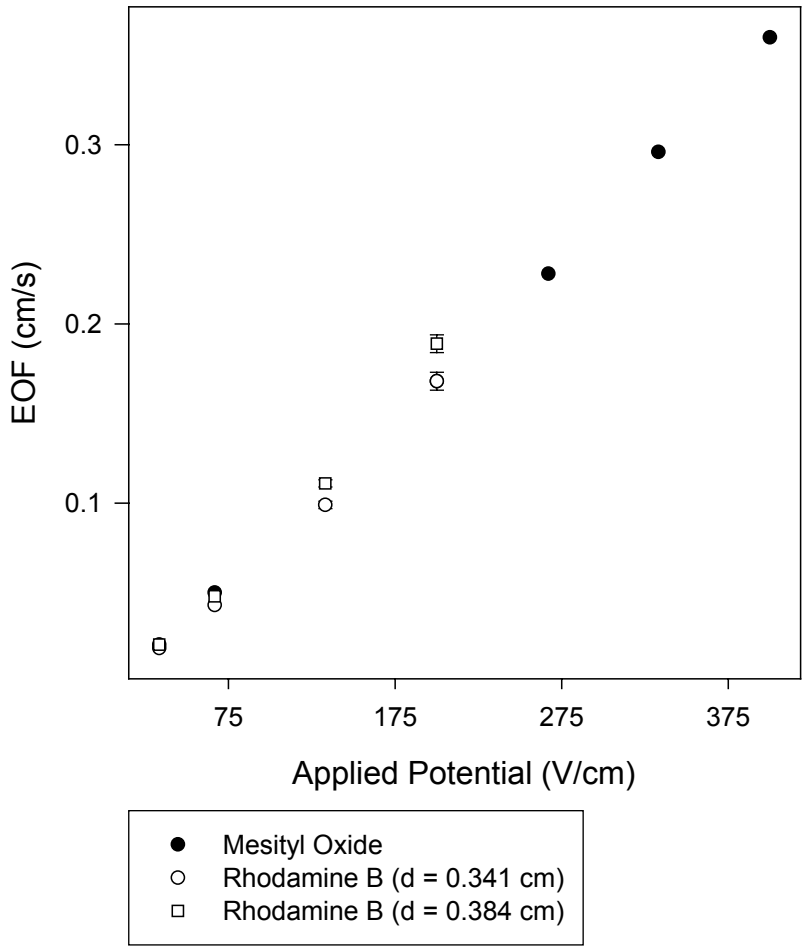

Figure A2-5. Flow rates measured using the secondary peak observed with 0.5 mM rhodamine B in 10 mM borate buffer (pH = 9.0). The distance between the heating beam and the detection beam (d) was calibrated with both the slowest and fastest flow rates measured with mesityl oxide which correspond to experiments where a secondary peak was observed with rhodamine B. (Heating beam λ = 514.5 nm; Slit width = 25 μm; Error bars are ± 1 SD).

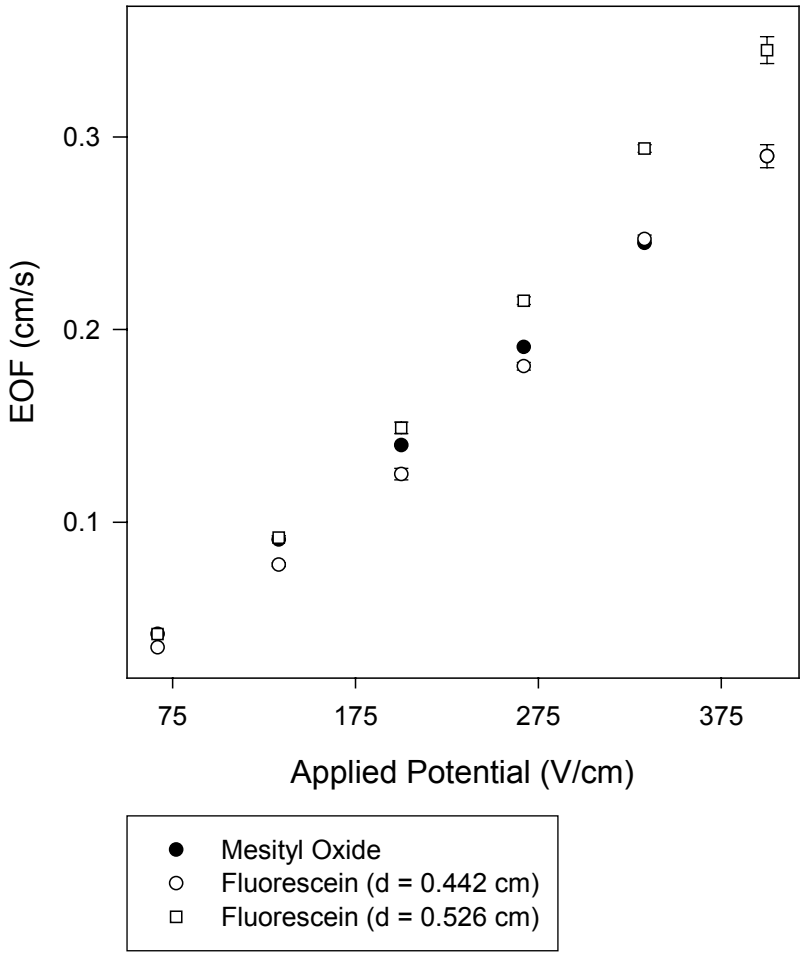

Figure A2-6. Flow rates measured using the secondary peak observed with 0.5 mM fluorescein in 10 mM borate buffer (pH = 9.0). The distance (d) between the heating beam and the detection beam was calibrated with both the slowest and fastest flow rates measured with mesityl oxide which correspond to experiments where a secondary peak was observed with fluorescein. (Heating beam λ = 488.0 nm; Slit width = 25 μm; Error bars are $\pm$ 1 SD).

slowest flow rates measured with mesityl oxide, respectively. A secondary RI peak for fluorescein was observable over flow rates of 0.0419 to 0.290 cm/s.

Hydrodynamic Flow Monitoring

Solution was flowed through the capillary hydrodynamically to determine if the method of heating a zone of solution in a capillary with a laser in order to measure flow rates in a capillary is a viable alternative to that presented by StClaire and Hayes.[15] The secondary RI event observed under electrophoretic conditions was not observed under conditions of hydrodynamic flow. This is true even at hydrodynamic flow rates of 0.10 cm/s, which overlap with flow rates observed with electrophoresis. This observation suggest that the presence of the secondary peak on the trailing edge of the larger primary peak is due to the electrophoretic separation of a photoproduct from the region of heated solution.

Figure A2-7A illustrates the most noticeable discrepancy in the hydrodynamic flow data. When *d* is calculated in the normal manner,[4-6] values of 1.265 to 5.155 cm are measured. However, when *d* is manually measured with a ruler at the capillary, values of ~3.5 to 7 mm are measured. Figures A2-7A illustrates how the calculated value of *d* varies with flow rate. This observation implies that it takes longer for the heated zone to travel from the heating beam to the detection beam than is expected. This effect is exaggerated at flow rates above 30 cm/s.

When measurements are taken from the center of the RI peak, the calculated flow rates versus the calibrated flow rate is not linear (Figure A2-7B). However, when measured from the peak front, the calculated values are closer to being linear (Figure A2-7C). Unfortunately, the values of *d* used for both figures are approximately a factor of 10 greater than the actual value for *d*. The results presented must be further analyzed and supported with literature before any firm conclusions can be made about the behavior of the RI flow monitoring system under both electrophoretic and hydrodynamic conditions.

This technique should be studied further so that an EOF monitoring method that does not require the addition of any buffer additives may be developed. The technique reported by StClaire and Hayes eliminated the need for a buffer additive by placing a resistive heating element around the capillary.[15] This method was simple and easily implemented; however, the amount of time for the heating element to reach the desired temperature and the amount of time for the heating element to cool following the removal of the applied current must be accounted for in the analysis of the data. Markov and Bornhop eliminated the resistive heating element and replaced it with an IR laser which was used to heat the aqueous solution in the capillary.[18] Markov and Bornhop also reported a novel method for the analysis of the data which eliminated some of the post-acquisition data processing used by StClaire and Hayes to achieve a linear calibration plot. Currently, the method reported by Markov and Bornhop method holds the greatest promise and should be explored further for use in capillary electrophoretic instruments.

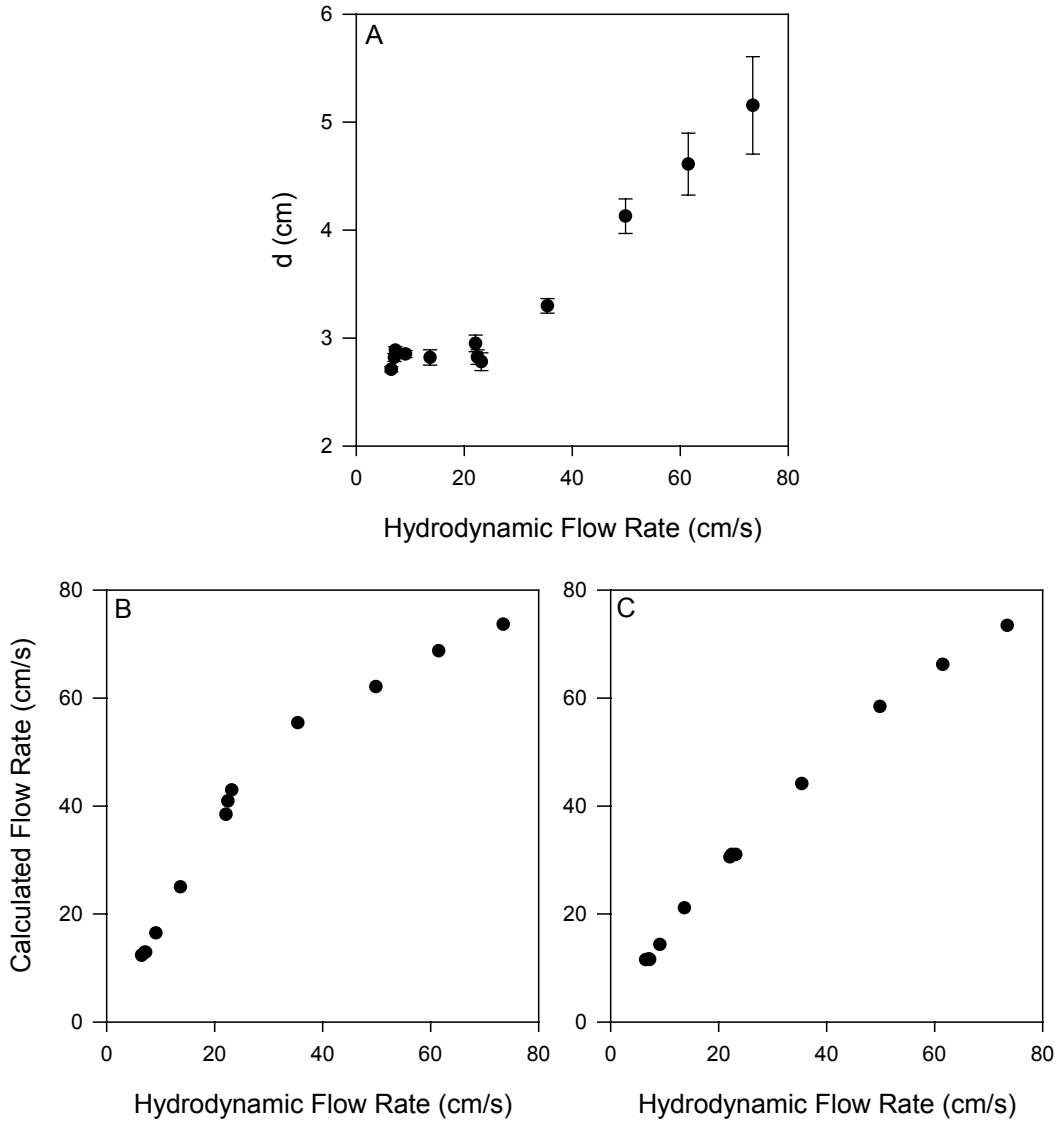

Figure A2-7. The (A) distance vs. calibrated flow rate measured from the center of the thermal peak. Calculated flow rate vs. calibrated flow rate where (B) d = 5.155 cm as measured from the center of the thermal peak and (C) d = 3.973 cm as measured from the front of the thermal peak at FWHM. Buffer solution was 10 mM borate buffer (pH = 9.00) with 0.5 mM phenol red. (Capillary 100 μm i.d.; Heating laser λ = 514.5 nm; Slit width = 25 μm).

Appendix II References

(1) Terabe, S.; Otsuka, K.; Ichikawa, J.; Tsuchiya, A.; Ando, T. *Anal. Chem.* **1984**, *56*, 111-113.

(2) Lukacs, K. D.; Jorgenson, J. W. *J. High Res. Chromatogr. Commun.* **1985**, *8*, 407-411.

(3) Huang, X.; Gordon, M. J.; Zare, R. N. *Anal. Chem.* **1988**, *60*, 1837-1838.

(4) Schrum, K. F.; Lancaster, J. M., III; Johnston, S. E.; Gilman, S. D. *Anal. Chem.* **2000**, *72*, 4317-4321.

(5) Pittman, J. L.; Schrum, K. F.; Gilman, S. D. *Analyst* **2001**, *126*, 1240-1247.

(6) Pittman, J. L.; Henry, C. S.; Gilman, S. D. *Anal. Chem.* **2003**, *Accepted for publication*.

(7) Altria, K. D.; Simpson, C. F. *Anal. Proc.* **1986**, *23*, 453-454.

(8) Altria, K. D.; Simpson, C. F. *Chromatographia* **1987**, *24*, 527-532.

(9) Bornhop, D. J.; Dovichi, N. J. *Anal. Chem.* **1986**, *58*, 504-505.

(10) Bruno, A. E.; Krattiger, B.; Maystre, F.; Widmer, H. M. *Anal. Chem.* **1991**, *63*, 2689-2697.

(11) Bornhop, D. J. *Appl. Optics* **1995**, *34*, 32343239.

(12) Tarigan, H. J.; Neill, P.; Kenmore, C. K.; Bornhop, D. J. *Anal. Chem.* **1996**, *68*, 1762-1770.

(13) Swinney, K.; Pennington, J.; Bornhop, D. J. *Analyst* **1999**, *124*, 221-225.

(14) Erickson, B. *Anal. Chem.* **2000**, *72*, 451A-452A.

(15) StClaire, J. C.; Hayes, M. A. *Anal. Chem.* **2000**, *72*, 4726-4730.

(16) Swinney, K.; Bornhop, D. J. *Analyst* **2000**, *125*, 1713-1717.

(17) Swinney, K.; Markov, D.; Bornhop, D. J. *Anal. Chem.* **2000**, *72*, 2690-2695.

(18) Markov, D. A.; Bornhop, D. J. *Fresenius J. Anal. Chem.* **2001**, *371*, 234-237.

(19) Markov, D.; Begari, D.; Bornhop, D. J. *Anal. Chem.* **2002**, *74*, 5438-5441.

(20) Woodruff, S. D.; Yeung, E. S. *Anal. Chem.* **1982**, *54*, 1174-1178.

(21) Kenmore, C. K.; Erskine, S. R.; Bornhop, D. J. *J. Chromatogr. A* **1997**, *762*, 219-225.

(22) Weimer, W. A.; Dovichi, N. J. *Appl. Optics* **1985**, *24*, 2981-2986.

(23) Bornhop, D. J.; Dovichi, N. J. *Anal. Chem.* **1987**, *59*, 1632-1636.

(24) Kenndler, E. In *High-Performance Capillary Electrophoresis*; Khaledi, M. G., Ed.; John Wiley & Sons, Inc.: New York, 1998; Vol. 146, pp 25-76.

(25) Sugarman, J. H.; Prud'homme, R. K. *Ind. Eng. Chem. Res.* **1987**, *26*, 1449-1454.

(26) van de Goor, A. A. A. M.; Wanders, B. J.; Everaerts, F. M. *J. Chromatogr.* **1989**, *470*, 95-104.

VITA

Jason Lasseter Pittman was born in Birmingham, AL on July 24, 1975. He was raised in Birmingham, AL and went to grade school at Mountain Brook Elementary School followed by Mountain Brook Junior High School. He graduated from Mountain Brook High School in 1993. From there he went to the University of the South in Sewanee, TN and received a B.S. in Chemistry in 1997.

Jason is currently pursuing his doctorate in chemistry at the University of Tennessee, Knoxville, TN.